Department of Physics and Astronomy
University of Heidelberg

Master Thesis in Physics
submitted by

Anna-Maria Elisabeth Glück

born in Horb am Neckar (Germany)

2024

Effective Field Theories for a Spin-1 Bose Gas Far From Equilibrium

This Master Thesis has been carried out by Anna-Maria Elisabeth Glück
at the
Kirchhoff Institute for Physics in Heidelberg
under the supervision of
Prof. Dr. Thomas Gasenzer.

Abstract

In the present work, we develop a low-energy effective field theory for the far-from-equilibrium spin-1 Bose gas after a parameter quench from the polar to the easy-plane phase. Inspired by the rich phase dynamics and self-similar spatio-temporal scaling of the transverse spin density observed in such a system, we integrate out the density fluctuations to find a theory only describing the phase degrees of freedom - the spinor phase φ_S and the Larmor phase φ_L. Expanding this theory around $\varphi_S = 2\mathbb{Z}\pi$, we obtain regular, uncoupled effective Lagrangians for the phases, with a free theory for φ_L and a sine-Gordon type theory with additional $\sin^2$-term for φ_S. The mass gap of the latter matches the Bogoliubov result and closely aligns with numerical data. The inclusion of higher-order density fluctuations does not significantly improve the agreement between the analytical and numerical results for the mass gap. We also perform an expansion about $\varphi_S = (2\mathbb{Z}+1)\pi$ by considering a theory set on the spin healing momentum scale and again find a free theory for φ_L and a sine-squared-Gordon theory for φ_S. In contrast with the expansion around $\varphi_S = 2\mathbb{Z}\pi$, the potential for φ_S expanded around $\varphi_S = (2\mathbb{Z}+1)\pi$ exhibits shallow local minima on top of the global maxima, which are in qualitative agreement with numerics.

Zusammenfassung

In dieser Arbeit entwickeln wir eine niedrigenergetische effektive Feldtheorie für ein spin-1 Bosegas weit vom Gleichgewicht nach einer rapiden Änderung der Parameter des Hamiltonian von der polaren in die Easy-Plane Phase. Von der reichhaltigen Dynamik der Phasen und dem selbst-ähnlichen raumzeitlichen Skalierungsverhalten der transversalen Spindichte inspiriert, integrieren wir die Dichtefluktuationen aus um eine Theorie zu erhalten, die nur die Phasenfreiheitsgrade beschreibt - die Spinorphase φ_S und die Larmorphase φ_L. Wenn wir die Theorie um $\varphi_S = 2\mathbb{Z}\pi$ entwickeln, erhalten wir regularisierte, ungekoppelte effektive Lagrangians für die Phasen, mit einer freien Theorie für φ_L und einer Theorie des sine-Gordon Typs mit einem extra $\sin^2$-Term für φ_S. Die Energielücke letzterer stimmt mit dem Resultat aus der Bogoliubov-Theorie und näherungsweise auch mit numerischen Daten überein. Die Einbeziehung von Termen höherer Ordnung in den Dichtefluktuationen verbessert die Übereinstimmung von analytischen und numerischen Resultaten für die Energielücke nicht signifikant. Auf der Energieskala des Healing-Impulses führen wir auch eine Entwicklung der Theorie um $\varphi_S = (2\mathbb{Z}+1)\pi$ durch und erhalten wieder eine freie Theorie für φ_L und eine sine-squared-Gordon Theorie für φ_S . Im Gegensatz zu der Entwicklung um $\varphi_S = 2\mathbb{Z}\pi$ zeigt das Potential für φ_S, das um $\varphi_S = (2\mathbb{Z}+1)\pi$ entwickelt wurde, flache Minima auf den globalen Maxima, die qualitativ mit der Numerik übereinstimmen.

Contents

1. Introduction

The question of how the universe came to be and how it has evolved to our current state has baffled humankind for centuries. With cosmological models as well as theories from all physical subfields, generations of physicists have come closer than ever to potentially understanding what the universe looked like in its very early stages [1]. However, the more we learn and theorize, the more physical questions open up as well. For example, subjects of current research are the thermalization and hadronization dynamics of the quark-gluon plasma that is hypothesized to be present in the universe before matter as we know it [2, 3], or the phase of reheating in the universe after the proposed period of inflation [4, 5].

As these phenomena are examples of isolated quantum many-body physics in extreme conditions far from equilibrium [6], this area of physics has gained interest in recent years. While the aforementioned systems cannot be directly studied, tabletop experiments with cold quantum gases provide a highly accessible way to probe the far-from-equilibrium dynamics of isolated quantum many-body systems [7] as these cold atom experiments allow for precise control of the initial conditions as well as the system parameters and realize almost perfectly isolated systems [8].

Because quantum many-body systems far from equilibrium in principle have an enormous number of degrees of freedom, the spectrum of phenomena that have been proposed for and observed in isolated cold atom systems out of equilibrium is broad [9], including but not limited to integrable dynamics [10–12], prethermalization [13–17], generalized Gibb's ensembles [18–22], many-body localization [23–26], critical and prethermal dynamics [27–30], wave turbulence [31, 32], decoherence and revivals [33], as well as universal spatio-temporal scaling dynamics [9, 34–41] and prescaling [42]. The beauty of many of these collective phenomena is, however, that despite the huge number of particles involved, they allow for a description of the relevant dynamics with only a few quantities.

Especially the universal scaling dynamics proposed for far-from-equilibrium systems and observed in cold atom experiments and numerical simulations of the latter is of interest in the current work. One can observe that correlation functions in different systems relaxing from an initial condition far from equilibrium can exhibit self-similar spatio-temporal scaling behavior

[34–37]. It is hypothesized that similarly to the notion of renormalization group fixed points governing universal scaling in equilibrium [43–48], such scaling occurs as a system approaches non-thermal fixed points in their time evolution to equilibrium [9, 34, 35, 40]. Once near such a fixed point, the system can then be described by only a small number of scaling exponents and functions, thus becoming independent of its exact initial conditions and microscopic degrees of freedom to a certain extent [49]. Similar to the universality classes in equilibrium, one may also be able to define such universality classes for the non-thermal fixed points [40, 49]. Thus, if the systems are in the same universality class, one may study the scaling behavior encountered in early-universe cosmology with tabletop cold atom experiments despite the vastly different energy scales of those systems.

In the current thesis, we want to contribute to the understanding of the universal scaling behavior observed in a spin-1 Bose-Einstein condensate (BEC) quenched far from equilibrium [37–39, 41]. Such a BEC can be described via three components, corresponding to the three magnetic sublevels of the spin-1 manifold. As a multi-component Bose gas allowing mixing between the different components, thus breaking $U(3)$ symmetry, it can exhibit phenomena not possible in single component gases, such as quantum phase transitions in the rich phase diagram, spin-mixing dynamics, as well as the formation and coarsening of spin domains [50]. It has been observed both experimentally [37] and numerically [38, 39, 41] that after quenching a spin-1 Bose gas from the polar to the easy-plane phase of the phase diagram, the transverse spin $F_\perp$, the order parameter of the easy-plane phase, exhibits self-similar scaling in the infrared according to

$$\langle |F_\perp(k)^2| \rangle =: S(k,t) = (t/t_{\text{ref}})^\alpha f_s \left([t/t_{\text{ref}}]^\beta k \right), \tag{1.1}$$

where f_s is a universal scaling function

$$f_s \sim 1/[1 + (k/k_\Lambda)^\kappa], \tag{1.2}$$

α, β, and κ are scaling exponents that are related to each other, k_Λ is the IR momentum scale, and t_{ref} is some reference time [38]. It has been discussed thoroughly that such self-similar scaling is due to quasiparticle transport to lower energies and energy transport to higher ones, as the initial momentum distribution $S(k,t)$ shortly after the quench is approximately a Heaviside function, overpopulating momenta around the spin-healing momentum compared to the equilibrium distribution [9, 38, 40]. However, it is not known which microscopic processes exactly drive these transport processes in momentum space. In the context of this self-similar scaling, rich phase dynamics including rogue waves and real-time instantons in the so-called Larmor phase between the $m = \pm 1$ components have been observed in one spatial dimension, as well as coarsening of these phenomena [41].

Thus, the goal of this work will be to develop a low-energy effective theory for the phase degrees of freedom in the spin-1 BEC in the hope of getting an intuition for the mechanisms behind the far-from-equilibrium self-similar scaling behavior observed in [38, 41]. Such an effective theory for the phases is much easier to interpret than the full spin-1 Bose action with all its degrees of freedom and can also be eventually used for numerical simulations of the far-from-equilibrium behavior of only the phase degrees of freedom. Especially, we want to use this effective theory to study the Larmor phase instantons observed in [41].

Moreover, it is worth noting that even though the far-from-equilibrium scaling behavior and the phase dynamics observed in [38] and [41] are the inspiration behind the effective field theories developed here, these theories could be of interest in general to the study of the phase degrees of freedom of the spin-1 Bose gas.

The current work is structured as follows: In the first chapter, Ch. 2, we want to give some background about the spin-1 Bose gas, its symmetries, its phase diagram, and the quench protocol used to study far-from-equilibrium phenomena in this system. Moreover, we recapitulate Bogoliubov theory for this system and set up a strategy to compare our results to the experiments carried out in Markus Oberthaler's group. Subsequently, in Ch. 3, we introduce some numerical methods used in the investigation of far-from-equilibrium physics and , thus, also in this work. As a first approach to develop an effective field theory for the spin-1 Bose gas, we employ the 2PI effective action formalism, deriving an effective action as well as equations of motion for the field expectation values and the statistical propagator up to leading order in $1/N$ in Ch. 4. While this method is useful for including non-equilibrium effects and initial conditions far from equilibrium, it is not suited well to reduce the degrees of freedom to only the phases of interest. Thus, in Ch. 5 we use the approach developed in [51], integrating out density fluctuations around the mean-field in order to obtain a low-energy effective theory only depending on the phase degrees of freedom of the spin-1 BEC near the easy-plane phase, i.e. the spinor phase φ_S of the 0-component and the relative Larmor phase φ_L between the $m = \pm 1$ components. We see that if we expand this theory for small values of φ_S, the theories for φ_L and φ_S decouple, yielding a free theory for φ_L and a sine-Gordon type theory for φ_S. These theories are then refined by including higher orders of the density fluctuations in the effective theory in Ch. 6. However, the theories developed in both chapters have the problem that they are only valid for values of the spinor phase φ_S around $2\pi\mathbb{Z}$ and diverge around the maxima of the sine-squared-Gordon potential for φ_S. Thus, in Ch. 7, we introduce a characteristic momentum for the density fluctuations, regulating the theory and enabling us to expand the effective theory around the potential maxima for φ_S, which then gives us a potential that is shaped as predicted by numerical simulations in the presence of instantons. In Ch. 8, we

finally sum up our results and discuss the next possible steps.

Unless otherwise noted, we use the Einstein summation convention throughout this work. Moreover, for the analytical chapters Ch. 4-7, we drop any explicit factors of $\hbar$ and c and use natural units $\hbar = c = 1$.

2. The spin-1 Bose gas

In this thesis, we want to develop a low-energy effective field theory for a spin-1 Bose-Einstein condensate (BEC) far from equilibrium after a quench from the polar to the easy-plane phase. We will use this chapter to lay out some theoretical background for that, discussing the Hamiltonian of the spin-1 Bose gas in Sec. 2.1 as well as its symmetries in Sec. 2.2. Thereafter, we consider the mean-field equation of motion as well as the different possible phases in the mean-field phase diagram of the condensate in Sec. 2.3, and explain how a quench from the polar to the easy-plane phase can be realized in Sec. 2.4. Subsequently, we derive the well-known Bogoliubov quasiparticle spectra in Sec. 2.5 for these two phases and discuss the emergence of dynamical instabilities following a quench. Lastly, we focus on how our analytical results can be reduced to one spatial dimension in order to be compared with a quasi-1d experiment with ^{87}Rb as it is studied in Prof. Markus Oberthaler's group in Heidelberg [37, 52–57].

For the most part, this chapter will follow [58] unless otherwise noted.

2.1. The spin-1 Hamiltonian

In this work, we consider a spin-1 Bose gas condensed to a BEC at zero temperature. Such a system of identical Bosons is best described by a three-component spinor of field operators Ψ_m with each component corresponding to a bosonic quantum field operator for the magnetic sublevels $m_F \in \{-1, 0, 1\}$ of the total spin $F = 1$[1] [58]

$$\hat{\boldsymbol{\Psi}} = \begin{pmatrix} \hat{\Psi_1} \\ \hat{\Psi_0} \\ \hat{\Psi_{-1}} \end{pmatrix}, \tag{2.1}$$

where we assume these operators to satisfy the canonical equal-time commutation relations

$$\left[\hat{\Psi}_i(\boldsymbol{x}, t), \hat{\Psi}_j(\boldsymbol{y}, t)\right] = 0 = \left[\hat{\Psi}_i^\dagger(\boldsymbol{x}, t), \hat{\Psi}_j^\dagger(\boldsymbol{y}, t)\right] \tag{2.2}$$

$$\left[\hat{\Psi}_i(\boldsymbol{x}, t), \hat{\Psi}_j^\dagger(\boldsymbol{y}, t)\right] = \delta_{ij}\delta^d(\boldsymbol{x} - \boldsymbol{y}). \tag{2.3}$$

[1] The notation m_F for the magnetic sublevels is chosen as the spinor components in atomic BECs are usually given by the sublevels of the fine structure manifold with total spin F, with $F = 1$ in this case.

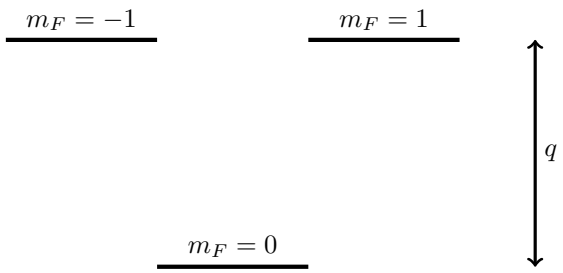

Figure 2.1.: Schematic picture of the energy shifts through the quadratic Zeeman effect.

In $1 + d$ space-time dimensions, the Hamiltonian for the weakly-interacting spin-1 Bose gas in an external magnetic field and potential is then given by [58–60]

$$\begin{aligned}\hat{H} = \int d^d\boldsymbol{x} \Bigg\{ \hat{\boldsymbol{\Psi}}^\dagger(\boldsymbol{x},t) \left[-\frac{\hbar^2}{2m}\nabla^2 + V(\boldsymbol{x}) + q f_z^2 \right] \hat{\boldsymbol{\Psi}}(\boldsymbol{x},t) \\ + \frac{1}{2} c_0 : \hat{n}^2(\boldsymbol{x},t) : + \frac{1}{2} c_1 : \hat{\boldsymbol{F}}^2(\boldsymbol{x},t) : \Bigg\},\end{aligned} \tag{2.4}$$

where :: denotes normal ordering of the operators. The quadratic part of this Hamiltonian involves the non-relativistic kinetic term, in which m denotes the mass of the bosons, the external trapping potential $V(\boldsymbol{x},t)$, and a term describing the quadratic Zeeman effect on the system's energy. We have already absorbed the linear Zeeman shift into a rotating frame of the spinors so that the quadratic Zeeman shift describes the lowest-order effect of an external magnetic field on the energy of the spinor BEC. Unlike the linear Zeeman effect, which shifts the magnetic sublevels $m_F = -1$ and $m_F = 1$ in opposite directions, the quadratic Zeeman effect causes the same shift in both levels with $m_F = \pm 1$, characterized by the coupling strength q, which can be experimentally tuned to different values as explained in Sec. 2.4. This effective detuning of the $m_F = \pm 1$ levels is illustrated in Fig. 2.1.

Moreover, there are two types of interaction terms: $U(3)$-symmetric density-density interactions governed by two normal-ordered powers of the number density operator

$$\hat{n}(\boldsymbol{x},t) = \hat{\Psi}_i^\dagger(\boldsymbol{x},t)\hat{\Psi}_i(\boldsymbol{x},t) \tag{2.5}$$

as well as spin-spin interactions involving the normal-ordered square of the spin density operator

$$\hat{\boldsymbol{F}} = \begin{pmatrix} \hat{\boldsymbol{\Psi}}^\dagger f_x \hat{\boldsymbol{\Psi}} \\ \hat{\boldsymbol{\Psi}}^\dagger f_y \hat{\boldsymbol{\Psi}} \\ \hat{\boldsymbol{\Psi}}^\dagger f_z \hat{\boldsymbol{\Psi}} \end{pmatrix}. \tag{2.6}$$

Here, the matrices $\boldsymbol{f} = (f_x, f_y, f_z)$ are the three spin-1 matrices corresponding to the generators of SO(3) in the three-dimensional irreducible representation in the spin-1 basis $|F = 1, m_F\rangle$

$$f_x = \frac{1}{\sqrt{2}} \begin{pmatrix} 0 & 1 & 0 \\ 1 & 0 & 1 \\ 0 & 1 & 0 \end{pmatrix} \quad f_y = \frac{1}{\sqrt{2}} \begin{pmatrix} 0 & -i & 0 \\ i & 0 & -i \\ 0 & i & 0 \end{pmatrix} \quad f_z = \begin{pmatrix} 1 & 0 & 0 \\ 0 & 0 & 0 \\ 0 & 0 & -1 \end{pmatrix} \tag{2.7}$$

so that the components of $\hat{\boldsymbol{F}}$ are given by multiplying these spin matrices by the spinor field from left and right, yielding scalar operators in each component:

$$\hat{\boldsymbol{F}} = \begin{pmatrix} \frac{1}{\sqrt{2}} \left((\hat{\Psi}_1^* + \hat{\Psi}_{-1}^*)\hat{\Psi}_0 + \hat{\Psi}_0^* (\hat{\Psi}_1 + \hat{\Psi}_{-1}) \right) \\ \frac{-i}{\sqrt{2}} \left((\hat{\Psi}_1^* - \hat{\Psi}_{-1}^*)\hat{\Psi}_0 - \hat{\Psi}_0^* (\hat{\Psi}_1 - \hat{\Psi}_{-1}) \right) \\ \left| \hat{\Psi}_1 \right|^2 - \left| \hat{\Psi}_{-1} \right|^2 \end{pmatrix} \tag{2.8}$$

The form of these interaction terms follows from group theory and symmetry arguments combined with the assumption of a dilute, weakly-interacting gas as explained in [58]. In such a gas, we can model interactions by only assuming s-wave scattering of two particles with pointlike scattering potential

$$v_{\mathcal{F}}(\boldsymbol{x}, \boldsymbol{y}) = g_{\mathcal{F}} \delta^d(\boldsymbol{x} - \boldsymbol{y}). \tag{2.9}$$

The total spin of the particles $\mathcal{F}$ must be conserved and can only be 0 or 2 for s-wave scattering of two bosons, such that the two scattering channels contribute to the Hamiltonian independently. The effective coupling constants $g_{\mathcal{F}}$ are related to the s-wave scattering lengths via

$$g_{\mathcal{F}} = \frac{4\pi\hbar^2}{m} a_{\mathcal{F}}. \tag{2.10}$$

By group-theoretic arguments, the operators corresponding to the 0- and 2-wave scattering channel can then be split into $\hat{n}^2$ and $\hat{\boldsymbol{F}}^2$ via Clebsch-Gordan coefficients, so that the interaction coefficients c_0 and c_1 are given by

$$c_0 = \frac{g_0 + 2g_2}{2} \quad c_2 = \frac{g_2 - g_0}{3}. \tag{2.11}$$

In the case of ^{87}Rb atoms experimentally considered in Prof. Dr. Markus Oberthaler's group [37, 52–57], the scattering lengths are given by $a_2 = (100.4 \pm 0.1)\, a_{\mathrm{B}}, a_0 = (101.8 \pm 0.2)\, a_{\mathrm{B}}$ [58], where a_{B} is the Bohr radius, such that $c_1 < 0$ and $|c_0| \gg |c_1|$.

The interaction term $\propto c_0$ consists of products of densities of the different components n_m. Such density-density interactions are the lowest-order $U(N)$ symmetric interaction one can

write down and, thus, appear also for any $U(N)$ symmetric theories. The term $\propto c_1$ is much more interesting, as it does not only contain products of component densities. Instead, this term governs the interaction between the spin densities Eq. (2.6). Consequently, it also allows for interactions in which the spin of the interacting particles changes and, thus, the different components mix.

Equivalently to the Hamiltonian, we can describe the spin-1 Bose gas with a partition function

$$Z = \int \mathcal{D}\Psi_1 \mathcal{D}\Psi_0 \mathcal{D}\Psi_{-1} e^{\frac{i}{\hbar} S[\Psi_1, \Psi_0, \Psi_{-1}]} \tag{2.12}$$

with the classical action obtained from the Hamiltonian Eq. (2.5) by a Legendre transformation

$$\begin{aligned} S = \int dt d^d\boldsymbol{x} \Big\{ & i\boldsymbol{\Psi}^\dagger(\boldsymbol{x},t)\partial_t \boldsymbol{\Psi}(\boldsymbol{x},t) - \boldsymbol{\Psi}^\dagger(\boldsymbol{x},t)\left[-\frac{\hbar^2}{2m}\nabla^2 + V(\boldsymbol{x}) + q f_z^2\right]\boldsymbol{\Psi}(\boldsymbol{x},t) \\ & -\frac{1}{2}c_0\left(\boldsymbol{\Psi}^\dagger(\boldsymbol{x},t)\boldsymbol{\Psi}(\boldsymbol{x},t)\right)^2 - \frac{1}{2}c_1\left(\boldsymbol{\Psi}^\dagger(\boldsymbol{x},t)\boldsymbol{f}\boldsymbol{\Psi}(\boldsymbol{x},t)\right)\left(\boldsymbol{\Psi}^\dagger(\boldsymbol{x},t)\boldsymbol{f}\boldsymbol{\Psi}(\boldsymbol{x},t)\right)\Big\}. \end{aligned} \tag{2.13}$$

or, written out,

$$\begin{aligned} S = \int dt d^d\boldsymbol{x} \Big\{ & i\left(\Psi_{-1}^\dagger \partial_t \Psi_{-1} + \Psi_0^\dagger \partial_t \Psi_0 + \Psi_1^\dagger \partial_t \Psi_1\right) \\ & - q\left(|\Psi_{-1}|^2 + |\psi_1|^2\right) - \frac{1}{2m}\left(\nabla\Psi_{-1}^\dagger \nabla\Psi_{-1} + \nabla\Psi_0^\dagger\nabla\Psi_0 + \nabla\Psi_1^\dagger\nabla\Psi_1\right) \\ & - \frac{c_0}{2}\left(|\psi_{-1}|^4 + |\Psi_0|^4 + |\Psi_1|^4 + 2|\Psi_{-1}|^2|\Psi_0|^2 + 2|\Psi_0|^2|\Psi_1|^2 + 2|\Psi_{-1}|^2|\Psi_1|^2\right) \\ & - \frac{c_1}{2}\left(|\Psi_{-1}|^4 + |\Psi_1|^4 + 2|\Psi_{-1}|^2|\Psi_0|^2 + 2|\Psi_0|^2|\Psi_1|^2 - 2|\Psi_{-1}|^2|\Psi_1|^2 + 2\Psi_0^2\Psi_{-1}^\dagger\Psi_1^\dagger + 2\bar{\Psi}_0^2\Psi_{-1}\Psi_1\right)\Big\}. \end{aligned} \tag{2.14}$$

Here the Ψ_i are classical, commuting fields. The functional integral measure is understood as the continuum limit of

$$\mathcal{D}\Psi_1\mathcal{D}\Psi_0\mathcal{D}\Psi_{-1} = \lim_{\delta\boldsymbol{x},\delta t\to 0} \Pi_{\boldsymbol{x},t}\Pi_{i\in\{-1,0,1\}} d\Psi_i(\boldsymbol{x},t) d\Psi_i^\dagger(\boldsymbol{x},t) \tag{2.15}$$

with discretized t and $\boldsymbol{x}$. The derivation of this formalism, especially for theories out of equilibrium, will be described in more detail in Sec.4.1.4.

From this written-out action, the mixing of components becomes especially visible. Here, one can see that there are terms in the interaction $\propto c_1$ that, for example, allow for two 0-component particles to become one +1- and one -1-particle in terms $\propto \Psi_0^{\dagger 2}\Psi_1\Psi_{-1}$ as illustrated in Fig. 2.3 (b).

2.2. Symmetries and Observables

Without the spin-changing interactions and the quadratic Zeeman shift terms, the Hamiltonian Eq. (2.5) would be invariant under $U(3)$ transformations. This symmetry is broken down to $SO(3) \times U(1)$ by the explicit appearance of the spin-1 matrices Eq. (2.7) in the spin-dependent interaction term. If, moreover, $q \neq 0$, the $SO(3)$ symmetry gets broken by the f_z^2 term such that the $SO(3)$ invariance reduces to $(D_\infty)_{f_z} = SO(2) \rtimes \mathbb{Z}_2$, singling out the z-axis while preserving invariance under rotations around this axis. Thus, the symmetries of the full spin-1 Hamiltonian can be described as $SO(2) \rtimes \mathbb{Z}_2 \times U(1)$.

Despite the Hamiltonian not being invariant under $SU(3)$ in the presence of all relevant terms to describe the spin-1 Bose gas, the 3-component field still allows us to observe the action of all $SU(3)$ generators in experiments with a spin-1 BEC, which correspond to the first 8 matrices in Tab. 2.1.

Subsets of these operators, in addition to some linear combinations, form representations of the generators for the $SU(2)$ subgroup of $SU(3)$ [62]:

$$\{\mathcal{O}_1, \mathcal{O}_2, \mathcal{O}_3\} \in \left\{ \left\{ \hat{F}_x, \hat{F}_y, \hat{F}_z \right\} ; \left\{ \hat{F}_x, \hat{Q}_{yz}, \hat{Q}_{zz} - \hat{Q}_{yy} \right\} ; \right. \tag{2.16}$$

$$\left\{ \hat{Q}_{xz}, \hat{Q}_{yz}, \hat{F}_z \right\} ; \left\{ \hat{F}_y, \hat{Q}_{xz}, \hat{Q}_{xx} - \hat{Q}_{zz} \right\} ; \tag{2.17}$$

$$\left\{ \hat{F}_x, \hat{Q}_{xz}, \hat{Q}_{xy} \right\} ; \left\{ \hat{F}_z, \hat{Q}_{xy}, \hat{Q}_{yy} - \hat{Q}_{xx} \right\} ; \tag{2.18}$$

$$\left. \left\{ \hat{F}_y, \hat{Q}_{yz}, \hat{Q}_{xy} \right\} \right\} \tag{2.19}$$

fulfilling the defining commutation relations

$$[\mathcal{O}_i, \mathcal{O}_j] = i\varepsilon_{ijk}\mathcal{O}_k. \tag{2.20}$$

2.3. Mean-field description

Now that we have discussed the Hamiltonian of the theory, let us get a better understanding of the system by considering a mean-field approximation. Such an approximation is purely classical and neglects any quantum and statistical fluctuations, thus only being valid for a gas made up of a very large number of very dilute weakly interacting atoms at very low temperatures [63]. However, this approximation is insightful for understanding the four phases with different groundstates we can expect for the theory as well as the relevant observables in these phases. Moreover, the truncated Wigner approximation (see Sec. 3.3), our main numerical technique, is based on the mean-field Gross-Pitaevskii equation, such that it makes sense to devote this section to the mean-field description of the spin-1 BEC.

$$f_x = \frac{1}{\sqrt{2}}\begin{pmatrix}0&1&0\\1&0&1\\0&1&0\end{pmatrix} \qquad \hat{F}_x = \frac{1}{\sqrt{2}}\hat{\Psi}_0^\dagger(\hat{\Psi}_1 + \hat{\Psi}_{-1}) + h.c.$$

$$f_y = \frac{1}{\sqrt{2}}\begin{pmatrix}0&-i&0\\i&0&-i\\0&i&0\end{pmatrix} \qquad \hat{F}_y = \frac{i}{\sqrt{2}}\hat{\Psi}_0^\dagger(\hat{\Psi}_1 - \hat{\Psi}_{-1}) + h.c.$$

$$f_z = \begin{pmatrix}1&0&0\\0&0&0\\0&0&-1\end{pmatrix} \qquad \hat{F}_z = \hat{n}_1 - \hat{n}_{-1}$$

$$q_{xz} = \frac{1}{\sqrt{2}}\begin{pmatrix}0&1&0\\1&0&-1\\0&-1&0\end{pmatrix} \qquad \hat{Q}_{xz} = \frac{1}{\sqrt{2}}\hat{\Psi}_0^\dagger(\hat{\Psi}_1 - \hat{\Psi}_{-1}) + h.c.$$

$$q_{yz} = \frac{i}{\sqrt{2}}\begin{pmatrix}0&-1&0\\1&0&1\\0&-1&0\end{pmatrix} \qquad \hat{Q}_{yz} = \frac{i}{\sqrt{2}}\hat{\Psi}_0^\dagger(\hat{\Psi}_1 + \hat{\Psi}_{-1}) + h.c.$$

$$q_{xy} = \begin{pmatrix}0&0&-i\\0&0&0\\i&0&0\end{pmatrix} \qquad \hat{Q}_{xy} = i\hat{\Psi}_{-1}^\dagger\hat{\Psi}_1 + h.c.$$

$$q_{xx} = \begin{pmatrix}-\frac{1}{3}&0&1\\0&\frac{2}{3}&0\\1&0&-\frac{1}{3}\end{pmatrix} \qquad \hat{Q}_{xx} = \frac{1}{3}(2\hat{n}_0 - \hat{n}_1 - \hat{n}_{-1}) + \hat{\Psi}_{-1}^\dagger\hat{\Psi}_1 + \hat{\Psi}_1^\dagger\hat{\Psi}_{-1}$$

$$q_{yy} = \begin{pmatrix}-\frac{1}{3}&0&-1\\0&\frac{2}{3}&0\\-1&0&-\frac{1}{3}\end{pmatrix} \qquad \hat{Q}_{yy} = \frac{1}{3}(2\hat{n}_0 - \hat{n}_1 - \hat{n}_{-1}) - \hat{\Psi}_{-1}^\dagger\hat{\Psi}_1 - \hat{\Psi}_1^\dagger\hat{\Psi}_{-1}$$

$$q_{zz} = \begin{pmatrix}\frac{2}{3}&0&0\\0&-\frac{4}{3}&0\\0&0&-\frac{2}{3}\end{pmatrix} \qquad \hat{Q}_{zz} = \frac{2}{3}(\hat{n}_1 + \hat{n}_{-1} - 2\hat{n}_0)$$

Table 2.1.: Spin-1 operators and the corresponding observables, built via $\hat{Q} = \mathbf{\Psi}^\dagger q \mathbf{\Psi}$. The first 8 matrices are linearly independent generators of $SU(3)$, while the last two are linear combinations. "$h.c.$" denotes the hermitian conjugate of the previous term. Table modified from [61].

2.3.1. The Gross-Pitavskii equation

To derive the mean-field description, we replace the fluctuating quantum field operators $\hat{\Psi}_i$ in the Hamiltonian by their expectation value:

$$\psi_i \equiv \langle \hat{\Psi}_i \rangle, \tag{2.21}$$

yielding the energy functional

$$\begin{aligned} E = \int d^d\boldsymbol{x}\boldsymbol{\psi}^\dagger(\boldsymbol{x},t)\left[-\frac{\hbar^2}{2m}\nabla^2 + V(\boldsymbol{x}) + qf_z^2\right]\boldsymbol{\psi}(\boldsymbol{x},t) \\ + \frac{1}{2}c_0 n^2(\boldsymbol{x},t) + \frac{1}{2}c_1\boldsymbol{F}^2(\boldsymbol{x},t). \end{aligned} \tag{2.22}$$

From the energy functional, we can derive the classical equation of motion using the variational principle

$$i\hbar\partial_t\psi_i = \frac{\delta E}{\delta\psi_i^\dagger}. \tag{2.23}$$

This yields

$$i\hbar\partial_t\boldsymbol{\psi}(\boldsymbol{x},\boldsymbol{t}) = \left[-\frac{\hbar^2}{2M}\nabla^2 + qf_z^2 + \frac{1}{2}c_0 n(\boldsymbol{x},t) + \frac{1}{2}c_1\boldsymbol{F}(\boldsymbol{x},t)\cdot\boldsymbol{f}\right]\boldsymbol{\psi}(\boldsymbol{x},t), \tag{2.24}$$

the Gross-Pitaevskii equation (GPE) for the spin-1 BEC.

Similarly, we can obtain this equation as the classical limit of the partition function Eq. (2.15): If we take $\hbar \to 0$, only the Ψ-configurations for which $\delta S = 0$ contribute non-zero Z[2]. Thus, the mean field ψ_i follows the classical equations of motion following from $\delta S = 0$, the Euler-Lagrange equations

$$\frac{d}{dt}\frac{\partial\mathcal{L}}{\partial\dot{\psi}_i} = \frac{\partial\mathcal{L}}{\partial\psi_i}, \tag{2.25}$$

which yield Eq. (2.70) as well.

2.3.2. The Mean-Field Phase diagram

Let us now consider a system without external trapping potential. Even without V, the spin-1 Lagrangian allows for a rich phase diagram for the mean-field expectation value as seen in Fig. 2.2. The different phases are caused by the interplay between the quadratic Zeeman shift

[2]Note that this is only strictly true if we shift time by a small imaginary part before sending it to infinity $t \to \infty(1 - i\varepsilon)$ [64].

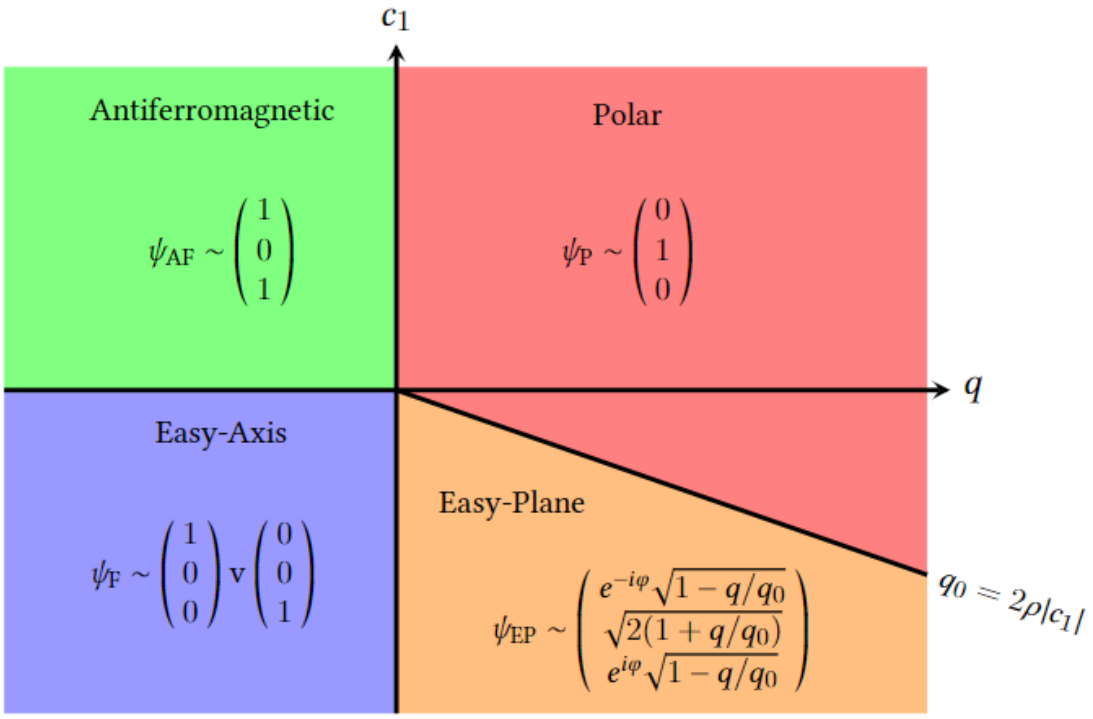

Figure 2.2.: Mean-field phase diagram for the spin-1 BEC. Figure taken from [65].

q and the interaction strength c_1 for spin-changing interactions. As coupling constants for the terms breaking the $U(3)$ invariance of the system, these quantities introduce competing energy scales that determine the ground state configuration of the mean field. In the following, we will elaborate on the different phases that can occur and what characterizes them.

Antiferromagnetic Phase

In the antiferromagnetic phase, we have $q < 0$ such that the $m_F = \pm 1$ levels are shifted downwards compared to the 0-level. Moreover, the antiferromagnetic interactions $c_1 > 0$ lead to a groundstate that is invariant under the $\mathbb{Z}_2$ symmetry of the Hamiltonian under the exchange of $m_F = 1$ and $m_F = -1$. Thus, we find a groundstate of the form

$$\psi_{AF} = \sqrt{\tilde{\rho}} \begin{pmatrix} e^{i\theta_1} \\ 0 \\ e^{i\theta_{-1}} \end{pmatrix} \tag{2.26}$$

with $\tilde{\rho}$ the homogeneous total density of the condensate. The mean-field expectation value for the spin density operator is then

$$\langle \hat{\boldsymbol{F}} \rangle = 0. \tag{2.27}$$

Easy-Axis or Ferromagnetic Phase

In the easy-axis or ferromagnetic phase, $q < 0$ like in the antiferromagnetic phase such that, again, the $m_F = \pm 1$ levels are energetically favorable. However, because of the ferromagnetic interactions $c_1 < 0$, we get spontaneous symmetry breaking of the $\mathbb{Z}_2$ phase as it becomes energetically more favorable to populate only one of the two energy levels $m_F = \pm 1$. In that case, we get a groundstate arbitrarily chosen between

$$\psi_F = e^{i\theta}\sqrt{\tilde{\rho}}\begin{pmatrix}1\\0\\0\end{pmatrix} \quad \text{and} \quad \psi_F = e^{i\theta}\sqrt{\tilde{\rho}}\begin{pmatrix}0\\0\\1\end{pmatrix} \tag{2.28}$$

with θ the global $U(1)$ phase. Thus, the mean-field spin density is of the form

$$\langle \hat{\boldsymbol{F}} \rangle = \sqrt{\tilde{\rho}}\begin{pmatrix}0\\0\\\pm 1\end{pmatrix}, \tag{2.29}$$

i.e. it is completely elongated in the z-direction, which is the name-giving characteristic for this phase.

Polar Phase

At positive $q > 0$, the $m_F = 0$ energy state is shifted downwards compared to $m_F = \pm 1$. Thus, for antiferromagnetic $c_1 > 0$ corresponding to repulsive spin-changing interactions, it is energetically most favorable to have all atoms occupying the 0-level, leading to a mean-field wave function of

$$\psi_P = \sqrt{\tilde{\rho}}e^{i\theta}\begin{pmatrix}0\\1\\0\end{pmatrix}. \tag{2.30}$$

and a spin density expectation value of

$$\langle \hat{\boldsymbol{F}} \rangle = 0 \tag{2.31}$$

like in the antiferromagnetic phase. Consequently, we need other observables from Tab. 2.1 to distinguish these two phases experimentally.

Note, however, that $q > 0$ and $c_1 > 0$ are not the only parameters for which the system occupies the polar phase. For small negative values of c_1, the spin-changing interactions compete with the Zeeman-splitting but they are not strong enough to produce a non-zero mean pop-

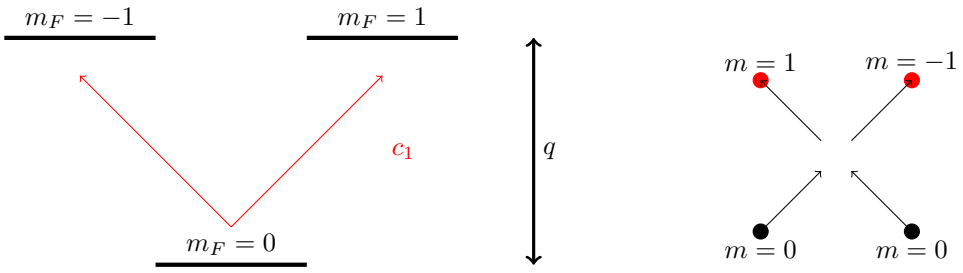

Figure 2.3.: (a) Schematic illustration of the Zeeman shift competing with spin-changing collisions. The quadratic Zeeman shift q determines the energy gap between the $m_F = 0$ and the $m_F = \pm 1$ components. For $q > 0$, depending on the strength of the spin-changing collisions, the latter can still be populated (easy-plane phase) or not (polar phase). (b) Schematic illustration of one possible spin-changing process, in which two $m_F = 0$ particles scatter to one $m_F = 1$ and one $m_F = -1$ particle.

ulation of the modes $m_F = \pm 1$ through interactions in which two atoms with $m_F = 0$ turn into one with $m_F = 1$ and one with $m_F = -1$ through processes as illustrated in Fig. 2.3.

Easy-Plane Phase

Only for $c_1 < 0$ and $|c_1| > q/2\tilde{\rho}$, the $m_F = \pm 1$ modes develop a non-zero mean field, leading to a mean-field spinor that can be parametrized by

$$\psi_{EP} = \begin{pmatrix} \sqrt{n} e^{\frac{i}{2}(\varphi_L + \theta)} \\ \sqrt{\tilde{\rho} - 2n} e^{\frac{i}{2}(\theta + \varphi_S)} \\ \sqrt{n} e^{-\frac{i}{2}(\varphi_L - \theta)} \end{pmatrix} \tag{2.32}$$

where

$$n = \frac{\tilde{\rho}}{4}(1 - q/q_0) \tag{2.33}$$

is the density of the $m_F = \pm 1$ modes and

$$q_0 = -2\tilde{\rho} c_1, \tag{2.34}$$

such that we can write

$$q = -2c_1(\tilde{\rho} - 4n). \tag{2.35}$$

This mean-field configuration corresponds to a symmetric occupation of $m_F = \pm 1$ only differing by a phase factor φ_L, which we call the Larmor phase, as well as a non-zero occupation of the 0-mode with phase evolution characterized by the so-called spinor phase φ_S in addition

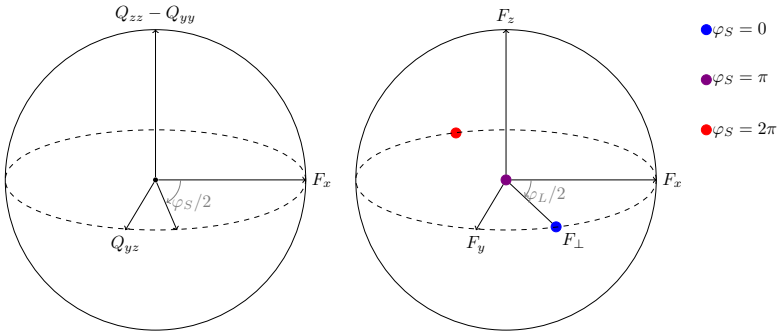

Figure 2.4.: Spin sphere spanned by $\{F_x, F_y, F_z\}$ (right) and spin-nematic sphere spanned by $\left\{F_x, Q_{yz}, Q_{z^2-y^2}\right\}$ (left) for the spin-1 BEC in the easy-plane phase. The Larmor phase φ_L rotates in the spin sphere, while the spinor phase φ_S rotates in the spin-nematic sphere. A rotation of the spinor phase affects the length of the spinor $F_\perp$ in the spin-nematic sphere such that at $\varphi_S = 0$ it is completely elongated, at $\varphi_S = \pi$ it has zero elongation, and at $\varphi_S = 2\pi$ it is elongated in the other direction. Similarly, a rotation of the Larmor phase affects the elongation as well as the height of the quantum state in the spin-nematic sphere.

to the global $U(1)$-phase θ.

The spin density operator has the expectation value

$$\langle \hat{\boldsymbol{F}} \rangle = \sqrt{8n(\tilde{\rho}-n)} \cos\frac{\varphi_S}{2} \begin{pmatrix} \cos\frac{\varphi_L}{2} \\ -\sin\frac{\varphi_L}{2} \\ 0 \end{pmatrix}, \tag{2.36}$$

which only has a magnetization in the $F_x - F_y$-plane with no magnetization in the F_z-direction, therefore naming this the easy-plane phase. The phase rotation in the $F_x - F_y$-plane is determined by the Larmor phase φ_L, while the length of $\langle \hat{\boldsymbol{F}} \rangle$ length is characterized by the spinor phase φ_S via $\sqrt{8n(\tilde{\rho}-n)}\cos\frac{\varphi_S}{2}$. The maximal elongation, thus, occurs for $\varphi_S = 2\pi\mathbb{Z}$ with $|F_\perp^{\max}| = \sqrt{8n(\tilde{\rho}-2n)} = \tilde{\rho}\sqrt{1-(q/q_0)^2}$.

If we define a further spin component

$$\hat{F}_\perp = \hat{F}_x + i\hat{F}_y = \sqrt{2}\left(\hat{\Psi}_1^\dagger \hat{\Psi}_0 + \hat{\Psi}_0^\dagger \hat{\Psi}_{-1}\right) \tag{2.37}$$

we find for its expectation value

$$\langle \hat{F}_\perp \rangle = |F_\perp| e^{i\varphi_L/2} \tag{2.38}$$

with

$$|F_\perp| = \sqrt{8n(\tilde{\rho}-n)}\left|\cos\frac{\varphi_S}{2}\right| \tag{2.39}$$

where we have absorbed sgn cos $\frac{\varphi_S}{2}$ in the Larmor phase. This rotation of $F_\perp$ in the spin sphere is illustrated on the right side of Fig 2.4. You can see that once φ_S crosses π, $|F_\perp|$ becomes negative such that the phase of $F_\perp$ as defined in Eq. (2.38) jumps by 2π.

To illustrate the mean-field dynamics of φ_S in the easy-plane phase, we consider the spin-nematic sphere spanned by $\{F_x, Q_{yz}, Q_{z^2-y^2}\}$ as seen on the left side of Fig. 2.4. As

$$\langle\hat{Q}_{yz}\rangle = \sqrt{8n(\tilde{\rho}-n)}\cos\frac{\varphi_L}{2}\sin\frac{\varphi_S}{2}, \tag{2.40}$$

the spinor phase rotates in the F_x, Q_{yz} plane in this spin-nematic phase with the Larmor phase determining the elongation in this sphere. Moreover, the Larmor phase determines the expectation value of $\hat{Q}_{z^2-y^2}$ via

$$\langle\hat{Q}_{z^2-y^2}\rangle = 4n - \tilde{\rho} + 2n\cos\varphi_L. \tag{2.41}$$

2.4. Quenching from the polar to the easy-plane phase

In the present work, we want to consider the spin-1 Bose gas driven far from equilibrium by a quench from the polar to the easy-plane phase. This particular problem has been studied in various experiments and numerical simulations such as [37–39, 41, 52–56], where $c_1 < 0$. Such a quench is realized by a sudden change of q from an initial value with $q > q_0 = -2\tilde{\rho}c_1$ to a value $q < q_0$, leading the system to undergo a quantum phase transition from the polar to the easy-plane phase and the order parameter $F_\perp$ of the easy-plane phase to develop a non-zero value. This is illustrated in Fig. 2.5. For experimental details of how this quench is carried out, see [37], for example.

2.5. Bogoliubov theory for the spin-1 BEC

One way to go beyond the mean-field is to include small fluctuations in the form of Bogoliubov modes. In the following, we will show a short derivation of the form of these quasiparticle excitations in the polar and the easy-plane phase. For this section, we will mainly follow [66], where one can also find a more detailed derivation than we will show here.

The first step for deriving the Bogoliubov spectrum in any phase is to go to momentum space,

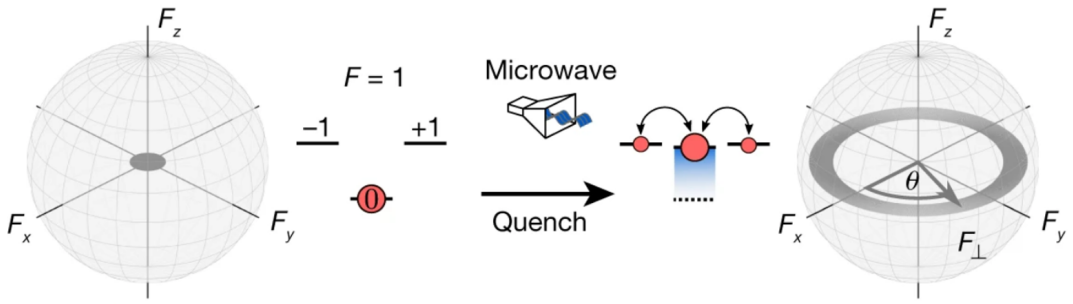

Figure 2.5.: Illustration of a quench from the polar to the easy-plane phase of a spin-1 Bose gas. In the polar phase, $\langle \hat{F} \rangle = 0$ and, at least in the mean-field approximation, only the $m_F = 0$ component is occupied. If q is tuned such that the energy gap between $m_F = 0$ and $m_F = \pm 1$ gets smaller, also the $m_F = \pm 1$ components develop a non-zero mean-field value and spin expectation value $F_\perp$, shown in the spin sphere. Figure taken from [37].

expanding each field operator as

$$\hat{\Psi}_m(\boldsymbol{x}) = \frac{1}{\sqrt{V}} \sum_{\boldsymbol{k}} \hat{a}_{\boldsymbol{k},m} e^{i\boldsymbol{k}\cdot\boldsymbol{x}}. \tag{2.42}$$

With this expansion, the Hamiltonian Eq. (2.5) becomes

$$\begin{aligned} \hat{H} = &\sum_{\boldsymbol{k}} (\varepsilon_{\boldsymbol{k}} + qm^2) \hat{a}^\dagger_{\boldsymbol{k},m} \hat{a}_{\boldsymbol{k},m} \\ &+ \frac{1}{2V} \sum_{\boldsymbol{k},\boldsymbol{p},\boldsymbol{q}} \left[c_0 \hat{a}^\dagger_{\boldsymbol{p},m} \hat{a}^\dagger_{\boldsymbol{q},m'} \hat{a}_{\boldsymbol{p}+\boldsymbol{k},m} \hat{a}_{\boldsymbol{q}-\boldsymbol{k},m'} + c_1 \boldsymbol{f}_{mm'} \cdot \boldsymbol{f}_{\mu\mu'} \hat{a}^\dagger_{\boldsymbol{p},m} \hat{a}^\dagger_{\boldsymbol{q},\mu} \hat{a}_{\boldsymbol{p}+\boldsymbol{k},m} \hat{a}_{\boldsymbol{q}-\boldsymbol{k},\mu'} \right], \end{aligned} \tag{2.43}$$

where we have introduced $\varepsilon_{\boldsymbol{k}} = \frac{\hbar^2 k^2}{2m}$.

In Bogoliubov theory, we assume that most but not all particles are occupying the $k = 0$-mode of the groundstate $|\Phi_0\rangle$ of the Bose gas, which is a coherent state obeying

$$\hat{a}_{0,m} |\Phi_0\rangle = \sqrt{N_0} \xi_m |\Phi_0\rangle \tag{2.44}$$

where $\sum_{m_F=-1}^{1} |\xi_m|^2 = 1$. On top of this groundstate, we assume there to be fluctuations, with the total particle number fulfilling

$$N = N_0 + \sum_{m,\boldsymbol{k}\neq 0} \hat{a}^\dagger_{\boldsymbol{k},m} \hat{a}_{\boldsymbol{k},m}, \tag{2.45}$$

and the fluctuations so small that we can expand the Hamiltonian to second order in $\hat{a}_{\boldsymbol{k}\neq 0,m}$ and $\hat{a}^\dagger_{\boldsymbol{k}\neq 0,m}$.

While the full Bogoliubov spectra for all phases of the spin-1 BEC are derived in [66] and listed in Tab. 7 in [58], we only want to focus on those for the polar and the easy-plane phase. These are of interest in the current work, where we study a spin-1 BEC quenched from the polar to the easy-plane phase. Thus we want to consider the Bogoliubov spectrum in the polar phase, as it can give us some information on how instabilities in the system develop after a quench. Moreover, we need the Bogoliubov spectrum for our numerical simulations, which are carried out in the truncated Wigner approximation (see Sec. 3.3). The spectrum in the easy-plane phase is of interest to us because at late times after the quench, the system's densities fluctuate closely around the mean-field equilibrium values as can be seen in Fig. 5.1a.

2.5.1. Bogoliubov spectrum in the polar phase and dynamical instabilities

In the polar phase we have $\xi = (0, 1, 0)^T$. Choosing

$$\hat{a}_{\boldsymbol{k},d} = \hat{a}_{\boldsymbol{k},0} \tag{2.46}$$

$$\hat{a}_{\boldsymbol{k},f_x} = \frac{1}{\sqrt{2}} \left(\hat{a}_{\boldsymbol{k},1} + \hat{a}_{\boldsymbol{k},1}\right) \tag{2.47}$$

$$\hat{a}_{\boldsymbol{k},f_y} = \frac{i}{\sqrt{2}} \left(\hat{a}_{\boldsymbol{k},1} - \hat{a}_{\boldsymbol{k},1}\right) \tag{2.48}$$

we find the Hamiltonian to second order in the fluctuations as

$$\hat{H}^{(2)} = \frac{V c_0 \tilde{\rho}^2}{2} + \sum_{\boldsymbol{k}\neq 0} \Bigg[(\varepsilon_{\boldsymbol{k}} + c_0\tilde{\rho}) \hat{a}^\dagger_{\boldsymbol{k},d} \hat{a}_{\boldsymbol{k},d} + \frac{c_0\tilde{\rho}}{2} \left(\hat{a}^\dagger_{\boldsymbol{k},d} \hat{a}^\dagger_{-\boldsymbol{k},d} + \hat{a}_{\boldsymbol{k},d} \hat{a}_{-\boldsymbol{k},d} \right) \tag{2.49}$$

$$+ \sum_{j=f_x,f_y} (\varepsilon_{\boldsymbol{k}} + c_1\tilde{\rho} + q) \hat{a}^\dagger_{\boldsymbol{k},f} \hat{a}_{\boldsymbol{k},f} + \frac{c_1\tilde{\rho}}{2} \left(\hat{a}^\dagger_{\boldsymbol{k},f} \hat{a}^\dagger_{-\boldsymbol{k},f} + \hat{a}_{\boldsymbol{k},f} \hat{a}_{-\boldsymbol{k},f} \right) \Bigg]$$

where $\tilde{\rho} = N/V$. This Hamiltonian is then diagonalized by the Bogoliubov transforms

$$\hat{b}_{\boldsymbol{k},d} = \sqrt{\frac{\varepsilon_{\boldsymbol{k}} + c_0\tilde{\rho} + E_{\boldsymbol{k},d}}{2E_{\boldsymbol{k},d}}} \hat{a}_{\boldsymbol{k},d} + \sqrt{\frac{\varepsilon_{\boldsymbol{k}} + c_0\tilde{\rho} - E_{\boldsymbol{k},d}}{2E_{\boldsymbol{k},d}}} \hat{a}^\dagger_{-\boldsymbol{k},d} \tag{2.50}$$

$$\hat{b}_{\boldsymbol{k},j} = \sqrt{\frac{\varepsilon_{\boldsymbol{k}} + c_1\tilde{\rho} + q + E_{\boldsymbol{k},f}}{2E_{\boldsymbol{k},f}}} \hat{a}_{\boldsymbol{k},j} + \sqrt{\frac{\varepsilon_{\boldsymbol{k}} + c_1\tilde{\rho} + q - E_{\boldsymbol{k},f}}{2E_{\boldsymbol{k},f}}} \hat{a}^\dagger_{-\boldsymbol{k},j} \tag{2.51}$$

such that

$$\hat{H}^{(2)} = E_0^P + \sum_{\boldsymbol{k}\neq 0} E_{\boldsymbol{k},d} \hat{b}^\dagger_{\boldsymbol{k},d} \hat{b}_{\boldsymbol{k},d} + E_{\boldsymbol{k},f} \left(\hat{b}^\dagger_{\boldsymbol{k},f_x} \hat{b}_{\boldsymbol{k},f_x} + \hat{b}^\dagger_{\boldsymbol{k},f_y} \hat{b}_{\boldsymbol{k},f_y} \right) \tag{2.52}$$

with Bogoliubov spectrum

$$E_{\boldsymbol{k},d} = \sqrt{\varepsilon_{\boldsymbol{k}}\left(\varepsilon_{\boldsymbol{k}} + 2\tilde{\rho}c_0\right)} \tag{2.53}$$

$$E_{\boldsymbol{k},f} = \sqrt{\left(\varepsilon_{\boldsymbol{k}} + q\right)\left(\varepsilon_{\boldsymbol{k}} + q + 2\tilde{\rho}c_1\right)}. \tag{2.54}$$

Thus, there is one gapless mode for the Goldstone£ boson corresponding to the spontaneous breaking of the total $U(1)$ symmetry when choosing a groundstate as Eq. (2.30), as well as two gapped modes. The gapless mode corresponds to the total phase of the condensate wave function, while the two gapped modes are related to the population of the $m_F = \pm 1$ modes.

In the polar phase, we have either $q > 0$ for positive c_1 or $q > -2\tilde{\rho}c_1$ for negative c_1. Thus, for parameters in the polar phase, the energies $E_{k,f}$ are always real. However, if we start in the polar phase and suddenly change $q > 0$ to be smaller than $-2\tilde{\rho}c_1$ for negative c_1, corresponding to a quench of the system to the easy-plane phase, we find that $E_{k,f}$ becomes imaginary, thus leading to instabilities of these modes. As the time evolution goes with $\propto e^{-iE_{k,f}t}$, the $m_F = \pm 1$ modes get populated exponentially, leading to a development of a non-zero mean field in $m_F = \pm 1$. Writing $E_{k,f} = i\hbar\gamma_{\boldsymbol{k}}$, one finds the occupations evolve in time as [67]

$$n_{\pm}(\boldsymbol{k}, t) = \left[\cosh^2\gamma_{\boldsymbol{k}}t + \left(\frac{\varepsilon_{\boldsymbol{k}} + q + \tilde{\rho}c1}{\hbar\gamma_{\boldsymbol{k}}}\right)^2 \sinh^2\gamma_{\boldsymbol{k}}t\right] n_{\pm}(\boldsymbol{k}, 0) \tag{2.55}$$

$$+ \left(\frac{\tilde{\rho}c_1}{\hbar\gamma_k}\right)^2 \sinh^2\gamma_{\boldsymbol{k}}t\left(n_{\mp}(-\boldsymbol{k}, 0) + 1\right) \tag{2.56}$$

such that non-zero occupations of $m_F = \pm 1$ can develop even if they are zero at the initial time.

2.5.2. Bogoliubov spectrum in the easy-plane phase

Now that we have discussed how amplified fluctuations in the polar phase after a quench to the easy-plane phase can lead to occupations of the $m_F = \pm 1$ components, let us look at the Bogoliubov spectrum in the easy-plane phase. In this phase, we have $\xi = (\sin\vartheta/\sqrt{2}, \cos\vartheta, \sin\vartheta/\sqrt{2})^T$ with $\sin\vartheta = \frac{1}{\sqrt{2}}\sqrt{1 - q/q_0}$. The Bogoliubov transformation is now more complex, but the procedure of expanding and diagonalizing the Hamiltonian is the same as in the polar phase. Omitting the details of the derivation, which can be found in [66], we get the diagonal Hamiltonian

$$\hat{H}^{(2)} = E_0^{BA} + \sum_{k\neq 0} E_{\boldsymbol{k},f_z}\hat{b}^{\dagger}_{\boldsymbol{k},f_z}\hat{b}_{\boldsymbol{k},f_z} + E_{\boldsymbol{k},+}\hat{b}^{\dagger}_{\boldsymbol{k},+}\hat{b}_{\boldsymbol{k},+} + E_{\boldsymbol{k},-}\hat{b}^{\dagger}_{\boldsymbol{k},-}\hat{b}_{\boldsymbol{k},-} \tag{2.57}$$

with Bogoliubov spectrum

$$E_{\boldsymbol{k},f_z} = \sqrt{\varepsilon_{\boldsymbol{k}}\left(\varepsilon_{\boldsymbol{k}} + q\right)} \tag{2.58}$$

and

$$E_{\boldsymbol{k},\pm} = \sqrt{\varepsilon_{\boldsymbol{k}}^2 + (c_0 - c_1)\tilde{\rho}\varepsilon_{\boldsymbol{k}} + 2(c_1\tilde{\rho})^2(1 - \frac{q^2}{(2\tilde{\rho}|c_1|)^2}) \pm \Lambda_{\boldsymbol{k}}} \tag{2.59}$$

where

$$\Lambda_{\boldsymbol{k}} = \sqrt{[(c_0 + 3c_1)\tilde{\rho}\varepsilon_{\boldsymbol{k}} + 2c_1(c_1\tilde{\rho})^2(1 - \frac{q^2}{(2\tilde{\rho}|c_1|)^2})]^2 - 4c_1(c_0 + 2c_1)\tilde{\rho}^2\frac{q^2}{(2\tilde{\rho}|c_1|)^2}\varepsilon_{\boldsymbol{k}}^2} \tag{2.60}$$

Note that in this phase, we have two gapless modes, E_{f_z} and E_-, for the Goldstone bosons corresponding to the spontaneous breaking of $U(1)$ symmetry and $SO(2)$ symmetry by the groundstate Eq. (2.32), represented by the total phase and the Larmor phase, respectively. The gapped mode corresponds to the spinor phase.

2.6. Crossover to 1d

The ultimate goal of any theory is to predict, describe, and explain experimental observations. For this thesis, the experimental inspiration comes mainly from investigations of far-from-equilibrium dynamics in a quasi-1d spin-1 Bose gas of ^{87}Rb-atoms in Markus Oberthaler's group [37, 52–57], for which the three magnetic sublevels $m_F = 0, \pm 1$ of the $F = 1$ hyperfine manifold form a spin-1 system with ferromagnetic interactions $c_1 < 0$. To achieve a quasi-1d condensate of these atoms, an anisotropic harmonic trap is applied to the 3d condensate in addition to laser barriers in the longitudinal direction of the gas, resulting in a very thin cigar-shaped condensate that can be considered as quasi-1d. This is illustrated in Fig. 2.6.

We can incorporate the harmonic trap into our action by including the external potential

$$V(\boldsymbol{x}) = \frac{\omega_\parallel^2}{2}x^2 + \frac{\omega_\perp^2}{2}(y^2 + z^2) \tag{2.61}$$

where the coordinate system is chosen as in Fig. 2.6 and $\omega_\perp$ and $\omega_\parallel$ are the trapping frequencies perpendicular and parallel to the relevant dimension, respectively. To obtain a quasi-1d condensate at zero temperature, $\omega_\perp$ has to be chosen such that the interactions are highly suppressed compared to the trapping energy in the perpendicular direction [68], i.e.

$$\hbar\omega_\perp \gg \tilde{\rho}c_0, \tilde{\rho}|c_1|. \tag{2.62}$$

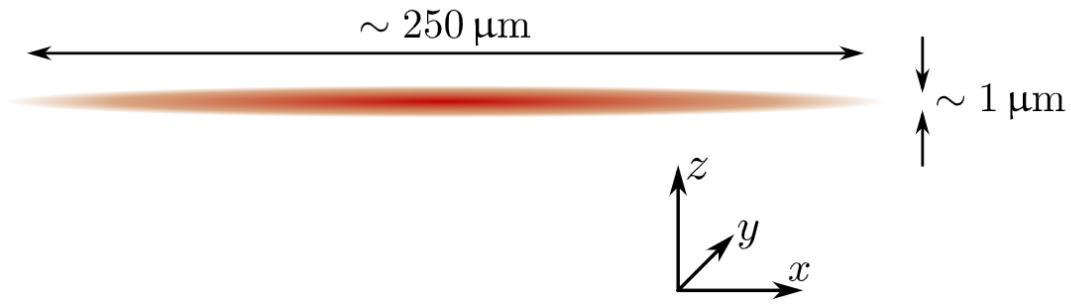

Figure 2.6.: Schematic illustration of the trap geometry in the ^{87}Rb in Markus Oberthaler's group. Figure taken from [61].

This condition can also be formulated in terms of lengthscales. For the two different interactions in the spin-1 BEC, we can define the density healing length ξ and the spin healing length ξ_s according to

$$\xi = \frac{\hbar}{\sqrt{2m\tilde{\rho}c_0}} \quad \text{and} \quad \xi_S = \frac{\hbar}{\sqrt{2m\tilde{\rho}|c_1|}}, \tag{2.63}$$

which describe the typical lengthscales at which the BEC "heals" from a defect in the mean density and spin density, respectively. Comparing this with the characteristic lengthscale of the transverse potential, the oscillation length describing the extent of the trap

$$a_\perp = \frac{\hbar}{\sqrt{m\omega_\perp}}, \tag{2.64}$$

the condition Eq. (2.62) translates to

$$a_\perp \ll \xi, \xi_S, \tag{2.65}$$

i.e. the trap size constraining the condensate in y- and z-direction has to be much smaller than the density and spin healing lengths. This condition then ensures that no significant dynamics can develop in these directions. Meanwhile,

$$a_\parallel \gg a_\perp \tag{2.66}$$

has to apply for there to be some significant elongation in x-direction in which quasi-1d physics can be studied.

For the condition Eq. (2.62), we can assume the system to be in the groundstate of the harmonic

oscillator in the perpendicular direction [69]

$$\left[-\frac{\hbar^2}{2m}\left(\nabla_y^2+\nabla_z^2\right)+\frac{m\omega_\perp^2}{2}(y^2+z^2)\right]\phi(\sqrt{y^2+z^2})=\mu_\perp\phi(\sqrt{y^2+z^2}) \tag{2.67}$$

which is given by

$$\phi_0(\sqrt{y^2+z^2})=\frac{1}{\sqrt{\pi a_\perp^2}}e^{\frac{-(y^2+z^2)}{2a_\perp^2}}. \tag{2.68}$$

We can then decompose the 3d wave function like

$$\Psi_m(\boldsymbol{x},t)=\Psi_m(x,t)\phi_0(\sqrt{y^2+z^2})e^{-\frac{i}{\hbar}\mu_\perp t}. \tag{2.69}$$

Plugging this into the GPE Eq. (2.70) and multiplying both sides by $\phi_0^\dagger(t,\sqrt{y^2+z^2})$, as well as integrating out y and z, we find that the resulting effective GPE for only the relevant x-direction is given by Eq. (2.70) in 1D [69]

$$i\hbar\partial_t\boldsymbol{\psi}(x,t)=\left[-\frac{\hbar^2}{2M}\nabla_x^2+qf_z^2+V(x)+\frac{1}{2}c_0^{1D}n(x,t)+\frac{1}{2}c_1^{1D}\boldsymbol{F}(x,t)\cdot\boldsymbol{f}\right]\boldsymbol{\psi}(x,t), \tag{2.70}$$

modified with effective couplings

$$c_i^{1D}=\frac{c_i}{2\pi a_\perp^2}. \tag{2.71}$$

In the following, we will work with the action in general d dimensions but remember that in order to compare to experimental quasi-1d results, one just has to modify the couplings $c_i\to c_i^{1D}$. For simplicity, we will also assume $V=0$ in the following.

3. Numerical Methods

Before we dig into the analytics of developing an effective field theory for the spin-1 Bose gas, we want to give an overview of the numerical methods used to study the far-from-equilibrium dynamics of this system. As detailed in the introduction, far from equilibrium physical systems exhibit a plethora of dynamical phenomena, from topological defects like real-time instantons to the general spatial coarsening of Larmor phase domains [41]. Due to this complexity, the most powerful way to theoretically study such systems is via numerical simulations. For such simulations, semi-classical truncated Wigner simulations are widely employed in the group of Thomas Gasenzer, in which noise is added to the GPE in order to perform calculations beyond the mean-field approximation. Using this method and the phenomenological insights from the numerical results has led to significant developments in the understanding of far-from-equilibrium dynamics of ultra-cold Bose gases and especially the spin-1 Bose gas in the past [38, 39, 41, 70–72].

Thus, even for the present work, which is mainly analytical, numerical simulations are hugely important. Firstly, due to the high complexity of out-of-equilibrium physics, numerical simulations can be a good guide to see what phenomena are interesting, such that we may make approximations to the theory based on the numerical results to get rid of irrelevant degrees of freedom. For example, the effective theories developed in Ch. 5-7 are all inspired by the numerical observation of the interesting phase dynamics of the spin-1 Bose gas including real-time instantons [41].

Moreover, once we have developed an analytical theory, numerical simulations make for a good sanity check of whether the analytical results accurately describe observations, and they will be used as such in this thesis. For these numerical simulations, we have used the spin-1 code developed in Thomas Gasenzer's group, with improvements in the past few years mainly attributable to Christian-Marcel Schmied and Ido Siovitz.

In the following chapter, we will sum up the most important methods used in the numerical simulation of far-from-equilibrium Bose gases in a semi-classical truncated Wigner approximation, with the first section Sec. 3.1 focusing on how the GPE can be discretized for numerical analysis, Sec. 3.2 explaining the split-step Fourier algorithm for the numerical time evolution

of nonlinear Schroedinger equations like GPEs, and the last section Sec. 3.3 giving some background on the truncated Wigner approximation.

3.1. Discretizing the GPE

To be able to numerically work with the GPE Eq. (2.70), we need to first discretize the equation. For that, we define the wave functions $\Psi(x)$ as a vector on a lattice of N points with lattice spacing Δx, which determines the length scale of the system and is related to the total physical length via $\Delta x = L/N$. Moreover, time is discretized and we define the time scale $\omega = \hbar/m\Delta x^2$. With this time and length scale, we can make all numerical quantities (marked by barring the quantities) dimensionless via

$$\bar{x} = \frac{x}{\Delta x};\;\; \bar{t} = \omega t;\;\; \bar{c}_i = \frac{c_i}{\hbar\omega\Delta x};\;\; \bar{\omega}_{\perp,\parallel} = \frac{\omega_{\perp,\parallel}}{\omega};\;\; \bar{q} = \frac{q}{\hbar\omega};\;\; \bar{\Psi}_i = \sqrt{\Delta x}\Psi_i. \tag{3.1}$$

For the rest of this chapter, we will drop the bar as we will only talk about the dimensionless quantities.

For a consistent definition of the discretized momenta in Fourier space, we expand the fields into discrete plane waves and demand that the discrete Laplacian for these plane waves on the lattice must fulfill

$$k^2\Psi_i = \Delta\Psi_i = \frac{\Psi_{i+1} - 2\Psi_j + \Psi_{j-1}}{\Delta x^2}. \tag{3.2}$$

Inserting the discrete plane waves into this equation, we find that the discrete momenta have to obey

$$k_n = \frac{2}{N}\sin\frac{\pi n}{N} \tag{3.3}$$

with $n \in [-N/2+1, N]$. This means that for small $|n|$, i.e. in the IR, the momenta are spaced approximately linearly as $\sin\phi \approx \phi$ for small values, while the spacing for high $|n|$ in the UV is denser.

3.2. The split-step Fourier method

To perform a time evolution of our system, we use the split-step Fourier approach [73] to solve the GPE Eq. (2.70), as this method is shown to conserve energy as well as particle number [73]. The GPE has the form of a non-linear Schrödinger equation

$$i\partial_t\Psi_j = H_{jk}\Psi_k, \tag{3.4}$$

where, usually, H consists of a kinetic term, which is diagonal in momentum space, and a nonlinear term in the fields, which is diagonal in position space. To be able to make use of the diagonality of the different parts of H in different spaces, we split H into its kinetic and the interaction part $H = K + I$ such that the time evolution of Ψ_j is given by

$$\Psi_j(t + \Delta t, x) = \left(e^{-iH\Delta t}\right)_{jk} \Psi_k(x, t) = \left(e^{-i(K+I)\Delta t}\right)_{jk} \Psi_k(x, t) \tag{3.5}$$

We can then use the Baker-Campbell-Hausdorff formula

$$e^{-i(K+I)\Delta t} = e^{-iK\Delta t} e^{-iI\Delta t} + \mathcal{O}(\Delta t^2) \tag{3.6}$$

to split the time evolution into a multiplication with $e^{-iK\Delta t}$, which is diagonal in momentum space, and one with $e^{-iI\Delta t}$, which is diagonal in position space with an error of $\mathcal{O}(\Delta t^2)$. Then, for small enough Δt, we can do the time propagation of Ψ_j via

$$\Psi_j(t + \Delta t, x) = \mathcal{F}^{-1}\left(\left(e^{-iK\Delta t}\right)_{jl} \mathcal{F}\left(\left(e^{-iI\Delta t}\right)_{lk} \Psi_k(x, t)\right)\right) + \mathcal{O}(\Delta t^2). \tag{3.7}$$

where $\mathcal{F}$ denotes the Fourier transformation.

3.3. The truncated Wigner Approximation

Finally, to go beyond mean-field simulations, we use the semi-classical truncated Wigner approximation (TWA). In this approximation, one first samples noise from the Wigner distribution, a classical (but not generally positive) quasi-probability distribution corresponding to the initial quantum state. In the following, we want to assume a homogeneous system without external potential for which most particles are in a coherent state like the ground state of the system. Moreover, we allow for small occupations of thermalized Bogoliubov quasiparticle modes. The Wigner distribution of this system is then a product of uncorrelated Gaussians, and the truncated Wigner noise can be added to the GPE by drawing noise from a Gaussian distribution, which at $T = 0$ corresponds to occupying each momentum mode with half a Bogoliubov quasiparticle

$$\langle \hat{b}^\dagger_{\boldsymbol{k},m} \hat{b}_{\boldsymbol{k}',m'} \rangle = \frac{1}{2} \delta_{mm'} \delta_{\boldsymbol{k}\boldsymbol{k}'}. \tag{3.8}$$

on average over many realizations. For a detailed derivation of this, see [74].

This noise is then added on top of the mean field before carrying out a real-time GPE simulation. Averaging over many different runs, one then recovers quantum physics as long as the condensate fraction stays large enough [74].

The discussion about dynamical instabilities in Sec. 2.5 makes it clear why adding this noise is crucial in order to describe the dynamics of a quantum system out of equilibrium. In a quench from the polar to the easy-plane phase, the non-zero occupation of the $m_F = \pm 1$ modes can only develop with quantum fluctuations in the initial polar state present.

4. The 2PI action for the spin-1 Bose gas

Now that we have introduced numerical methods to study far-from-equilibrium physics, we want to start developing an effective field theory for the spin-1 Bose gas far from equilibrium. A natural formalism for the analytical study of far-from-equilibrium quantum field theories is the Schwinger-Keldysh formalism and the 2PI effective action [6, 15]. Thus, in this chapter, we will apply these methods to the spin-1 Bose gas after an explanation of these formalisms in Sec. 4.1.

With these methods, we will obtain quantum equations of motion for the field expectation value ψ in Sec. 4.3 as well as the full propagator in Sec. 4.4, all up to a self-consistent 1-loop approximation. However, we will find that these equations are difficult to interpret and do not allow for a reduction of the theory to only the phase degrees of freedom.

Note that for the background in Sec. 4.1, we will mainly follow [6, 15], [75], and [76]. For the calculation thereafter, we have adapted the derivation in [76] from the spin-1/2 to the spin-1 case. In this and the following chapters, we will use natural units such that $\hbar = 1 = c$.

4.1. Functional methods for nonequilibrium field theories

4.1.1. Notation

In this chapter, we will use a different notation for the complex N-component scalar field. We define

$$\phi_\alpha = \begin{pmatrix} \psi_1 \\ \psi_1^\dagger \\ \vdots \\ \psi_N \\ \psi_N^\dagger \end{pmatrix} \quad \text{and} \quad \phi_\alpha^\dagger = \begin{pmatrix} \psi_1^\dagger & \psi_1 & \dots & \psi_N^\dagger & \psi_N \end{pmatrix} \tag{4.1}$$

and write convolutions as

$$J^\dagger \cdot \phi \equiv \int d^d\boldsymbol{x} \int_{\mathcal{C}} dt J^\dagger_\alpha(\boldsymbol{x},t)\phi_\alpha(\boldsymbol{x},t) \tag{4.2}$$

$$\phi^\dagger \cdot R \cdot \phi \equiv \int\int d^d\boldsymbol{x} d^d\boldsymbol{y} \int\int_{\mathcal{C}} dt dt' \phi^\dagger_\alpha(\boldsymbol{x},t) R_{\alpha\beta}(\boldsymbol{x},t;\boldsymbol{y},t')\phi_\beta(\boldsymbol{y},t') \tag{4.3}$$

for $\mathcal{C}$ the Keldysh time contour defined in the next section [76].

In this notation, the equal-time commutation relations of the quantum fields

$$\left[\hat\Psi_i(\boldsymbol{x},t), \hat\Psi^\dagger_j(\boldsymbol{y},t)\right] = \delta_{ij}\delta(\boldsymbol{x}-\boldsymbol{y}) \tag{4.4}$$

and

$$\left[\hat\Psi_i(\boldsymbol{x},t), \hat\Psi_j(\boldsymbol{y},t)\right] = 0 = \left[\hat\Psi_i(\boldsymbol{x},t), \hat\Psi^\dagger_j(\boldsymbol{y},t)\right] \tag{4.5}$$

become

$$\left[\hat\phi_\alpha(\boldsymbol{x},t), \hat\phi^\dagger_\beta(\boldsymbol{y},t)\right] = V_{\alpha\beta}\delta(\boldsymbol{x}-\boldsymbol{y}) \tag{4.6}$$

with

$$V = \begin{pmatrix} 1 & 0 & 0 & 0 & 0 & 0 \\ 0 & -1 & 0 & 0 & 0 & 0 \\ 0 & 0 & 1 & 0 & 0 & 0 \\ 0 & 0 & 0 & -1 & 0 & 0 \\ 0 & 0 & 0 & 0 & 1 & 0 \\ 0 & 0 & 0 & 0 & 0 & -1 \end{pmatrix} \tag{4.7}$$

Note that we use this notation because it gives a natural way to not only study correlation functions like $\langle\hat\Psi_i\hat\Psi^\dagger_j\rangle$ but also anomalous correlators like $\langle\hat\Psi_i\hat\Psi_j\rangle$ and $\langle\hat\Psi^\dagger_i\hat\Psi^\dagger_j\rangle$, all in the notation of $\langle\hat\phi_\alpha\hat\phi^\dagger_\beta\rangle$ with the quantum operators $\hat\phi$ canonically quantizing the fields ϕ.

4.1.2. The generating functional

Consider now a quantum many-body system governed by some Hamiltonian $H(t)$, which at some time t_0 was in a state described by the density matrix $\rho(t_0) = \rho_0$. Its unitary time evolution is completely determined by the Hamiltonian via

$$\rho(t) = U_{t,t_0}\rho_0 U^\dagger_{t,t_0} = U_{t,t_0}\rho_0 U_{t_0,t} \tag{4.8}$$

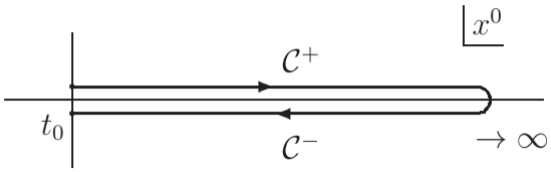

Figure 4.1.: Closed real-time Keldysh contour [6]. The shift of the curves away from the real axis is merely to illustrate the time contour better.

with

$$U_{t,t'} = \mathcal{T} \exp\left(-i \int_{t'}^{t} H(\tilde{t}) d\tilde{t}\right), \tag{4.9}$$

where $\mathcal{T}$ is the time-ordering operator [75]. Observables can then be calculated via

$$\langle \mathcal{O} \rangle(t) = \frac{\mathrm{Tr}\rho(t)O}{\mathrm{Tr}\rho(t)} = \frac{\mathrm{Tr}\rho_0 U_{t_0,t} O U_{t,t_0}}{\mathrm{Tr}\rho_0}, \tag{4.10}$$

where in the last step we have used that $U_{t_0,t}U_{t,t_0} = 1$ and the cyclicity of the trace. Because $\mathrm{Tr}\rho_0 = 1$ for any density matrix, we are left with

$$\langle \mathcal{O} \rangle(t) = \mathrm{Tr}\rho_0 U_{t_0,t} O U_{t,t_0} = \mathrm{Tr}\rho_0 O(t) \tag{4.11}$$

if we consider $O(t)$ in the Heisenberg picture.

Note that Eq. (4.11) involves a forward and backward evolution from t_0 to t in contrast to the case of real-time vacuum QFT, where we don't need the backward evolution because of the translation invariance of the vacuum. One can now insert $1 = U_{t,\infty}U_{\infty,t}$ into this expectation value in order to obtain $\langle \mathcal{O} \rangle(t) = \mathrm{Tr}\rho_0 U_{t_0,\infty} U_{\infty,t} O U_{t,t_0}$ to extend the closed time path $\mathcal{C}$, also known as the Keldysh contour [77], to $t = \infty$ in the future (see Fig. 4.1), with an operator insertion on the forward path $\mathcal{C}^+$. Similarly, you could insert the operator on the backward path or take the average of both.

Let us now specify our considerations for a complex N-component scalar quantum field theory. To know such a quantum field theory - in as well as out of equilibrium - means knowing all correlation functions. Thus, we can define the generating functional with respect to the sources J and R as

$$Z[J, R; \rho_0] = \mathrm{Tr}\rho_0 \mathcal{T}_\mathcal{C} e^{iJ^\dagger \cdot \phi + \frac{i}{2}\phi^\dagger \cdot R \cdot \phi}. \tag{4.12}$$

Here, $\mathcal{T}_\mathcal{C}$ denotes time ordering along the closed time contour, with times on C^+ considered earlier than times on C^-. Note that due to the closed time path, Z is already normalized to 1

in absence of any sources.

4.1.3. Non-equilibrium correlation functions

From the generating functional Eq. (4.28), we can derive non-equilibrium correlation functions by taking functional derivatives with respect to the sources J and R. For example, the one-point function is given by

$$\langle\hat{\phi}_\alpha(\boldsymbol{x},t)\rangle = \left.\frac{\delta Z[J,R]}{i\delta J^\dagger_\alpha(\boldsymbol{x},t)}\right|_{J,R=0} = \Phi_\alpha(\boldsymbol{x},t) \tag{4.13}$$

which together with the time-ordered two-point function

$$\langle\mathcal{T}_\mathcal{C}\hat{\phi}_\alpha(\boldsymbol{x},t)\hat{\phi}^\dagger_\beta(\boldsymbol{y},t')\rangle = \left.\frac{\delta^2 Z[J,R]}{i\delta J^\dagger_\alpha(\boldsymbol{x},t)i\delta J_\beta(\boldsymbol{y},t')}\right|_{J,R=0}. \tag{4.14}$$

forms the propagator or connected two-point function

$$G_{\alpha\beta}(\boldsymbol{x},t;\boldsymbol{y},t') = \langle\mathcal{T}_\mathcal{C}\hat{\phi}_\alpha(\boldsymbol{x},t)\hat{\phi}^\dagger_\beta(\boldsymbol{y},t')\rangle - \Phi_\alpha(\boldsymbol{x},t)\Phi^\dagger_\beta(\boldsymbol{y},t'). \tag{4.15}$$

Defining the commutator and the anticommutator

$$\rho_{\alpha\beta}(\boldsymbol{x},t;\boldsymbol{y},t') = i\langle\left[\hat{\phi}_\alpha(\boldsymbol{x},t),\hat{\phi}^\dagger_\beta(\boldsymbol{y},t')\right]\rangle \tag{4.16a}$$

$$F_{\alpha\beta}(\boldsymbol{x},t;\boldsymbol{y},t') = \frac{1}{2}\langle\left\{\hat{\phi}_\alpha(\boldsymbol{x},t),\hat{\phi}^\dagger_\beta(\boldsymbol{y},t')\right\}\rangle - \Phi_\alpha(\boldsymbol{x},t)\Phi^\dagger_\beta(\boldsymbol{y},t'), \tag{4.16b}$$

we can decompose the propagator

$$G_{\alpha\beta}(\boldsymbol{x},t;\boldsymbol{y},t') = F_{\alpha\beta}(\boldsymbol{x},t;\boldsymbol{y},t') - \frac{i}{2}\rho_{\alpha\beta}(\boldsymbol{x},t;\boldsymbol{y},t')\mathrm{sgn}_\mathcal{C}(t-t'). \tag{4.17}$$

where we call ρ the spectral and F the statistical component of the propagator. As it involves the commutator, the spectral function contains the terms that are not analytic at $t-t'=0$, while the statistical part is analytic everywhere. We can interpret ρ as giving information about the available states of the theory, while F tells us about their occupation [6].

Note that in thermal equilibrium, the spectral and statistical functions are related through the fluctuation-dissipation relation [6]. Out of equilibrium, this is generally not the case and ρ and F are independent degrees of freedom. We only use two independent functions F and ρ to describe non-equilibrium propagators, despite the fields ϕ^+ and ϕ^- being separate degrees of

freedom suggesting we have four independent propagators

$$iG^{+-}(\boldsymbol{x},t;\boldsymbol{y},t') = \langle\hat{\phi}^{+}(\boldsymbol{x},t)\hat{\phi}^{\dagger-}(\boldsymbol{y},t')\rangle \tag{4.18}$$

$$iG^{-+}(\boldsymbol{x},t;\boldsymbol{y},t') = \langle\hat{\phi}^{-}(\boldsymbol{x},t)\hat{\phi}^{\dagger+}(\boldsymbol{y},t')\rangle \tag{4.19}$$

$$iG^{++}(\boldsymbol{x},t;\boldsymbol{y},t') = \langle\hat{\phi}^{+}(\boldsymbol{x},t)\hat{\phi}^{\dagger+}(\boldsymbol{y},t')\rangle$$

$$iG^{--}(\boldsymbol{x},t;\boldsymbol{y},t') = \langle\hat{\phi}^{-}(\boldsymbol{x},t)\hat{\phi}^{\dagger-}(\boldsymbol{y},t')\rangle. \tag{4.20}$$

This is due to the fact that at $R = J = 0$, these are related via the two relations [6]

$$G^{+-}(\boldsymbol{x},t;\boldsymbol{y},t') = G^{-+}(\boldsymbol{y},t';\boldsymbol{x},t) \tag{4.21}$$

and

$$G^{++}(\boldsymbol{x},t;\boldsymbol{y},t') + G^{--}(\boldsymbol{x},t;\boldsymbol{y},t') = G^{+-}(\boldsymbol{x},t;\boldsymbol{y},t') + G^{-+}(\boldsymbol{x},t;\boldsymbol{y},t'). \tag{4.22}$$

4.1.4. The functional integral formalism

We can now write the generating functional in terms of a path integral by inserting coherent states for ϕ at each $(\boldsymbol{x},t)$ on the contour, taking space and time as continuum limits of discrete lattices. For details on this construction, see any of the following [6, 15, 75], also for subtleties about convergence and well-definedness. This construction then yields

$$Z[J,R;\rho_0] = \underbrace{\int[d\phi_0^+]\int[d\phi_0^-]\,\langle\phi_0^+|\,\rho_0\,|\phi_0^-\rangle}_{\text{initial conditions}}\underbrace{\int_{\phi^+(t_0)=\phi_0^+}^{\phi^-(t_0)=\phi_0^-}\mathcal{D}'\phi e^{iS[\phi]+iJ^\dagger\cdot\phi+\frac{i}{2}\phi^\dagger\cdot R\cdot\phi}}_{\text{quantum d}^{\text{d}}\text{ynamics}} \tag{4.23}$$

where ϕ are "classical" fields and $S[\phi]$ is the classical action determined by a Legendre transform and time integration of the classical Hamiltonian. Moreover, the functional integral measure is given by

$$\int_{\phi^+(t_0)=\phi_0^+}^{\phi^-(t_0)=\phi_0^-}\mathcal{D}'\phi = \lim_{N\to\infty}\int\prod_{i=1}^{N-1}\prod_{\boldsymbol{x},\alpha}d\phi_\alpha(\boldsymbol{x},t_i)(2\pi i\Delta t)^{-\frac{1}{2}} \tag{4.24}$$

with $t_{\mathcal{C}} = N\Delta t$ discretizing the time along the Keldysh contour and the initial field configurations fixed to $\phi(t_0,x) = \phi^+(t_0,x) = \phi_0^+(x)$ as well as $\phi(t_N,x) = \phi^-(t_0,x) = \phi_0^-(x)$. In the initial conditions part of the functional integral, these constraints are also integrated over via

$$\int[d\phi_0^\pm] \equiv \int\prod_{\boldsymbol{x},\alpha}d\phi_0^{\alpha\pm}(x). \tag{4.25}$$

Gaussian initial conditions

If ρ_0 is a Gaussian density matrix, which we can assume in many physical cases, the matrix element $\langle \phi_0^+ | \, \rho_0 \, | \phi_0^- \rangle$ can be parametrized via

$$\langle \phi_0^+ | \, \rho_0^{\text{gaussian}} \, | \phi_0^- \rangle = \mathcal{N} \exp i \left(\alpha_0 + \alpha_1^\dagger \cdot \phi + \frac{1}{2} \phi^\dagger \cdot \alpha_2 \cdot \phi \right), \tag{4.26}$$

where $\alpha_1(\boldsymbol{x}, t), \alpha_2(\boldsymbol{x}, t; \boldsymbol{y}, t')$ vanish for $t \neq t_0$ as the initial density matrix is only specified at t_0 [6]. Because this is only quadratic in the fields, we can absorb α_1 and α_2 in the source terms. Redefining

$$J + \alpha_1 \to J; \quad R + \alpha_2 \to R \tag{4.27}$$

and including the integrals over $\phi_0^\pm$ as well as any irrelevant normalizations in the integral measure $\int \mathcal{D}\phi$, we get

$$Z[J, R; \rho_0^{\text{gaussian}}] \to Z[J, R] = \int \mathcal{D}\phi e^{iS[\phi] + iJ^\dagger \cdot \phi + \frac{i}{2} \phi^\dagger \cdot R \cdot \phi}, \tag{4.28}$$

where now the initial conditions are encoded in the sources at $t = t_0$ and the integral measure is given by

$$\int \mathcal{D}\phi = \mathcal{N} \lim_{N \to \infty} \int \prod_{i=0}^{N} \prod_{\boldsymbol{x}, \alpha} d\phi_\alpha(\boldsymbol{x}, t_i) (2\pi i \Delta t)^{-\frac{1}{2}}. \tag{4.29}$$

In this notation, it looks like the contours $\mathcal{C}^\pm$ decouple. However, we have to keep in mind that $\phi_0^\pm$ are still coupled through the initial conditions, and the kinetic part of $S[\phi]$ introduces further coupling between ϕ^+ and ϕ^- at $t \to \infty$.

Gaussian density matrices are completely sufficient for our purposes. For example, a box in momentum space, which is encountered for $S(k, t)$ shortly after a quench from the polar to the easy-plane phase [38] and which drives the transport processes leading to the scaling is given by the Gaussian density matrix

$$\rho_0 = \prod_k \frac{1}{2\pi} \int_{-\pi}^{\pi} d\theta \, | \sqrt{f_0} \Theta(k_{\xi_S} - k) e^{i\theta} \rangle \, \langle \sqrt{f_0} \Theta(k_{\xi_S} - k) e^{i\theta} | \tag{4.30}$$

with Θ the Heaviside step function, f_0 the constant value for $S(k, t)$ and $|\sqrt{f_0} \Theta(k_{\xi_S} - k) e^{i\theta}\rangle$ the coherent state with eigenvalue $\sqrt{f_0} e^{i\theta}$ for $k \leq k_{\xi_S}$ and the vacuum for $k > k_{\xi_S}$[78].

4.1.5. The 2PI action formalism

In the following, we want to derive an effective action for the complex scalar N-component field. Such an effective action is useful since effective actions provide a way to obtain a closed set of evolution equations for correlation functions once an order of approximation is specified at the level of the effective action [6]. This method then, for example, avoids the appearance of secular terms, i.e. terms growing polynomially in time, which even for weakly coupled theories can occur in regular perturbation theory [6]. Moreover, the effective action is formulated in terms of the correlation functions instead of the sources, for which the initial conditions are harder to access in an experimental setup.

From vacuum field theory, we are used to dealing with the 1PI effective action, which is obtained as a Legendre transform of the generating function with respect to the linear source J. In general, for an arbitrary number of sources, this can be generalized to the nPI effective action by carrying out n Legendre transforms. In the case of non-equilibrium field theories with Gaussian initial conditions, the only relevant sources are J and R, such that we only need $n = 2$ to obtain the useful 2PI effective action [6].

To obtain the 2PI effective action, we proceed step by step as detailed in [6] and first define the generating functional for connected diagrams $W[J, R]$ via

$$W[J, R] = -i \log Z[J, R], \tag{4.31}$$

as well as the expectation values of the field $\Phi_{J,R}$ and the propagator $G_{J,R}$ in terms of the sources J, R analogously to Eqs. (4.13) and (4.15) as

$$\Phi_{\alpha;J,R}(\boldsymbol{x}, t) \equiv \frac{\delta W[J, R]}{\delta J^{\dagger}_{\alpha}(\boldsymbol{x}, t)} \tag{4.32a}$$

$$\frac{1}{2}\left(\Phi_{\beta,J,R}(\boldsymbol{y}, t')\Phi^{\dagger}_{\alpha;J,R}(\boldsymbol{x}, t) + G_{\beta\alpha;J,R}(\boldsymbol{y}, t'; \boldsymbol{x}, t)\right) \equiv \frac{\delta W[J, R]}{\delta R_{\alpha\beta}(\boldsymbol{x}, t; \boldsymbol{y}, t')} \tag{4.32b}$$

The 1PI effective action can now be derived from W by a Legendre transform with respect to J. Assuming that $J_{\phi,R}$ is invertible with inverse $\Phi_{J,R}$, we get

$$\Gamma^{R}[\Phi] = W[J_{\phi,R}, R] - J^{\dagger}_{\Phi,R} \cdot \Phi \tag{4.33}$$

which governs the evolution equations

$$\frac{\delta\Gamma^R[\Phi]}{\delta\Phi_\alpha(\boldsymbol{x},t)} = -J^\dagger_{\alpha,\Phi,R}(\boldsymbol{x},t) \tag{4.34a}$$

$$\frac{\delta\Gamma^R[\Phi]}{\delta R_{\alpha\beta}(\boldsymbol{x},t;\boldsymbol{y},t')} = \frac{\delta W[J,R]}{\delta R_{\alpha\beta}(\boldsymbol{x},t;\boldsymbol{y},t')}. \tag{4.34b}$$

Note that for $R = 0$, this 1PI effective action is well-known from vacuum field theory. In particular, we know that to 1-loop order, $\Gamma^{R=0}$ is given by (see Appendix B.1 for a derivation)

$$\Gamma^{R=0,1-\text{loop}} = S[\Phi] + \frac{i}{2}\text{Tr}\log\left[G_0^{-1}\right] \tag{4.35}$$

where

$$\left(G_0^{-1}\right)_{\alpha\beta}(\boldsymbol{x},t;\boldsymbol{y},t') = -i\frac{\delta S}{\delta\Phi^\dagger_\alpha(\boldsymbol{x},t)\Phi_\beta(\boldsymbol{y},t')}. \tag{4.36}$$

We can easily transfer this to $R \neq 0$ by defining

$$S^R[\Phi] = S[\Phi] + \frac{1}{2}\phi^\dagger \cdot R \cdot \phi \tag{4.37}$$

such that

$$\Gamma^{R,1-\text{loop}} = S^R[\Phi] + \frac{i}{2}\text{Tr}\log\left[G_0^{R\,-1}\right] \tag{4.38}$$

with

$$\left(G_0^{R\,-1}\right)_{\alpha\beta} = -i\frac{\delta S^R}{\delta\Phi^\dagger_\alpha\Phi_\beta} = \left(G_0^{-1}\right)_{\alpha\beta} - iR_{\alpha\beta} \tag{4.39}$$

such that

$$\Gamma^{R,1-\text{loop}} = S^R[\Phi] + \frac{i}{2}\text{Tr}\log\left[G_0^{-1} - iR\right]. \tag{4.40}$$

A further Legendre transform with regard to R, assuming invertible $R_{\Phi,G}$ with inverse $G_{\Phi,R}$

then gives us the 2PI effective action:

$$\Gamma[\Phi, G] = \Gamma^R[\Phi] - \int_{x,y,\mathcal{C}} \frac{\delta\Gamma^R[\Phi]}{\delta R_{\alpha\beta}(\boldsymbol{x}, t; \boldsymbol{y}, t')} R_{\alpha\beta}(\boldsymbol{x}, t; \boldsymbol{y}, t') \tag{4.41}$$

$$= \Gamma^R[\Phi] - \int_{x,y,\mathcal{C}} \frac{1}{2} \left(\Phi_\beta(\boldsymbol{y}, t')\Phi^\dagger_\alpha(\boldsymbol{x}, t) + G_{\beta\alpha}(\boldsymbol{y}, t'; \boldsymbol{x}, t) \right) R_{\alpha\beta}(\boldsymbol{x}, t; \boldsymbol{y}, t') \tag{4.42}$$

$$= W[J, R] - J^\dagger \cdot \Phi - \int_{x,y,\mathcal{C}} \frac{1}{2} \left(\Phi_\beta(\boldsymbol{y}, t')\Phi^\dagger_\alpha(\boldsymbol{x}, t) + G_{\beta\alpha}(\boldsymbol{y}, t'; \boldsymbol{x}, t) \right) R_{\alpha\beta}(\boldsymbol{x}, t; \boldsymbol{y}, t') \tag{4.43}$$

where we have used Eqs. (4.34b) and (4.32b) in the second and Eq. (4.33) in the last step and we have dropped explicitly writing the dependence of the sources on the fields. From this, we get the equations of motion

$$\frac{\delta\Gamma[\Phi]}{\delta\Phi_\alpha(\boldsymbol{x}, t)} = -J^\dagger_\alpha(\boldsymbol{x}, t) - \int_{y,\mathcal{C}} \Phi^\dagger_\beta(\boldsymbol{y}, t') R_{\beta\alpha}(\boldsymbol{y}, t'; \boldsymbol{x}, t) \tag{4.44a}$$

$$\frac{\delta\Gamma[\Phi]}{\delta G_{\alpha\beta}(\boldsymbol{x}, t; \boldsymbol{y}, t')} = -\frac{1}{2} R_{\beta\alpha}(\boldsymbol{y}, t'; \boldsymbol{x}, t). \tag{4.44b}$$

The 2PI effective action is now a function of the full 1- and 2-point function, such that the equations of motion Eqs (4.44a) and (4.44b) give the full quantum mechanical equations of motion for Φ and G.

For the 2PI action, we can use our 1PI 1-loop result to determine

$$\Gamma^{1-\text{loop}}[\Phi, G] = \Gamma^{R,1-\text{loop}} - \int_{x,y,\mathcal{C}} \frac{1}{2} \left(\Phi_\beta(\boldsymbol{y}, t')\Phi^\dagger_\alpha(\boldsymbol{x}, t) + G_{\beta\alpha}(\boldsymbol{y}, t'; \boldsymbol{x}, t) \right) R_{\alpha\beta}(\boldsymbol{x}, t; \boldsymbol{y}, t')$$

$$= S[\Phi] + \frac{i}{2}\text{Tr}\log\left[G_0^{-1} - iR\right] - \frac{1}{2}\text{Tr}G \cdot R \tag{4.45}$$

where in the last step we have put Eq. (4.38) into the first line. This yields a consistent result with Eq. (4.44b) if we set

$$G^{-1} = G_0^{-1} - iR \tag{4.46}$$

to 1-loop order such that

$$\Gamma^{1-\text{loop}}[\Phi, G] = S[\Phi] + \frac{i}{2}\text{Tr}\log G^{-1} + \frac{i}{2}\text{Tr}G_0^{-1} \cdot G. \tag{4.47}$$

Adding a term $\Gamma_2[\Phi, G]$ including all higher orders, we finally get

$$\Gamma[\Phi, G] = S[\Phi] + \frac{i}{2}\text{Tr}\log G^{-1} + \frac{i}{2}\text{Tr}G_0^{-1} \cdot G + \Gamma_2[\Phi, G] \tag{4.48}$$

where we have now separated out the 1-loop part. For an interpretation of $\Gamma_2[\Phi, G]$, we look at the equation of motion Eq. (4.44b) and find

$$G^{-1} = G_0^{-1} - iR - \Sigma[\Phi, G] \tag{4.49}$$

where

$$\Sigma[\Phi, G] \equiv 2i\frac{\delta\Gamma_2[\Phi, G]}{\delta G}. \tag{4.50}$$

Eq. (4.49) tells us that Σ is the proper self-energy, with which $G - G_0$ can be written as a geometric sum, which in matrix notation reads (for simplicity at $R = 0$)

$$G - G_0 = G \cdot \Sigma[\Phi, G] \cdot G - G \cdot \Sigma[\Phi, G] \cdot G \cdot \Sigma[\Phi, G] \cdot G + \dots \tag{4.51}$$

with 1-particle irreducible $\Sigma[\Phi, G]$, meaning that by cutting a single propagator line in $\Sigma[\Phi, G]$ the diagram cannot be disintegrated. This implies now that $\Gamma_2[\Phi, G]$, from which Σ is obtained by a derivative with respect to the propagator, has to be 2-particle irreducible, i.e. the diagrams contributing to $\Gamma_2[\Phi, G]$ cannot be reduced to two individual diagrams by cutting two propagator lines.

Thus, to determine Γ_2, we have to consider all closed diagrams which have at least two loops and are two-particle irreducible. The latter condition considerably restricts the number of diagrams that have to be considered. Moreover, note that instead of the bare propagator entering diagrams or expansions, in the 2PI formalism, we expand in terms of the full propagator, thus leading to a self-consistent treatment of the propagator, which is the key to avoiding secular terms.

Having thoroughly discussed the equation of motion Eq. (4.44b), we want to close this subsection by giving an explicit expression for Eq. (4.44a). Using the form of the effective action in Eq. (4.48), we find

$$\frac{\delta\Gamma_2[\Phi, G]}{\delta\Phi} = -\frac{\delta S[\Phi]}{\delta\Phi} - \frac{i}{2}\frac{\delta \mathrm{Tr} G_0^{-1}(\Phi) G}{\delta\Phi} - J^\dagger - \Phi^\dagger \cdot R \tag{4.52}$$

4.1.6. Propagator evoluation equations

Eq. (4.49) gives us an integral equation for the propagator, which in the following we want to turn into partial differential equations for the spectral and the statistical part of G, which can then be solved together with the initial conditions at $t = t_0$. For these derivations, we will

mainly follow [76]. Rewriting Eq. (4.49), we find

$$\int_{y,\mathcal{C}} \left[\left(G_0^{-1}\right)_{\alpha\beta}(\boldsymbol{x},t;\boldsymbol{y},t') - iR_{\alpha\beta}(\boldsymbol{x},t;\boldsymbol{y},t') - \Sigma_{\alpha\beta}(\boldsymbol{x},t;\boldsymbol{y},t') \right] G_{\beta\gamma}(\boldsymbol{y},t';\boldsymbol{z},t'') = \delta_{\alpha\gamma}\delta(t-t'')\delta(\boldsymbol{x}-\boldsymbol{z}). \tag{4.53}$$

We can now split the propagator according to Eq. (4.17) Moreover, because J and R are only non-vanishing at $t = t_0$, they have vanishing support in the integral and can be neglected in the following. Furthermore, we can split G_0^{-1} into the part involving time derivatives and the "mass" (including the spatial derivatives) according to

$$\left(G_0^{-1}\right)_{\alpha\beta}(\boldsymbol{x},t;\boldsymbol{y},t') = \delta(t-t')\delta(\boldsymbol{x}-\boldsymbol{y})\left[V_{\alpha\beta}\partial_t + iM_{\alpha\beta}(\boldsymbol{x},t)\right]. \tag{4.54}$$

Thus, Eq (4.53) becomes

$$\int_{y,\mathcal{C}} \left[\delta(t-t')\delta(\boldsymbol{x}-\boldsymbol{y})\left[V_{\alpha\beta}\partial_t + iM_{\alpha\beta}(\boldsymbol{x},t)\right] - \Sigma_{\alpha\beta}(\boldsymbol{x},t;\boldsymbol{y},t')\right] \cdot \left[F_{\beta\gamma}(\boldsymbol{y},t';\boldsymbol{z},t'') - \frac{i}{2}\rho_{\beta\gamma}(\boldsymbol{y},t';\boldsymbol{z},t'')\mathrm{sgn}_{\mathcal{C}}(t'-t'')\right] = \delta_{\alpha\gamma}\delta(t-t'')\delta(\boldsymbol{x}-\boldsymbol{z}). \tag{4.55}$$

Applying the time derivative and using the product rule along with

$$\partial_{t'}\mathrm{sgn}_{\mathcal{C}}(t'-t'') = \delta(t'-t'') \tag{4.56}$$

and the equal-time commutation

$$\rho_{\beta\gamma}(t',y;t',z) = i\delta(\boldsymbol{y}-\boldsymbol{z})V_{\beta\gamma}, \tag{4.57}$$

we find

$$\begin{aligned} 0 = &\int_{y,\mathcal{C}} \left[\delta(t-t')\delta(\boldsymbol{x}-\boldsymbol{y})\left[V_{\alpha\beta}\partial_t + iM_{\alpha\beta}(\boldsymbol{x},t)\right] - \Sigma_{\alpha\beta}(\boldsymbol{x},t;\boldsymbol{y},t')\right] F_{\beta\gamma}(\boldsymbol{y},t';\boldsymbol{z},t'') \\ &- \frac{i}{2}\mathrm{sgn}_{\mathcal{C}}(t'-t'')\left[\left(\delta(t-t')\delta(\boldsymbol{x}-\boldsymbol{y})\left[V_{\alpha\beta}\partial_t + iM_{\alpha\beta}(\boldsymbol{x},t)\right] - \Sigma_{\alpha\beta}(\boldsymbol{x},t;\boldsymbol{y},t')\right]\rho_{\beta\gamma}(\boldsymbol{y},t';\boldsymbol{z},t'')\right. \end{aligned} \tag{4.58}$$

as the derivative term involving $\mathrm{sgn}_{\mathcal{C}}$ cancels the right hand side. For further simplification, we can now also decompose Σ into a local Σ^0 and a non-local part $\bar{\Sigma}$

$$\Sigma_{\alpha\beta}(\boldsymbol{x},t;\boldsymbol{y},t') = -i\delta(\boldsymbol{x}-\boldsymbol{y})\delta(t-t')\Sigma^0(\boldsymbol{x},t) + \bar{\Sigma}(\boldsymbol{x},t;\boldsymbol{y},t') \tag{4.59}$$

and further split $\bar{\Sigma}$ similarly to the propagator

$$\Sigma_{\alpha\beta}(\boldsymbol{x},t;\boldsymbol{y},t') = \Sigma^F_{\alpha\beta}(\boldsymbol{x},t;\boldsymbol{y},t') - \frac{i}{2}\mathrm{sgn}_{\mathcal{C}}(t-t')\Sigma^\rho_{\alpha\beta}. \tag{4.60}$$

Moreover, we find that integrating functions regular in time over a closed time contour with insertions of $\mathrm{sgn}_{\mathcal{C}}$ simplifies the expressions to

$$\int_{\mathcal{C}} dt f(t) dt = 0 \tag{4.61}$$

$$\int_{\mathcal{C}} dt f(t) \mathrm{sgn}_{\mathcal{C}}(t - t_1) dt = -2 \int_0^{t_1} f(t) dt \tag{4.62}$$

$$\int_{\mathcal{C}} dt f(t) \mathrm{sgn}_{\mathcal{C}}(t - t_1) \mathrm{sgn}_{\mathcal{C}}(t - t_2) dt = -2 \mathrm{sgn}_{\mathcal{C}}(t_1 - t_2) \int_{t_1}^{t_2} f(t) dt \tag{4.63}$$

Using all this as well as carrying out the delta-functions in Eq. (4.59), we get

$$\begin{aligned} 0 = &\left[V_{\alpha\beta}\partial_t + iM_{\alpha\beta}(\boldsymbol{x}, t) + i\Sigma^0_{\alpha\beta}(\boldsymbol{x}, t)\right] F_{\beta\gamma}(\boldsymbol{x}, t; \boldsymbol{z}, t'') \\ &+ i \int_{t_0}^{t} dt' \int d^d\boldsymbol{y} \Sigma^{\rho}_{\alpha\beta}(\boldsymbol{x}, t; \boldsymbol{y}, t') F_{\beta\gamma}(\boldsymbol{y}, t'; \boldsymbol{z}, t'') \\ &- \frac{i}{2} \mathrm{sgn}_{\mathcal{C}}(t - t'') \left[V_{\alpha\beta}\partial_t + iM_{\alpha\beta}(\boldsymbol{x}, t) + i\Sigma^0_{\alpha\beta}(\boldsymbol{x}, t)\right] \rho_{\beta\gamma}(\boldsymbol{x}, t; \boldsymbol{z}, t'') \\ &- i \int_{t_0}^{t''} dt' \int d^d\boldsymbol{y} \Sigma^{F}_{\alpha\beta}(\boldsymbol{x}, t; \boldsymbol{y}, t') \rho_{\beta\gamma}(\boldsymbol{y}, t'; \boldsymbol{z}, t'') \\ &- \frac{1}{2} \mathrm{sgn}_{\mathcal{C}}(t - t'') \int_{t}^{t''} dt' \int d^d\boldsymbol{y} \Sigma^{\rho}_{\alpha\beta}(\boldsymbol{x}, t; \boldsymbol{y}, t') \rho_{\beta\gamma}(\boldsymbol{y}, t'; \boldsymbol{z}, t''). \end{aligned} \tag{4.64}$$

Finally, we can also decompose this equation into the parts multiplying $\mathrm{sgn}_{\mathcal{C}}(t - t'')$ and those that don't, yielding the coupled equations

$$iV_{\alpha\beta}\partial_t F_{\beta\gamma}(\boldsymbol{y}, t'; \boldsymbol{z}, t'') = \left[M_{\alpha\beta}(\boldsymbol{x}, t) + \Sigma^0_{\alpha\beta}(\boldsymbol{x}, t)\right] F_{\beta\gamma}(\boldsymbol{x}, t; \boldsymbol{z}, t'') \tag{4.65}$$

$$+ \int_{t_0}^{t} dt' \int' \Sigma^{\rho}_{\alpha\beta}(\boldsymbol{x}, t; \boldsymbol{y}, t') F_{\beta\gamma}(\boldsymbol{y}, t'; \boldsymbol{z}, t'') \tag{4.66}$$

$$- \int_{t_0}^{t''} dt' \int' \Sigma^{F}_{\alpha\beta}(\boldsymbol{x}, t; \boldsymbol{y}, t') \rho_{\beta\gamma}(\boldsymbol{y}, t'; \boldsymbol{z}, t'') \tag{4.67}$$

and

$$iV_{\alpha\beta}\partial_t \rho_{\beta\gamma}(\boldsymbol{y}, t'; \boldsymbol{z}, t'') = \left[M_{\alpha\beta}(\boldsymbol{x}, t) + \Sigma^0_{\alpha\beta}(\boldsymbol{x}, t)\right] \rho_{\beta\gamma}(\boldsymbol{x}, t; \boldsymbol{z}, t'') \tag{4.68}$$

$$+ \int_{t}^{t''} dt' \int' \Sigma^{\rho}_{\alpha\beta}(\boldsymbol{x}, t; \boldsymbol{y}, t') \rho_{\beta\gamma}(\boldsymbol{y}, t'; \boldsymbol{z}, t''). \tag{4.69}$$

Note that now there are no integrals over the time contour left, and we have transformed Eq. (4.49) to an ordinary set of coupled partial differential equations only involving "normal" integrals. These integrals remain due to the fact that even though we start with a Gaussian matrix at t_0, out-of-equilibrium non-Gaussianities will develop such that these equations do not hold for a different starting time. Thus, the integrals preserve the "memory" of the system

at earlier times.

4.1.7. The $1/N$ expansion

So far, all formulas have been exact to all orders. However, to actually be able to calculate anything with this formalism, we have to make approximations by only including certain diagrams in the 2PI effective action Γ_2. One could simply do a loop expansion - however, such an expansion is not valid in the vicinity of phase transitions with high fluctuations [6].

Another possible way of approximating Γ_2 without this shortcoming is the $1/N$ expansion [15, 79, 80], which is valid for sufficiently symmetric symmetric N-component models with N large enough. For this approximation, instead of expanding in powers of a weak coupling, we expand in orders of $1/N$, such that

$$\Gamma_2[\Phi, G] = \underset{\propto N^1}{\Gamma_2^{\text{LO}}}[\Phi, G] + \underset{\propto N^0}{\Gamma_2^{\text{NLO}}}[\Phi, G] + \underset{\propto N^{-1}}{\Gamma_2^{\text{NNLO}}}[\Phi, G] + \dots \tag{4.70}$$

This formalism is mainly useful for $O(N)$ invariant theories, for which we know that $O(N)$ irreducible invariants like TrG or $\phi^\dagger\phi$ all scale $\propto N$. Moreover, to obtain β-functions for c_0 and c_1 that are independent of N, each bare coupling has to scale with $1/N$ such that every vertex carries a factor of $1/N$. Thus, the order in $1/N$ for a given diagram in Γ_2 is given by

$$\mathcal{O}(1/N) = \frac{\text{\#vertices}}{\text{\#irreducible invariants}} \tag{4.71}$$

in an $O(N)$ invariant theory [6].

4.2. The 2PI action for the spin-1 Bose gas

We can now apply the 2PI action formalism to the spin-1 Bose gas. For that, we first need to convert the action Eq. (2.14) to the notation in Sec. 4.1.1. This yields

$$\begin{aligned} S = \int_{x,\mathcal{C}} & \frac{i}{2}\phi_\alpha^\dagger (V)_{\alpha\beta}\partial_t\phi_\beta - \frac{1}{4m}\nabla\phi_\alpha^\dagger\nabla\phi_\alpha - \frac{q}{2}\phi_\alpha^\dagger(\tilde{f}_z^2)_{\alpha\beta}\phi_\beta \\ & - \frac{c_0}{8}(\phi_\alpha^\dagger\phi_\alpha)^2 - \frac{c_1}{8}(\phi_\alpha^\dagger(\tilde{f}_a)_{\alpha\beta}\phi_\beta)(\phi_\gamma^\dagger(\tilde{f}_a)_{\gamma\delta}\phi_\delta) \end{aligned} \tag{4.72}$$

where

$$\tilde{f}_x = \frac{1}{\sqrt{2}} \begin{pmatrix} 0 & 0 & 1 & 0 & 0 & 0 \\ 0 & 0 & 0 & 1 & 0 & 0 \\ 1 & 0 & 0 & 0 & 1 & 0 \\ 0 & 1 & 0 & 0 & 0 & 1 \\ 0 & 0 & 1 & 0 & 0 & 0 \\ 0 & 0 & 0 & 1 & 0 & 0 \end{pmatrix}; \; \tilde{f}_y = \frac{1}{\sqrt{2}} \begin{pmatrix} 0 & 0 & -i & 0 & 0 & 0 \\ 0 & 0 & 0 & -i & 0 & 0 \\ i & 0 & 0 & 0 & -i & 0 \\ 0 & i & 0 & 0 & 0 & -i \\ 0 & 0 & i & 0 & 0 & 0 \\ 0 & 0 & 0 & i & 0 & 0 \end{pmatrix}; \tag{4.73}$$

$$\tilde{f}_z = \begin{pmatrix} 1 & 0 & 0 & 0 & 0 & 0 \\ 0 & 1 & 0 & 0 & 0 & 0 \\ 0 & 0 & 0 & 0 & 0 & 0 \\ 0 & 0 & 0 & 0 & 0 & 0 \\ 0 & 0 & 0 & 0 & -1 & 0 \\ 0 & 0 & 0 & 0 & 0 & -1 \end{pmatrix} \tag{4.74}$$

are 6×6 matrices and we have adjusted the prefactors of all terms to keep the equations of motion unchanged compared to the formulation in Eq. (2.14).

From this, we can now compute the effective action Γ in Eq. (4.48) as well as the equations of motion Eq. (4.44). In the following, we want to do this to leading order in $1/N$. For $q = 0$, the $1/N$ expansion is valid as we then have a $SO(3)$-symmetric theory, and though $N = 3$ is not particularly large, the $1/N$ expansion has been show to lead to reasonable results even for moderate N [81]. According to [82], a large N expansion may be interpreted as an approximation on the quasiparticle level, mainly taking into account the Goldstone modes in a given theory. As such, we will, therefore, also employ the $1/N$ expansion for our parameters in the easy-plane phase with non-zero q.

Let us first look at the 1-loop terms. While $\mathrm{Tr} \log G^{-1}$, is purely of leading order in $1/N$, this is not so simple for $\mathrm{Tr}(G_0^{-1} G)$. The inverse free propagator for the spin-1 action amounts to

$$\begin{aligned} (G_0^{-1})_{\alpha\beta}(x,t,y,t') = \delta(\boldsymbol{x}-\boldsymbol{y})\delta(t-t') \Big[(V)_{\alpha\beta}\partial_t - \frac{i}{2m}\partial_x^2 \delta_{\alpha\beta} + iq(\tilde{f}_z)_{\alpha\beta} \\ + \frac{ic_0}{4}\left(\delta_{\alpha\beta}\Phi_\gamma^\dagger\Phi_\gamma + 2\Phi_\beta^\dagger\Phi_\alpha\right) + \frac{ic_1}{4}\left((\tilde{f}_a)_{\alpha\beta}\Phi_\gamma^\dagger(\tilde{f}_a)_{\gamma\delta}\Phi_\delta + 2(\tilde{f}_a)_{\alpha\gamma}\Phi_\gamma\Phi_\delta^\dagger(\tilde{f}_a)_{\delta\beta}\right)\Big] \end{aligned} \tag{4.75}$$

where we have used that

$$(\tilde{f}_a)_{\alpha\gamma}\Phi_\gamma = \Phi_\gamma^\dagger(\tilde{f}_a)_{\gamma\alpha}. \tag{4.76}$$

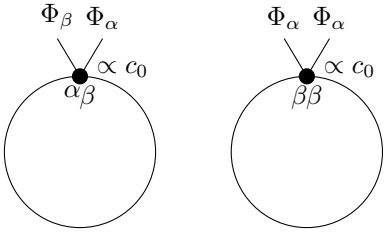

Figure 4.2.: Index structure of the 1-loop contributions to the effective action with density-density interaction vertices $\propto c_0$. The lines correspond to the full propagator G and the full quantum fields Φ are denoted as such.

Thus, $\mathrm{Tr}(G_0^{-1}G)$ yields

$$\begin{aligned}
&\mathrm{Tr}(G_0^{-1}[\Phi]G) \qquad (4.77)\\
&= \int_{x,y,\mathcal{C}} \delta(\boldsymbol{x}-\boldsymbol{y})\delta(t-t')\left[(V)_{\alpha\beta}\partial_t - \frac{i}{2m}\partial_x^2\delta_{\alpha\beta}\right] G_{\beta\alpha}(\boldsymbol{x},t;\boldsymbol{y},t') + \int_{x,\mathcal{C}} iq\mathrm{Tr}F(\boldsymbol{x},t;\boldsymbol{x},t)\\
&\quad + \int_{x,\mathcal{C}} \frac{ic_0}{4}\left(\mathrm{Tr}(F(\boldsymbol{x},t;\boldsymbol{x},t))\Phi^\dagger_\alpha(\boldsymbol{x},t)\Phi_\alpha(\boldsymbol{x},t) + 2\Phi^\dagger_\alpha(\boldsymbol{x},t)F_{\alpha\gamma}(\boldsymbol{x},t;\boldsymbol{x},t)\Phi_\gamma(\boldsymbol{x},t)\right)\\
&\quad + \int_{x,\mathcal{C}} \frac{ic_1}{4}\Big(\mathrm{Tr}(\tilde{f}_a F(\boldsymbol{x},t;\boldsymbol{x},t))\Phi^\dagger_\alpha(\boldsymbol{x},t)(\tilde{f}_a)_{\alpha\gamma}\Phi_\gamma(\boldsymbol{x},t)\\
&\qquad\qquad +2\Phi^\dagger_\alpha(\boldsymbol{x},t)(\tilde{f}_a)_{\alpha\beta}F_{\beta\gamma}(\boldsymbol{x},t;\boldsymbol{x},t)(\tilde{f}_a)_{\gamma\delta}\Phi_\delta(\boldsymbol{x},t)\Big)\,.
\end{aligned}$$

Note that here, we have explicitly included the integrals over space and time instead of absorbing them in "Tr". Moreover, we have neglected the spectral function component of G. This was done because at equal time and space, the spectral function is trivially determined by the commutator relation, such that it does not influence the evolution equations. We follow [76] in defining $G(\boldsymbol{x},t;\boldsymbol{x},t) \equiv \frac{1}{2}\left(\lim_{t'\searrow t} G(\boldsymbol{x},t;\boldsymbol{x},t') + \lim_{t'\nearrow t} G(\boldsymbol{x},t;\boldsymbol{x},t')\right) = F(\boldsymbol{x},t;\boldsymbol{x},t)$ to avoid the contributions from ρ in the equal-time 2-point function in the following. Note that for both c_0 and c_1, the first term always in $\mathrm{Tr}(G_0^{-1}G)$ involves two $O(3)$ invariants, while the second term only involves one. Thus, the first terms are of leading order, while the second terms are both next-to-leading order. For c_0, this is illustrated in Fig. 4.2, and for the spin-density interactions, the same arguments apply, just with an additional factor of the spin matrices f at the vertex.

Now we consider Γ_2. For the 2-loop contribution, there are also both leading and next-to-leading order contributions. Fig. 4.3 shows this once more for the example of the c_0 interaction. For the double-bubble with two vertices, the indexing of the diagram matters, as the left diagram traces over both loops separately, such that it is leading order in $1/N$, while the right diagram only involves one trace, therefore being next to leading order. As the diagram with two vertices gets an additional factor of $1/N$ through the additional vertex, it is next-to-leading

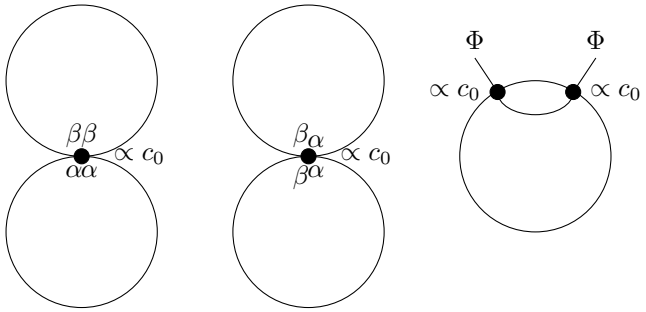

Figure 4.3.: 2-loop contributions to the effective action, limited to those with only density-density interaction vertices $\propto c_0$. Again, the lines correspond to the full propagator G. The double bubble diagram is shown with the two possible index structures.

or higher order for all indexing [15]. The same is also true for all diagrams with more than two loops, such that we can neglect them here. Again, these arguments also apply to the diagrams involving the spin-density vertices or, in the case of more than one vertex, a mix of both interactions. If we only consider the LO term in Γ_2, we get from the diagrams involving two traces for both our interactions

$$\Gamma_2^{\mathrm{LO}} = -i\int_{x,t}(-i\frac{c_0}{8})(\mathrm{Tr}G(\boldsymbol{x},t;\boldsymbol{x},t))^2 + (-i\frac{c_1}{8})\mathrm{Tr}G(\boldsymbol{x},t;\boldsymbol{x},t)\tilde{f}_a\mathrm{Tr}G(\boldsymbol{x},t;\boldsymbol{x},t)\tilde{f}_a \tag{4.78}$$

which is independent of the field expectation value Φ

$$\Gamma_2^{\mathrm{LO}}[\Phi,G] = \Gamma_2^{\mathrm{LO}}[G]. \tag{4.79}$$

Thus, we find the effective action with Γ_2 to leading order

$$\begin{aligned}
\Gamma^{\mathrm{LO}} = &\int_{\mathcal{C},x}\Big\{\frac{i}{2}\Phi_\alpha^\dagger(\boldsymbol{x},t)(V)_{\alpha\beta}\partial_t\Phi_\beta(\boldsymbol{x},t) - \frac{1}{4M}\nabla\Phi_\alpha^\dagger(\boldsymbol{x},t)\nabla\Phi_\alpha(\boldsymbol{x},t) - \frac{q}{2}\Phi_\alpha^\dagger(\boldsymbol{x},t)(\tilde{f}_z^2)_{\alpha\beta}\Phi_\beta(\boldsymbol{x},t)\\
&- \frac{c_0}{8}(\Phi_\alpha^\dagger(\boldsymbol{x},t)\Phi_\alpha(\boldsymbol{x},t))^2 - \frac{c_1}{8}(\Phi_\alpha^\dagger(\boldsymbol{x},t)(\tilde{f}_a)_{\alpha\beta}\Phi_\beta(\boldsymbol{x},t))(\Phi_\gamma^\dagger(\boldsymbol{x},t)(\tilde{f}_a)_{\gamma\delta}\Phi_\delta(\boldsymbol{x},t))\\
&+ \int_{y,\mathcal{C}}\left\{\delta(\boldsymbol{x}-\boldsymbol{y})\delta(t-t')\left[(V)_{\alpha\beta}\partial_t - \frac{i}{2m}\partial_x^2\delta_{\alpha\beta}\right]G_{\beta\alpha}(\boldsymbol{x},t;\boldsymbol{y},t')\right\}\\
&+ iq\mathrm{Tr}F(\boldsymbol{x},t;\boldsymbol{x},t) + \frac{i}{2}\mathrm{Tr}\log G^{-1}\\
&+ \frac{ic_0}{4}\Big(\mathrm{Tr}(F(\boldsymbol{x},t;\boldsymbol{x},t))\Phi_\alpha^\dagger(\boldsymbol{x},t)\Phi_\alpha(\boldsymbol{x},t) + 2\Phi_\alpha^\dagger(\boldsymbol{x},t)F_{\alpha\gamma}(\boldsymbol{x},t;\boldsymbol{x},t)\Phi_\gamma(\boldsymbol{x},t)\Big)\\
&+ \frac{ic_1}{4}\Big(\mathrm{Tr}(\tilde{f}_aF(\boldsymbol{x},t;\boldsymbol{x},t))\Phi_\alpha^\dagger(\boldsymbol{x},t)(\tilde{f}_a)_{\alpha\gamma}\Phi_\gamma(\boldsymbol{x},t) + 2\Phi_\alpha^\dagger(\boldsymbol{x},t)(\tilde{f}_a)_{\alpha\beta}F_{\beta\gamma}(\boldsymbol{x},t;\boldsymbol{x},t)(\tilde{f}_a)_{\gamma\delta}\Phi_\delta(\boldsymbol{x},t)\Big)\\
&- \frac{c_0}{8}(\mathrm{Tr}F(\boldsymbol{x},t;\boldsymbol{x},t))^2 - \frac{c_1}{8}\mathrm{Tr}F(\boldsymbol{x},t;\boldsymbol{x},t)\tilde{f}_a\mathrm{Tr}F(\boldsymbol{x},t;\boldsymbol{x},t)\tilde{f}_a\Big\}
\end{aligned} \tag{4.80}$$

4.3. The equation of motion for the field expectation value

With these ingredients, we can now calculate the equation of motion for the field expectation value according to Eq. (4.44a). As there is no field-dependence of Γ_2 to leading order, we find

$$\begin{aligned} i(V)_{\alpha\beta}\partial_t\Phi_\beta =& -\frac{1}{2M}\partial_x^2\Phi_\alpha + q(\tilde{f}_z^2)_{\alpha\beta}\Phi_\beta + \frac{c_0}{4}\Phi_\alpha(\Phi_\beta^\dagger\Phi_\beta) + \frac{c_1}{4}(\tilde{f}_a)_{\alpha\beta}\Phi_\beta(\Phi_\gamma^\dagger(\tilde{f}_a)_{\gamma\delta}\Phi_\delta) \\ & - \frac{i}{2}\frac{\delta \mathrm{Tr} G_0^{-1}(\Phi)G}{\delta\Phi^\dagger} - J - R\cdot\Phi \qquad (4.81) \\ =& -\frac{1}{2M}\partial_x^2\Phi_\alpha + q(\tilde{f}_z^2)_{\alpha\beta}\Phi_\beta + \frac{c_0}{4}\Phi_\alpha(\Phi_\beta^\dagger\Phi_\beta) + \frac{c_1}{4}(\tilde{f}_a)_{\alpha\beta}\Phi_\beta(\Phi_\gamma^\dagger(\tilde{f}_a)_{\gamma\delta}\Phi_\delta) \\ & + \frac{c_0}{2}\left(\mathrm{Tr}(F)\Phi_\alpha + 2F^{\alpha\gamma}\Phi_\gamma\right) \\ & + \frac{c_1}{2}\left(\mathrm{Tr}(\tilde{f}_a F)(\tilde{f}_a)^{\alpha\gamma}\Phi_\gamma + 2(\tilde{f}_a)^{\alpha\beta}F^{\beta\gamma}(\tilde{f}_a)^{\gamma\delta}\Phi^\delta\right) \qquad (4.82) \end{aligned}$$

where we have omitted the explicit space- and time-dependencies and where the second equation is true for all $t > t_0$ as the sources vanish for those times. They have to be considered, however, in the form of initial conditions. Let us now take a closer look at what the traces of the statistical propagator look like. In Eq. (4.16b), the statistical propagator is defined via the anticommutator of the fields

$$\begin{aligned} F_{\alpha\beta}(\boldsymbol{x},t;\boldsymbol{y},t') &= \frac{1}{2}\langle\phi^\alpha(\boldsymbol{x},t)\phi_\beta^\dagger(\boldsymbol{y},t') + \phi_\beta^\dagger(\boldsymbol{y},t')\phi^\alpha(\boldsymbol{x},t)\rangle_{\mathrm{conn}} \\ &= \begin{pmatrix} f_{11} & h_{11} & f_{10} & h_{10} & f_{1-1} & h_{1-1} \\ h_{11}^* & f_{11}^* & h_{10}^* & f_{10}^* & h_{1-1}^* & f_{1-1}^* \\ f_{01} & h_{01} & f_{00} & h_{00} & f_{0-1} & h_{0-1} \\ h_{01}^* & f_{01}^* & h_{00}^* & f_{00}^* & h_{0-1}^* & f_{0-1}^* \\ f_{-11} & h_{-11} & f_{-10} & h_{-10} & f_{-1-1} & h_{-1-1} \\ h_{-11}^* & f_{-11}^* & h_{-10}^* & f_{-10}^* & h_{-1-1}^* & f_{-1-1}^* \end{pmatrix} \end{aligned} \qquad (4.83)$$

where

$$f_{ij}(\boldsymbol{x},t;\boldsymbol{y},t') = \frac{1}{2}\langle\psi_i(\boldsymbol{x},t)\psi_j^\dagger(\boldsymbol{y},t') + \psi_j^\dagger(\boldsymbol{y},t')\psi_i(\boldsymbol{x},t)\rangle_{\mathrm{conn}} = f_{ji}^*(\boldsymbol{y},t';\boldsymbol{x},t) \qquad (4.84)$$

$$h_{ij}(\boldsymbol{x},t;\boldsymbol{y},t') = \frac{1}{2}\langle\psi_i(\boldsymbol{x},t)\psi_j(\boldsymbol{y},t') + \psi_j(\boldsymbol{y},t')\psi_i(\boldsymbol{x},t)\rangle_{\mathrm{conn}} = h_{ji}(\boldsymbol{y},t';\boldsymbol{x},t). \qquad (4.85)$$

At equal time and place, f_{ii} describe the densities of excitations above the condensate, while the h_{ij} correspond to anomalous averages. We define

$$n_{ij}(\vec{x}) \equiv f_{ij}(\boldsymbol{x}, t; \boldsymbol{x}, t) \tag{4.86}$$

$$m_{ij}(\vec{x}) \equiv h_{ij}(\boldsymbol{x}, t; \boldsymbol{x}, t) \tag{4.87}$$

$$N(\vec{x}) \equiv \sum_i n_{ii}(\vec{x}) \tag{4.88}$$

such that the relations

$$n_{ij} = n_{ji}^* \tag{4.89}$$

$$m_{ij} = m_{ji} \tag{4.90}$$

apply. Then, the traces occuring in Eq. (4.80) yield

$$\mathrm{Tr}(F) = 2N \tag{4.91}$$

$$\mathrm{Tr}(\tilde{f}_x F) = \sqrt{2}\,(n_{10} + n_{01} + n_{0-1} + n_{-10}) \tag{4.92}$$

$$\mathrm{Tr}(\tilde{f}_y F) = 0 \tag{4.93}$$

$$\mathrm{Tr}(\tilde{f}_z F) = 2(n_{11} - n_{-1-1}) \tag{4.94}$$

and the matrices $\tilde{f}_a$ multiplied with $F(\vec{x})$ are given by

$$\tilde{f}_x \cdot F \cdot \tilde{f}_x = \tag{4.95}$$

$$\frac{1}{2}\begin{pmatrix} n_{00} & m_{00} & n_{01}+n_{0-1} & m_{10}+m_{0-1} & n_{00} & m_{00} \\ m_{00}^* & n_{00} & m_{10}^*+m_{0-1}^* & n_{10}+n_{-10} & m_{00}^* & n_{00} \\ n_{10}+n_{-10} & m_{10}+m_{0-1} & n_{11}+n_{1-1}+n_{-11}+n_{-1-1} & m_{11}+2m_{1-1}+m_{-1-1} & n_{10}+n_{-10} & m_{10}+m_{0-1} \\ m_{10}^*+m_{0-1}^* & n_{01}+n_{0-1} & m_{11}^*+2m_{1-1}^*+m_{-1-1}^* & n_{11}+n_{1-1}+n_{-11}+n_{-1-1} & m_{10}^*+m_{0-1}^* & n_{01}+n_{0-1} \\ n_{00} & m_{00} & n_{01}+n_{0-1} & m_{10}+m_{0-1} & n_{00} & m_{00} \\ m_{00}^* & n_{00} & m_{10}^*+m_{0-1}^* & n_{10}+n_{-10} & m_{00}^* & n_{00} \end{pmatrix}$$

$$\tilde{f}_y \cdot F \cdot \tilde{f}_y = \tag{4.96}$$

$$\frac{1}{2}\begin{pmatrix} n_{00} & m_{00} & n_{0-1}-n_{01} & m_{0-1}-m_{10} & -n_{00} & -m_{00} \\ m_{00}^* & n_{00} & m_{0-1}^*-m_{10}^* & n_{-10}-n_{10} & -m_{00}^* & -n_{00} \\ n_{-10}-n_{10} & m_{0-1}-m_{10} & n_{11}-n_{1-1}-n_{-11}+n_{-1-1} & m_{11}-2m_{1-1}+m_{-1-1} & n_{-10}-n_{10} & m_{10}-m_{0-1} \\ m_{0-1}^*-m_{10}^* & n_{0-1}-n_{01} & m_{11}^*-2m_{1-1}^*+m_{-1-1}^* & n_{11}-n_{1-1}-n_{-11}+n_{-1-1} & m_{10}^*-m_{0-1}^* & n_{01}-n_{0-1} \\ -n_{00} & -m_{00} & n_{01}-n_{0-1} & m_{10}-m_{0-1} & n_{00} & m_{00} \\ -m_{00}^* & -n_{00} & m_{10}^*-m_{0-1}^* & n_{10}-n_{-10} & m_{00}^* & n_{00} \end{pmatrix}$$

$$\tilde{f}_z \cdot F \cdot \tilde{f}_z = \tag{4.97}$$

$$\begin{pmatrix} n_{11} & m_{11} & 0 & 0 & -n_{1-1} & -m_{1-1} \\ m_{11}^* & n_{11} & 0 & 0 & -m_{1-1}^* & -n_{1-1} \\ 0 & 0 & 0 & 0 & 0 & 0 \\ 0 & 0 & 0 & 0 & 0 & 0 \\ -n_{-11} & -m_{1-1} & 0 & 0 & n_{-1-1} & m_{-1-1} \\ -m_{1-1}^* & -n_{1-1} & 0 & 0 & m_{-1-1}^* & n_{-1-1} \end{pmatrix}.$$

4.3.1. The Hartree-Fock-Bogoliubov-Popov approximation

We can now assume that only the diagonal terms n_{ii} in F are non-zero, corresponding to the Hartree-Fock-Bogoliubov-Popov approximation as in [75, 83]. In that special case, the matrix

products are reduced to

$$\tilde{f}_x \cdot F \cdot \tilde{f}_x = \frac{1}{2}\begin{pmatrix} n_{00} & 0 & 0 & 0 & n_{00} & 0 \\ 0 & n_{00} & 0 & 0 & 0 & n_{00} \\ 0 & 0 & n_{11}+n_{-1-1} & 0 & 0 & 0 \\ 0 & 0 & 0 & n_{11}+n_{-1-1} & 0 & 0 \\ n_{00} & 0 & 0 & 0 & n_{00} & 0 \\ 0 & n_{00} & 0 & 0 & 0 & n_{00} \end{pmatrix}$$

$$\tilde{f}_y \cdot F \cdot \tilde{f}_y = \frac{1}{2}\begin{pmatrix} n_{00} & 0 & 0 & 0 & -n_{00} & 0 \\ 0 & n_{00} & 0 & 0 & 0 & -n_{00} \\ 0 & 0 & n_{11}+n_{-1-1} & 0 & 0 & 0 \\ 0 & 0 & 0 & n_{11}+n_{-1-1} & 0 & 0 \\ -n_{00} & 0 & 0 & 0 & n_{00} & 0 \\ 0 & -n_{00} & 0 & 0 & 0 & n_{00} \end{pmatrix}$$

$$\tilde{f}_z \cdot F \cdot \tilde{f}_z = \begin{pmatrix} n_{11} & 0 & 0 & 0 & 0 & 0 \\ 0 & n_{11} & 0 & 0 & 0 & 0 \\ 0 & 0 & 0 & 0 & 0 & 0 \\ 0 & 0 & 0 & 0 & 0 & 0 \\ 0 & 0 & 0 & 0 & n_{-1-1} & 0 \\ 0 & 0 & 0 & 0 & 0 & n_{-1-1} \end{pmatrix} \tag{4.98}$$

Thus, the equation of motion Eq. (4.82) becomes

$$\begin{aligned} &i(V)_{\alpha\beta}\partial_t\Phi_\beta = -\frac{1}{2M}\partial_x^2\Phi_\alpha + q(\tilde{f}_z^2)_{\alpha\beta}\Phi_\beta + \frac{c_0}{4}\Phi_\alpha(\Phi_\beta^\dagger\Phi_\beta) + \frac{c_1}{4}(\tilde{f}_a)_{\alpha\beta}\Phi_\beta(\Phi_\gamma^\dagger(\tilde{f}_a)_{\gamma\delta}\Phi_\delta) \\ &+ \frac{c_0}{2}\mathrm{diag}\left(2N+2n_{11}, 2N+2n_{11}, 2N+2n_{00}, 2N+2n_{00}, 2N+2n_{-1-1}, 2N+2n_{-1-1}\right)_\beta^\alpha \Phi^\beta \\ &+ \frac{c_1}{2}\mathrm{diag}\left(2(n_{11}-n_{-1-1})+2n_{00}+2n_{11}, 2(n_{11}-n_{-1-1})+2n_{00}+2n_{11}, 2n_{11}+2n_{-1-1},\right. \\ &\left. 2n_{11}+2n_{-1-1}, 2(n_{-1-1}-n_{11})+2n_{00}+2n_{-1-1}, 2(n_{-1-1}-n_{11})+2n_{00}+2n_{-1-1}\right)_\beta^\alpha \Phi^\beta \\ &= -\frac{1}{2M}\partial_x^2\Phi_\alpha + q(\tilde{f}_z^2)_{\alpha\beta}\Phi_\beta + \frac{c_0}{4}\Phi_\alpha(\Phi_\beta^\dagger\Phi_\beta) + \frac{c_1}{4}(\tilde{f}_a)_{\alpha\beta}\Phi_\beta(\Phi_\gamma^\dagger(\tilde{f}_a)_{\gamma\delta}\Phi_\delta) + K_{\alpha\beta}\Phi_\beta \\ &= \frac{\delta H}{\delta\phi_\alpha^\dagger} + K_{\alpha\beta}\Phi_\beta \end{aligned} \tag{4.99}$$

where

$$K = \begin{pmatrix} K_1 & 0 & 0 & 0 & 0 & 0 \\ 0 & K_1 & 0 & 0 & 0 & 0 \\ 0 & 0 & K_2 & 0 & 0 & 0 \\ 0 & 0 & 0 & K_2 & 0 & 0 \\ 0 & 0 & 0 & 0 & K_3 & 0 \\ 0 & 0 & 0 & 0 & 0 & K_3 \end{pmatrix} \tag{4.100}$$

with

$$K_1 = (c_0 + c_1)(2n_{11} + n_{00}) + (c_0 - c_1)n_{-1-1} \tag{4.101}$$

$$K_2 = (c_0 + c_1)N + (c_0 - c_1)n_{00} \tag{4.102}$$

$$K_3 = (2n_{-1-1} + n_{00}) + (c_0 - c_1)n_{11} \tag{4.103}$$

In the last line of Eq. (4.99), we have written the equation of motion in terms of the classical Hamiltonian, the Legendre transform of the Lagrangian Eq. (4.72). From this line, it becomes obvious that in this approximation, the quantum equation of motion for the field expectation value is given by the usual GPE in addition to an extra term $K_{\alpha\beta}\Phi_\beta$, effectively shifting the quadratic term in the action by some m_F-dependent values that involve the statistical propagator.

4.4. Evolution equation for the statistical propagator

Thus, to solve the equation of motion for the condensate fields, we need an equation governing the evolution of the statistical propagator as well. In our case, Γ_2 Eq. (4.78) leads to a completely local self-energy

$$\Sigma(x, t; y, t') = -i\delta(\boldsymbol{x} - \boldsymbol{y})\delta(t - t')\Sigma^{(0)}(\boldsymbol{x}, t). \tag{4.104}$$

with

$$(\Sigma^0)_{\alpha\beta} = \frac{c_0}{2}\mathrm{Tr}\left(F(\boldsymbol{x}, t; \boldsymbol{x}, t)\right)\delta_{\alpha\beta} + \frac{c_1}{2}\mathrm{Tr}\left(F(\boldsymbol{x}, t; \boldsymbol{x}, t)\tilde{f}_a\right)(\tilde{f}_a)_{\alpha\beta} \tag{4.105}$$

Using this, the evolution of F according to Eq. (4.67) is just given by

$$i(V)_{\alpha\beta}\partial_t F_{\beta\gamma}(\boldsymbol{x}, t; \boldsymbol{y}, t') = [M_{\alpha\beta}(x, t) + \Sigma^{(0)}_{\alpha\beta}(x, t)]F_{\beta\gamma}(\boldsymbol{x}, t; \boldsymbol{y}, t') \tag{4.106}$$

with

$$M^{\alpha\beta}(\boldsymbol{x},t) = -\frac{1}{2m}\partial_x^2\delta_{\alpha\beta} + q(\tilde{f}_z)_{\alpha\beta} + \frac{c_0}{4}\left(\delta_{\alpha\beta}\Phi_\gamma^\dagger\Phi_\gamma + 2\Phi_\beta^\dagger\Phi_\alpha\right) + \frac{c_1}{4}\left((\tilde{f}_a)_{\alpha\beta}\Phi_\gamma^\dagger(\tilde{f}_a)_{\gamma\delta}\Phi_\delta + 2(\tilde{f}_a)_{\alpha\gamma}\Phi_\gamma\Phi_\delta^\dagger(\tilde{f}_a)_{\delta\beta}\right) \tag{4.107}$$

For densities at equal time, the evolution is governed by the commutator

$$iV\partial_t F(\boldsymbol{x},t;\boldsymbol{x},t) = \left[M + \Sigma^{(0)}, F(\boldsymbol{x},t;\boldsymbol{x},t)\right] \tag{4.108}$$

as

$$iV\partial_{t'}F(\boldsymbol{x},t;\boldsymbol{y},t')\big|_{x=y} \overset{(4.83)}{=} \left[-iV\partial_{t'}F(\boldsymbol{y},t';\boldsymbol{x},t)\right]^\dagger\Big|_{x=y} \tag{4.109}$$

$$\overset{(4.106)}{=} -\left[\left(M+\Sigma^{(0)}\right)F(\boldsymbol{y},t';\boldsymbol{x},t)\right]^\dagger\Big|_{x=y} \tag{4.110}$$

$$= -F(\boldsymbol{x},t;\boldsymbol{x},t)(M+\Sigma^0) \tag{4.111}$$

With Eqs (4.82) and (4.108), we now have a self-consistent set of equations to leading order describing the spin-1 Bose gas out of equilibrium with the full field expectation value Φ and propagator G. These are extremely helpful in order to compare to numerical simulations of the far-from-equilibrium dynamics of the system and to determine how big a role higher-order terms than we have included in the analytic equations play. All these investigations are subject to future work.

However, these equations are still written in terms of all the degrees of freedom of our system and now that we have formulated everything in terms of the expectation values of the fields and the propagator, it is not possible anymore to integrate out any degrees of freedom not of interest to us. Thus, in the next chapters, we will use a different approach to develop low-energy effective theories only dependent on the phase degrees of freedom that interest us following the numerical observations in [41].

5. A first low-energy effective field theory for the phase degrees of freedom

In the last chapter, we developed a theory to describe the spin-1 Bose gas in a setting out of equilibrium to leading order. These considerations are certainly very useful to make comparisons with numerical truncated Wigner simulations of the spin-1 Bose gas far from equilibrium and to determine how much higher-order terms actually play a role in its dynamics.

However, the results from Ch. 4 are still not easy to interpret, as we get equations for three complex fields, as well as the full statistical propagator F. These of course have physical interpretations like the condensate wave function and the matrix containing occupation numbers. Nevertheless, they are not particularly useful for making sense of the rich phase dynamics in the spinor and Larmor phase shown to appear in numerical simulations of the spin-1 Bose gas after a quench from the polar to the easy-plane phase as seen in [41].

Bogoliubov theory tells us (see Sec. 2.5) that in the easy-plane phase, the mass gaps for the density fluctuations are much higher than those of the phase degrees of freedom. Therefore, we can assume that at least at times in the dynamics when we are close to the equilibrium easy-plane phase, the relevant degrees of freedom at low energies are the Larmor and the spinor phase, as the overall phase is not physically relevant. Thus, we want to spend the remainder of this thesis developing a low-energy effective field theory for these two phases, thereby dramatically decreasing the number of degrees of freedom we consider from 6 real degrees of freedom (or 12 if we count the doubling of degrees of freedom out of equilibrium) to only 2.

To develop such an effective field theory, we cannot continue down the 2PI path. Because in the 2PI formalism, the number of degrees of freedom is kept the same and the sources are replaced by the full quantum field and propagator, the evolution equations Eqs (4.82) and (4.108) we have obtained also still include all degrees of freedom, and there is no way of isolating the phase dynamics.

Instead, to obtain a theory only for the phase degrees of freedom, we will follow another procedure, which is inspired by [51]. For that, we will expand our theory around constant, homogeneous mean-field values for the densities. Then, we integrate out the density fluctuations

using Gaussian integrals to obtain a theory in which the only variables are the phases. Note that for these considerations, we will also abolish the Keldysh time path used in the previous chapter. This is justified because for the theory developed in this and the following chapters, we assume that we are in the scaling regime, where there is supposed to be little dependence on the initial condition, and numerical simulations show the fields to be near their equilibrium values (see Fig. 5.1).

To lowest order, this calculation has already been performed by Ido Siovitz [84], such that the first section of this chapter, Sec. 5.1, is mainly a recap of his results, with the addition of the imaginary part of the effective action. In Sec. 5.1.3 it will turn out that for small spinor phases φ_S, the theories for the Larmor and the spinor phases decouple, resulting in a free theory for the Larmor phase and a modified sine-Gordon model for the spinor phase. For a first sanity check for these effective theories, we then compare the analytical result for the mass gap of φ_S to numerical simulations in Sec. 5.2.

In this and the following chapters, we will assume that we are in the parameter regime of the easy-plane phase with $c_1 < 0$ and in any numerical simulations, we work with the parameters for the ^{87}Rb experiment by Markus Oberthaler as seen in Tab. A.1 in App. A.

5.1. Lowest order LEEFT

5.1.1. A coordinate transformation of the action

Like in [51], we work in the path integral formalism and start out with the spin-1 action Eq. (2.14). At this point, the theory is written in terms of the fundamental fields Eq. (2.1) with six real degrees of freedom, given by the three complex fields Ψ_i. Equivalently, we can write the theory in terms of densities and phases, splitting

$$\Psi_i = \sqrt{\rho_i} e^{i\phi_i}. \tag{5.1}$$

Inspired by the mean-field spinor in the easy-plane phase Eq. (2.32), we can further transform these coordinates via

$$\rho = \frac{\rho_1 + \rho_{-1}}{2};\ \ \varepsilon = \frac{\rho_1 - \rho_{-1}}{2};\ \ \theta = \phi_1 + \phi_{-1};\ \ \varphi_L = \phi_1 - \phi_{-1};\ \ \varphi_S = 2\phi_0 - \theta \tag{5.2}$$

such that

$$\Psi_{-1} = \sqrt{\rho - \varepsilon} e^{\frac{i}{2}(\theta - \varphi_L)};\ \ \Psi_1 = \sqrt{\rho + \varepsilon} e^{\frac{i}{2}(\theta + \varphi_L)};\ \ \Psi_0 = \sqrt{\tilde{\rho} - 2\rho} e^{\frac{i}{2}(\theta + \varphi_S)}. \tag{5.3}$$

Here, $\tilde{\rho}$ has the intuitive interpretation of the total density, while ρ is the density that depletes the $m_F = 0$ component symetrically in favor of the $m_F = \pm 1$ components, and ε is the density difference between the $m_F = 1$ and $m_F = -1$ component. Moreover, θ plays the role of the total $U(1)$ phase, the spinor phase φ_S describes the phase rotation of the $m_F = 0$-component, and the Larmor phase φ_L is the relative phase between the $m_F = 1$ and $m_F = -1$ component. In these new variables, the Lagrangian of Eq. (2.14) becomes

$$\begin{aligned}\mathcal{L} =& -\varepsilon\dot{\varphi}_L + \rho\dot{\varphi}_S - \frac{\tilde{\rho}}{2}\left(\dot{\varphi}_S + \dot{\theta}\right) - 2q\rho \\ &- \frac{1}{8m}\left[(\rho-\varepsilon)(\nabla\log(\rho-\varepsilon))^2 + (\rho+\varepsilon)(\nabla\log(\rho+\varepsilon))^2 + (\tilde{\rho}-2\rho)(\nabla\log(\tilde{\rho}-2\rho))^2\right] \\ &- \frac{\rho}{4m}(\nabla\varphi_L)^2 - \frac{\tilde{\rho}-2\rho}{8m}(\nabla\varphi_S)^2 - \frac{\tilde{\rho}}{8m}(\nabla\theta)^2 - \frac{1}{2m}\left(\varepsilon\nabla\theta\nabla\varphi_L + \frac{\tilde{\rho}-2\rho}{2}\nabla\theta\nabla\varphi_S\right) \\ &- \frac{c_0}{2}\tilde{\rho}^2 - 2c_1\left[\varepsilon^2 - 2\rho^2 + \rho\tilde{\rho} + \sqrt{\rho^2-\varepsilon^2}(\tilde{\rho}-2\rho)\cos\varphi_S\right].\end{aligned} \tag{5.4}$$

Note that through the spin-density interactions $\propto c_1$, a term $\propto \cos\varphi_S$ enters the Lagrangian, stemming from the part of the action $\propto c_1(\Psi_0^2\Psi_{-1}^\dagger\Psi_1^\dagger + \Psi_0^{\dagger 2}\Psi_{-1}\Psi_1)$ that encodes the part of the interaction involving the spin-changing collisions in which two $m_F = 0$ particles become a pair of $m_F = \pm$ particles or vice versa as illustrated in Fig. 2.3.

5.1.2. Integrating out density fluctuations

Numerical simulations of a quench from the polar to the easy-plane phase via TWA show the fluctuations of the densities ρ and ε to be small compared to the dynamics of the phase at the energies considered in experiment, as can be seen in Fig. 5.1b. Moreover, they show the fluctuations to be mainly about a homogeneous background corresponding to the easy-plane mean-field configuration (see Fig. 5.1a). Thus, we want to integrate out the density fluctuations in order to develop an effective theory only for φ_S and φ_L. The strategy for that is to first expand ρ and ε around the homogeneous mean-field background with

$$\rho = n + \delta\rho \quad \varepsilon = 0 + \delta\varepsilon, \tag{5.5}$$

and

$$\tilde{\rho} = \text{const.}; \quad n = \text{const.}; \quad \langle\delta\rho\rangle = 0 = \langle\delta\varepsilon\rangle. \tag{5.6}$$

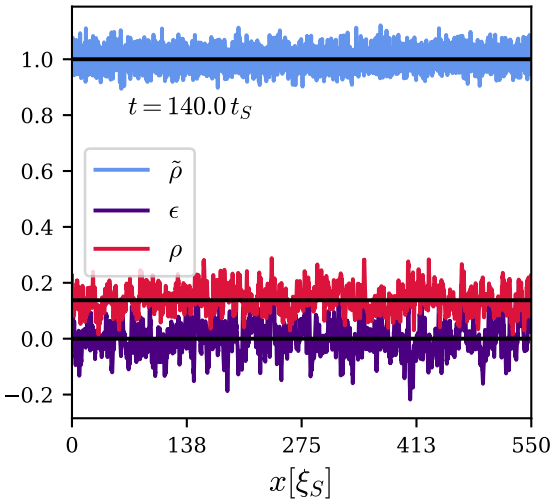

(a) $\tilde{\rho}$, ρ, and ε in units of the initial density $\tilde{\rho}(t = 0)$ in a (1+1)d spin-1 Bose gas after a quench from the polar to the easy-plane phase with $q = -0.9c_1\tilde{\rho}$. The values are shown at a time $t = 140t_S$, which is right in the scaling regime according to [41]. One can see that all quantities only fluctuate slightly around the homogeneous mean-field values predicted for the easy-plane phase in equilibrium, which are shown in black.

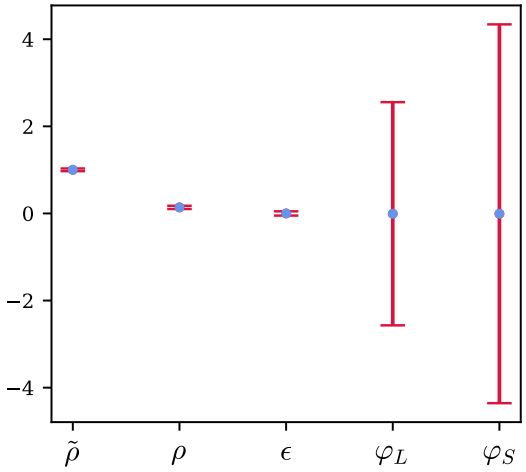

(b) Means and standard deviations of the density and phase degrees of freedom over time and space in a (1+1)d spin-1 Bose gas after a quench from the polar to the easy-plane phase with $q = -0.9c_1\tilde{\rho}$. The values for the densities are given in terms of $\tilde{\rho}$. As can be seen, the standard deviations for the density degrees of freedom are significantly smaller than those for the phases, justifying our approximation to integrate out the density fluctuations.

Figure 5.1.: Numerical results for the fluctuations of the density degrees of freedom. Data taken from the truncated Wigner simulations carried out in [41].

We then expand the Lagrangian to second order in these fluctuations $\boldsymbol{\delta\rho} = (\delta\rho, \delta\varepsilon)^T$[1]:

$$\mathcal{L} = \mathcal{L}^0 + \mathcal{L}^1 + \mathcal{L}^2 + \mathcal{O}(\delta^3) = \mathcal{L}^0 + \boldsymbol{\delta\rho}^T \boldsymbol{J_0} + \frac{1}{2}\boldsymbol{\delta\rho}^T \boldsymbol{G_0^{-1}} \boldsymbol{\delta\rho} + \mathcal{O}(\delta^3), \tag{5.7}$$

such that the partition function approximately becomes

$$Z = \int \mathcal{D}\rho\mathcal{D}\varepsilon\mathcal{D}\theta\mathcal{D}\varphi_S\mathcal{D}\varphi_L e^{iS[\rho,\varepsilon,\varphi_S,\varphi_L]} \tag{5.8}$$

$$= \int \mathcal{D}\delta\rho\mathcal{D}\delta\varepsilon\mathcal{D}\theta\mathcal{D}\varphi_S\mathcal{D}\varphi_L e^{i\int_{t,x}\mathcal{L}^0 + \boldsymbol{\delta\rho}^T\boldsymbol{J_0} + \frac{1}{2}\boldsymbol{\delta\rho}^T\boldsymbol{G_0^{-1}}\cdot\boldsymbol{\delta\rho} + \mathcal{O}(\delta^3)} \tag{5.9}$$

Then, through Gaussian integration of the density fluctuations, using the Fresnel integral

$$\int \exp\left(\frac{i}{2}x\cdot A\cdot x + iJ\cdot x\right) d^n x = \sqrt{\frac{(2\pi i)^n}{\det A}} \exp\left(-\frac{i}{2}J\cdot A^{-1}\cdot J\right) \tag{5.10}$$

for a symmetric, real $n \times n$ matrix A without singularities, we get

$$Z \approx \int \mathcal{D}\delta\rho\mathcal{D}\delta\varepsilon\mathcal{D}\theta\mathcal{D}\varphi_S\mathcal{D}\varphi_L e^{i\int_{t,x}\mathcal{L}^0 + \boldsymbol{\delta\rho}^T\boldsymbol{J_0} + \frac{1}{2}\boldsymbol{\delta\rho}^T\boldsymbol{G_0^{-1}}\cdot\boldsymbol{\delta\rho}} \tag{5.11}$$

$$= C\int \mathcal{D}\theta\mathcal{D}\varphi_S\mathcal{D}\varphi_L \underbrace{e^{i\int_{t,x}\left[\mathcal{L}^0 - \frac{1}{2}\boldsymbol{J_0^T G_0 J_0}\right] - \frac{1}{2}\log\det \boldsymbol{G_0^{-1}}}}_{e^{iS^{\text{eff}}}} \tag{5.12}$$

such that we obtain the effective action

$$S^{\text{eff}} = \int_{t,x}\left[\mathcal{L}^0 - \frac{1}{2}\boldsymbol{J_0^T G_0 J_0}\right] + \frac{i}{2}\log\det \boldsymbol{G_0^{-1}}. \tag{5.13}$$

Comparing to Eq. (4.35), we find that such a Gaussian integration corresponds to a 1-loop approximation of the action. Note, however, that we have the extra term $-\frac{1}{2}\boldsymbol{J_0^T G_0 J_0}$ in Eq. (5.13) compared to Eq. (4.35). This is due to the fact that in the derivation of Eq. (4.35) in App. B.1, the linear term cancels with the term stemming from the Legendre transformation to 1-loop order.

For our low-energy effective action, however, instead of performing a Legendre transformation and getting a theory that depends on $\langle\rho\rangle$ and $\langle\varepsilon\rangle$ fulfilling an equation of motion like $\frac{\delta\Gamma}{\delta\boldsymbol{\rho}} = -\boldsymbol{J^T}$, we just assume that at zero external sources, we have the constant, homogeneous mean-field values $\langle\rho\rangle = n$ and $\langle\varepsilon\rangle = 0$ and no mean fluctuations. Consequently, we cannot make a similar cancellation to what is done in App. B.1 and are left with the linear term in $\boldsymbol{\delta\rho}$, which then gives $-\frac{1}{2}\boldsymbol{J_0^T G_0 J_0}$ upon Gaussian integration.

[1]Note that we have defined $G_0^{-1} = \frac{\delta^2 S}{\delta\boldsymbol{\delta\rho}\delta\boldsymbol{\delta\rho}}$ without the factor of $-i$ in Eq. (4.36) such that G_0^{-1} is real. As for a purely real positive number a, $\log -ia = a + i\frac{3\pi}{2} = \log a + \text{const.}$, this does not matter in the log det term of the effective action and we get the same log det term as in Eq. (4.35).

Let us now apply this strategy to our Lagrangian Eq. (5.4). After expanding ρ and ε according to Eq. (5.5), we obtain

$$\begin{aligned}\mathcal{L} = &-\delta\varepsilon\dot{\varphi}_L + \delta\rho\dot{\varphi}_S - \frac{\tilde{\rho}}{2}\left(\dot{\theta}+\dot{\varphi}_S\right) - 2q\delta\rho - \frac{c_0}{2}\tilde{\rho}^2 \\ &- \frac{1}{8m}\Big[(n+\delta\rho-\delta\varepsilon)(\nabla\log(n+\delta\rho-\delta\varepsilon))^2 + (n+\delta\rho+\delta\varepsilon)(\nabla\log(\rho+\varepsilon))^2 \\ &+(\tilde{\rho}-2n-2\delta\rho)(\nabla\log(\tilde{\rho}-2n-2\delta\rho))^2\Big] - \frac{n+\delta\rho}{4m}(\nabla\varphi_L)^2 - \frac{\tilde{\rho}-2n-2\delta\rho}{8m}(\nabla\varphi_S)^2 \\ &- \frac{\tilde{\rho}}{8m}(\nabla\theta)^2 - \frac{1}{2m}(\delta\varepsilon\nabla\theta\nabla\varphi_L - (n+\delta\rho)\nabla\theta\nabla\varphi_S) \\ &- 2c_1\left[\delta\varepsilon^2 - 2n^2 - 2\delta\rho^2 - 4n\delta\rho + n\tilde{\rho} + \delta\rho\tilde{\rho} + \sqrt{n^2+\delta\rho^2+2n\delta\rho-\delta\varepsilon^2}(\tilde{\rho}-2n-2\delta\rho)\cos\varphi_S\right].\end{aligned} \tag{5.14}$$

We then expand this Lagrangian Eq. (5.14) to second order in the fluctuations to obtain an effective action like in Eq. (5.9). If we carry out this expansion, we find (details about this expansion in App. B.2):

$$\begin{aligned}\mathcal{L}^0 = &-\frac{n}{4m}(\nabla\varphi_L)^2 - \frac{\tilde{\rho}-2n}{8m}(\nabla\varphi_S)^2 - \frac{\tilde{\rho}}{8m}(\nabla\theta)^2 - \frac{\tilde{\rho}-2n}{4m}\nabla\theta\nabla\varphi_S \\ &- 2c_1 n(\tilde{\rho}-2n)(1+\cos\varphi_S)\end{aligned} \tag{5.15}$$

$$\boldsymbol{J_0} = \begin{pmatrix}\dot{\varphi}_S - 2q - \frac{1}{4m}\left((\nabla\varphi_L)^2 - (\nabla\varphi_S)^2 - 2\nabla\theta\nabla\varphi_S\right) - 2c_1(\tilde{\rho}-4n)(1+\cos\varphi_S) \\ -\dot{\varphi}_L - \frac{1}{2m}\nabla\theta\nabla\varphi_L\end{pmatrix} \tag{5.16}$$

$$\boldsymbol{G_0^{-1}} = \begin{pmatrix}\frac{\tilde{\rho}}{2m}\frac{\nabla^2}{n(\tilde{\rho}-2n)} + 8c_1(1+\cos\varphi_S) & 0 \\ 0 & \frac{\nabla^2}{2mn} - 2c_1\left(2+\left(2-\frac{\tilde{\rho}}{n}\right)\cos\varphi_S\right).\end{pmatrix} \tag{5.17}$$

Note that here, we have neglected terms such as $\frac{c_0}{2}\tilde{\rho}^2$, $4c_1n^2$ or $\frac{\tilde{\rho}}{2}\left(\dot{\theta}+\dot{\varphi}_S\right)$, which are just constants or a total derivative, respectively, if we assume $\tilde{\rho}$ and n to be constant.

So far, the Lagrangian includes terms involving the spatial derivative of the total phase $\nabla\theta$, as they do not automatically vanish in the above approximations. However, as θ is not even dynamical if we assume $\tilde{\rho} = $ const. and we are not interested in the total phase anyway, we can assume a spatially constant total phase and in the following neglect all terms involving $\nabla\theta$.

In the following, we also want to neglect the ∇^2 terms in the inverse free propagator for two reasons. Firstly, we want to look at a low-energy effective theory, corresponding to small values of k. And indeed, even momenta at the spin healing length $k_{\xi_S} = 1/\xi_S = \sqrt{2m\tilde{\rho}|c_1|}$ lead to a small kinetic term compared to the prefactor $\propto 8c_1$ of the other term in $\boldsymbol{G_0^{-1}}$. Moreover, even if we wanted to include these terms, we would have a non-diagonal inverse propagator as the terms $\propto \nabla^2$ are diagonal in Fourier space, while the other terms are diagonal in position

space.

Neglecting these derivative terms, we get

$$\begin{aligned}\frac{1}{2}\boldsymbol{J_0^T G_0 J_0} =&\frac{1}{2}\left[\frac{n^3\dot{\varphi}_L^2}{-2n^2c_1(2n+(2n-\tilde{\rho})\cos\varphi_S)}\right.\\ &\left.+\frac{\left(\dot{\varphi}_S-2q-\frac{(\nabla\varphi_L)^2-(\nabla\varphi_S)^2}{4m}-2c_1(\tilde{\rho}-4n)(1+\cos\varphi_S)\right)^2}{8c_1(1+\cos\varphi_S)}\right]\end{aligned} \tag{5.18}$$

and

$$\begin{aligned}&\log\det\boldsymbol{G_0^{-1}} = \operatorname{tr}\log\boldsymbol{G_0^{-1}}\\ =&\frac{1}{\Delta t(\Delta x)^d}\int_{t,x}\left[\log\left(\frac{8c_1(1+\cos\varphi_S)}{16c_1}\right)+\log\left(\frac{-2c_1\left(2+\left(2-\frac{\tilde{\rho}}{n}\right)\cos\varphi_S\right)}{2c_1\left(\frac{\tilde{\rho}}{n}-4\right)}\right)\right].\end{aligned} \tag{5.19}$$

where Δt and Δx are the time- and lengthscales relevant for regularization, defined by $\sum_{t,x} = \frac{1}{\Delta t(\Delta x)^d}\int_{t,x}$ [85]. As such, they are related to the system's volume in Fourier space. Moreover, we have normalized the log terms to vanish for $\varphi_S = 0$. Combining all terms as in Eq. (5.13), we find for the effective Lagrangian

$$\begin{aligned}\mathcal{L}^{\text{eff}} =&-\frac{n}{4m}(\nabla\varphi_L)^2-\frac{\tilde{\rho}-2n}{8m}(\nabla\varphi_S)^2-2c_1n(\tilde{\rho}-2n)(1+\cos\varphi_S)\\ &-\frac{1}{2}\left[\frac{n^3\dot{\varphi}_L^2}{-2n^2c_1(2n+(2n-\tilde{\rho})\cos\varphi_S)}\right.\\ &\left.+\frac{\left(\dot{\varphi}_S-2q-\frac{(\nabla\varphi_L)^2-(\nabla\varphi_S)^2}{4m}-2c_1(\tilde{\rho}-4n)(1+\cos\varphi_S)\right)^2}{8c_1(1+\cos\varphi_S)}\right]\\ &+\frac{i}{2\Delta t(\Delta x)^d}\left[\log\left(\frac{8c_1(1+\cos\varphi_S)}{16c_1}\right)+\log\left(\frac{-2c_1\left(2+\left(2-\frac{\tilde{\rho}}{n}\right)\cos\varphi_S\right)}{2c_1\left(\frac{\tilde{\rho}}{n}-4\right)}\right)\right].\end{aligned} \tag{5.20}$$

Note that for $\varphi_S = (2\mathbb{Z}+1)\,\pi$, the effective action diverges as the term $\propto(1+\cos\varphi_S)$ in the numerator of the second term in $\frac{1}{2}\boldsymbol{J_0^T G_0 J_0}$ goes to zero. The reason for this is that because we have neglected the derivative terms, the inverse free propagator $\boldsymbol{G_0^{-1}}$ has a zero eigenvalue at $\varphi_S = (2\mathbb{Z}+1)\,\pi$, making the Gaussian integral divergent. However, if we are nowhere near $\varphi_S = (2\mathbb{Z}+1)\,\pi$, we can still use this theory as an approximation.

Note also that due to the Gaussian integration yielding an effective action quadratic in $\boldsymbol{J_0}$, the non-relativistic theory in the densities becomes a relativistic theory in the phases φ_L and φ_S

as $\boldsymbol{J_0} \propto \dot{\varphi}$. For this effective theory, we can interpret the fact that the derivative terms in φ_L are divided by φ_S-dependent terms as φ_S influencing the speed of sound for the dispersion of φ_L. We can also see that only the coupling c_1 appears in this action, which makes sense as this is the coupling for the spin-density interactions, which, contrary to the density-density interactions, affect the complex phases of the quantum fields describing the spin-1 Bose gas.

5.1.3. Expansion around $\varphi_S = 2\pi\mathbb{Z}$

We see in numerical simulations that φ_S mostly lies around multiples of 2π, $\varphi_S \approx 2\pi N$ for $N \in \mathbb{Z}$ (see Fig. 5.2b). This makes sense as φ_S is predicted to be a gapped mode by Bogoliubov theory, with minimal energy at $\varphi_S = 2\pi\mathbb{Z}$. For φ_S around $2\pi\mathbb{Z}$, we can use

$$1 + \cos\varphi_S = 2\left(1 - \sin^2\frac{\varphi_S}{2}\right) \tag{5.21}$$

to expand our effective action around small values of $\sin^2\frac{\varphi_S}{2}$.

For the real part, we expand $\frac{1}{1+\cos\varphi_S}$ up to $\mathcal{O}(\sin^4\frac{\varphi_S}{2})$

$$\frac{1}{1+\cos\varphi_S} = \frac{1}{2}\left(1 + \sin^2\frac{\varphi_S}{2} + \sin^4\frac{\varphi_S}{2}\right) + \mathcal{O}(\sin^6), \tag{5.22}$$

and for the imaginary part, we do the same using

$$\log\left(1 + a\sin^2\frac{\varphi_S}{2}\right) = a\sin^2\frac{\varphi_S}{2} - \frac{a^2}{2}\sin^4\frac{\varphi_S}{2} + \mathcal{O}(\sin^6). \tag{5.23}$$

If we, moreover, use $q = -2c_1(\tilde{\rho} - 4n)$, which holds in the groundstate of the easy-plane phase (see Eq. (2.35)) and neglect any terms involving $\dot{\varphi}\sin^2$, $\nabla^2\varphi\sin^2$ and higher, as well as higher than second order derivative terms, we find that the Lagrangians for φ_S and φ_L decouple and we get

$$\mathcal{L}^{\text{eff}}_{\varphi_L} = \frac{\dot{\varphi_L}^2 n}{2q} - \frac{n}{4m}\left(\nabla\varphi_L\right)^2 + \mathcal{O}\left(\dot{\varphi}\sin^2, \nabla\varphi\sin^2, \dot{\varphi}\nabla^2\varphi, \nabla^3\varphi\right) \tag{5.24}$$

and

$$\begin{aligned}\mathcal{L}^{\text{eff}}_{\varphi_S} =& -\frac{1}{32c_1}\dot{\varphi}_S^2 - \frac{\tilde{\rho}-2n}{8m}(\nabla\varphi_S)^2 - 2c_1 n(\tilde{\rho}-2n)\cos\varphi_S \\ &+ \tilde{A}\sin^2\frac{\varphi_S}{2} + \tilde{B}\sin^4\frac{\varphi_S}{2} + \mathcal{O}\left(\sin^6, \dot{\varphi}\sin^2, \nabla\varphi\sin^2, \dot{\varphi}\nabla^2\varphi, \nabla^3\varphi\right).\end{aligned} \tag{5.25}$$

where

$$\tilde{A} = -\frac{i}{2\Delta t(\Delta x)^d}\left(1 + 2\frac{\tilde{\rho}-2n}{\tilde{\rho}-4n}\right) \tag{5.26}$$

and

$$\tilde{B} = -\frac{q^2}{8c_1} - \frac{i}{2\Delta t(\Delta x)^d}\left(\frac{1}{2} + 2\left(\frac{\tilde{\rho}-2n}{\tilde{\rho}-4n}\right)^2\right). \tag{5.27}$$

For the final step, we want to write the theory for φ_S such that the trigonometric functions all take the same argument. For that, we use the relations

$$\sin^2(\varphi/2) = -\frac{1}{2}\cos(\varphi) + \frac{1}{2} \tag{5.28}$$

and

$$\sin^4(\varphi/2) = -\frac{1}{2}\cos(\varphi) - \frac{1}{4}\sin^2(\varphi) + \frac{1}{2}, \tag{5.29}$$

and find for the effective Lagrangian for the spinor phase

$$\begin{aligned}\mathcal{L}^{\text{eff}}_{\varphi_S} = &-\frac{1}{32c_1}\dot{\varphi}_S^2 - \frac{\tilde{\rho}-2n}{8m}(\nabla\varphi_S)^2 - A\cos\varphi_S + B\sin^2\varphi_S \\ &+ \mathcal{O}\left(\sin^6, \dot{\varphi}\sin^2, \nabla\varphi\sin^2, \dot{\varphi}\nabla^2\varphi, \nabla^3\varphi\right)\end{aligned} \tag{5.30}$$

with

$$A = 2c_1 n(\tilde{\rho}-2n) - \frac{q^2}{16c_1} - \frac{i}{4\Delta t(\Delta x)^d}\left(\frac{3}{2} + \frac{2(\tilde{\rho}-2n)}{(\tilde{\rho}-4n)} + \frac{2(\tilde{\rho}-2n)^2}{(\tilde{\rho}-4n)^2}\right) \tag{5.31}$$

and

$$B = \frac{q^2}{32c_1} + \frac{i}{8\Delta t(\Delta x)^d}\left(\frac{1}{2} + \frac{2(\tilde{\rho}-2n)^2}{(\tilde{\rho}-4n)^2}\right). \tag{5.32}$$

Let us take a closer look and interpret the theories we have obtained for φ_S and φ_L. The Lagrangian for the Larmor phase Eq. (5.24) is that of a free theory. This makes sense as φ_L is the Goldstone boson corresponding to the spontaneous symmetry breaking of the $SO(2)$ symmetry by Eq. (2.32), and we can associate the massless Bogoliubov mode E_- (see Eq. (2.59)) with it. Thus, if we go back to Fig. 2.4, a free theory for φ_L means a free rotation of $F_\perp$ in the spin sphere.

The Lagrangian for φ_S Eq. (5.31) is more complicated. In the approximation of small φ_S, the periodic potential with divergences at $\varphi_S = \pi + 2\pi\mathbb{Z}$ turns into a sine-Gordon type theory with a $\sin^2$-term in the potential along with the cos-term. This theory is regular as for $\varphi_S \approx 2\pi\mathbb{Z}$, the theory does not "see" the divergences. The real part of the potential for φ_S as in Eq. (5.31) is pictured in Fig. 5.2a. As this figure shows the potential not only near $\varphi_S = 2\pi\mathbb{Z}$ but also for values of φ_S for which the approximations made in the derivation do not hold, this illustration should be taken with a grain of salt. However, it gives a good intuition of the periodicity of

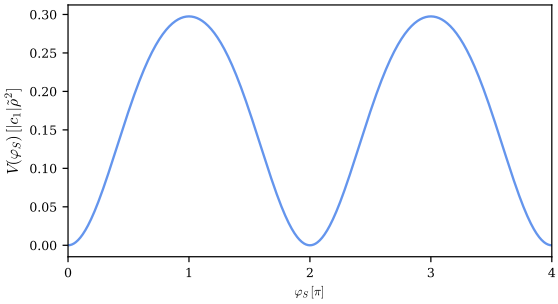

(a) Real part of the potential for φ_S as in Eq. (5.31) in units of $|c_1|\tilde{\rho}^2$. We have used $q = -0.9\tilde{\rho}c_1$ to compare with the experiment and numerical simulations.

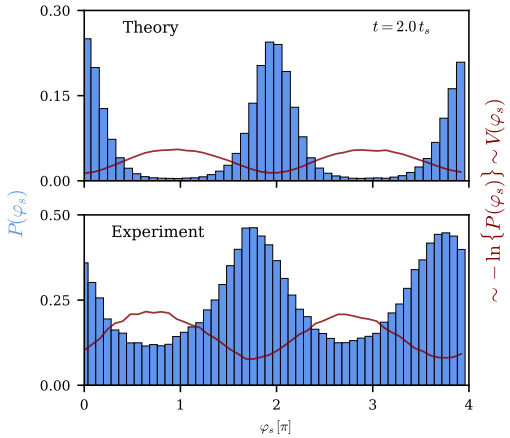

(b) Experimental and numerical data showing the potential of φ_S. For the numerical simulation, $q = -0.9\tilde{\rho}c_1$ was used [84].

Figure 5.2.: Comparison of the analytical form of the potential for φ_s as in Eq. (5.31) with numerical and experimental results of the (1+1)d spin-1 Bose gas.

the potential for φ_S.

If we compare this potential to results from the experiment as well as numerical simulations [84], which are shown in Fig. 5.2b, we see the same 2π periodicity, and as most numerical datapoints are around $\varphi_S = 2\pi\mathbb{Z}$ with close to none at $\varphi_S = (2\mathbb{Z}+1)\,\pi$, our assumption of small φ_S seems to describe most of the dynamics well[2].

However, there has to be some mechanism allowing to hop between the minima, as several minima are populated in the experiment and the simulations and this hopping of 2π in the phase φ_S then also causes the phase of $F_\perp$, or the Larmor phase as defined in Eq. (2.38), to jump by 2π, as can be seen in Fig. 2.4. Thus, jumps between the minima of the periodic potential of φ_S correspond to the (anti)-instantons seen in the numerical simulations in [41]. As the theory developed in this chapter loses its validity around the maxima, we cannot use it, however, to study what exactly happens for the phase degrees of freedom at these (anti)-instantons. Thus, the next two chapters will focus on improving the low-energy effective theory developed here in order to also describe what is happening at the maxima of the potential.

Before we get into this, we want to make one more comment about the imaginary part of the effective action. In Fig. 5.2a, we have only shown the real part of the potential. However, as

[2]Note that the plateaus in the experimental data around $\varphi_S = (2\mathbb{Z}+1)\,\pi$ are only due to the experiment not purely measuring the phase φ_S but the orientation of the field in the $\hat{F}_x - \hat{Q}_{yz}$-plane, which leads to plateaus at the minima.

Eq. (5.31) shows, there is a non-negligible part to $\mathcal{L}^{\text{eff}}$, namely

$$\begin{aligned}\Im\mathcal{L}^{\text{eff}}_{\varphi_S} =&\frac{1}{4\Delta t(\Delta x)^d}\left[\left(\frac{3}{2}+\frac{2(\tilde{\rho}-2n)}{(\tilde{\rho}-4n)}+\frac{2(\tilde{\rho}-2n)^2}{(\tilde{\rho}-4n)^2}\right)\cos\varphi_S+\left(\frac{1}{4}+\frac{(\tilde{\rho}-2n)^2}{(\tilde{\rho}-4n)^2}\right)\sin^2\varphi_S\right]\\&+\text{const.}+\mathcal{O}(\sin^6).\end{aligned} \tag{5.33}$$

For $|\varphi_S| \mod 2\pi < \pi/2$, which holds in the approximation of small $\sin^2\varphi_S$, this imaginary part is strictly positive, such that multiplied with i this term simply gives a damping of the partition function. In the following, we will, therefore, mainly focus on the real part of the effective action.

5.2. Mass gap of the effective theory

For even more sanity checks on the applicability of our low-energy effective field theory, we want to compare the dispersion relation and specifically the mass gap of our effective theory for φ_S with numerical results from truncated Wigner simulations of the full spin-1 Bose gas in (1+1)d. To derive the analytical form for the dispersion relation, let us first consider the equations of motion that follow from just the real part of the action

$$\Re\mathcal{L}^{\text{eff}}_{\varphi_S} = -\frac{1}{32c_1}\dot{\varphi}_S^2-\frac{\tilde{\rho}-2n}{8m}(\nabla\varphi_S)^2-\left[2c_1n(\tilde{\rho}-2n)-\frac{q^2}{16c_1}\right]\cos\varphi_S+\frac{q^2}{32c_1}\sin^2\varphi_S,$$

which are given by

$$-\frac{\ddot{\varphi}_S}{16c_1}=\frac{\tilde{\rho}-2n}{4m}\nabla^2\varphi_S+\left[2c_1n(\tilde{\rho}-2n)-\frac{q^2}{16c_1}\right]\sin\varphi_S+\frac{q^2}{16c_1}\sin\varphi_S\cos\varphi_S. \tag{5.34}$$

To obtain a dispersion relation from this equation, we first expand sine and cosine to the first order in φ_S:

$$-\frac{\ddot{\varphi}_S}{16c_1}=\frac{\tilde{\rho}-2n}{4m}\nabla^2\varphi_S+2c_1n(\tilde{\rho}-2n)\varphi_S. \tag{5.35}$$

Now we perform a 2d Fourier transform, yielding the following dispersion relation:

$$\frac{\omega^2}{16c_1}=-\frac{\tilde{\rho}-2n}{4m}k^2+2c_1n(\tilde{\rho}-2n) \tag{5.36}$$

Thus, for $k=0$ we obtain the mass gap

$$m_{\text{GAP}}=\sqrt{32c_1^2n(\tilde{\rho}-2n)} \tag{5.37}$$

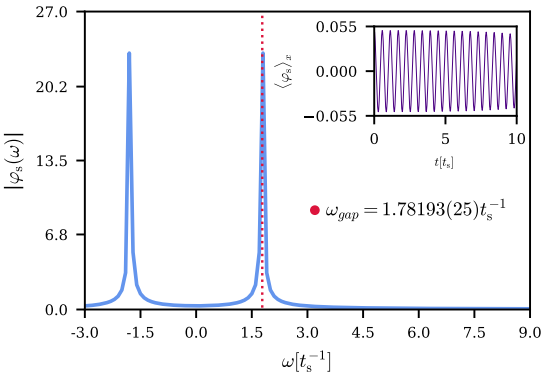

(a) Numerical results for the Fourier spectrum of an oscillation of the spinor phase after a rotation $\Psi_{\pm1} \to \Psi_{\pm1}e^{\pm i\alpha}$ with $\alpha = 0.032\pi$. The simulations were performed via truncated Wigner simulations of the full (1+1)d spin-1 Bose gas at $q = -0.9c_1\tilde{\rho}$. The blue lines show the Fourier spectrum, while the inlay shows the oscillation of φ_S. The red dotted line represents the fit result for the mass gap from the oscillation via fitting a function $a\cos(\omega t)$.

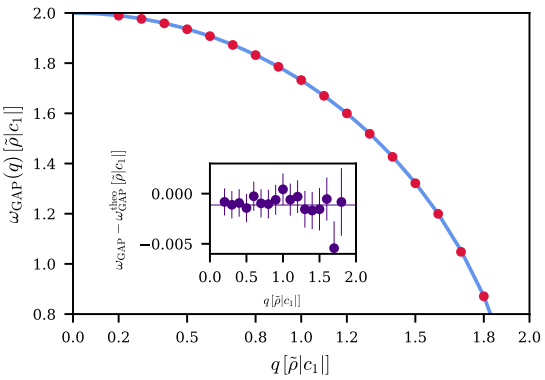

(b) Numerical results (red) for the mass gap of the spinor phase dispersion relation compared to the analytic result from the Bogoliubov relation as well as the effective theory (blue). The numerical values have been computed with truncated Wigner simulations of the full spin-1 gas, while the analytical curve follows Eq. (5.37). The inset shows the difference between analytic and numerical results.

Figure 5.3.: Mass gap of the spinor phase in the (1+1)d spin-1 Bose gas.

This coincides with the mass gap from the E_+ Bogoliubov dispersion relation Eq. (2.59), which for $k = 0$ becomes

$$E_{+1} = 2\sqrt{1 - \frac{q^2}{(2\tilde{\rho}|c_1|)^2}}|c_1|\tilde{\rho}. \tag{5.38}$$

Using $q = -2c_1(\tilde{\rho} - 4n)$ (Eq. (2.35)), this exactly gives our analytical mass gap Eq. (5.37).

To compare this to numerical results, we have carried out truncated Wigner simulations of the (1+1)d spin-1 Bose gas in the easy-plane phase with $q = -0.9c_1\tilde{\rho}$. To introduce a small perturbation to the system, we performed a rotation of the spinor phase $\Psi_{\pm1} \to \Psi_{\pm1}e^{\pm i\alpha}$ with $\alpha = 0.032\pi$, giving rise to an oscillatory behavior of the spinor phase as shown in the inlay of Fig. 5.3a. The Fourier spectrum shown in the same figure exhibits two clear peaks corresponding to the oscillation frequency $\omega = 1.78193(25)\tilde{\rho}|c_1|$ as well as its negative. The frequency was determined to this precision via a fit to the data with the function $f(t) = a\sin\omega t$ up until $t = 2.4\,t_S$. This value is only slightly smaller than the analytically determined mass gap for $q = -0.9c_1\tilde{\rho}$, which is given by $\omega = 1.78606\tilde{\rho}|c_1|$.

Repeating this numerical determination of ω_{GAP} for different q, we also find good agreement with the functional q-dependence of the theoretical prediction Eq. (5.37) as shown in Fig. 5.3b.

Note, however, that the inset in Fig. 5.3b shows the numerical values to be systematically lower than the theoretical prediction. Though this systematic shift is still within the error bars of the numerical values, it is interesting to examine whether this shift could be compensated by including higher-order density fluctuation corrections to the effective action.

6. Including higher-order density fluctuations

Given the problem that at $k = 0$ and $\varphi_S = (2\mathbb{Z} + 1)\pi$ our low-energy effective field theory becomes divergent, we want to investigate in this chapter whether this divergence is intrinsic to the theory or if this issue can be fixed by including higher orders in the fluctuations, which may stabilize the theory. Thus, in Sec. 6.1, we include higher orders of the density fluctuations $\delta\rho$ and $\delta\varepsilon$ into our theory in the spirit of the Hartree-Fock-Bogoliubov-Popov approximation. This then leads us to a self-consistent equation for the fluctuation correlations $\langle\delta\rho(\boldsymbol{x}, t)\delta\rho(\boldsymbol{x}, t)\rangle$ and $\langle\delta\varepsilon(\boldsymbol{x}, t)\delta\varepsilon(\boldsymbol{x}, t)\rangle$ in Sec. 6.3. However, as it turns out, including higher orders of fluctuations like that will not rid our effective theory of the divergences at $k = 0$ and $\varphi_s = (2\mathbb{Z} + 1)\,\pi$. This will be discussed in Sec. 6.1.1. Still, the density fluctuation corrections lead to a change in our theory for small angles φ_S, which will be derived in Sec. 6.2. For this theory, we again calculate the mass gap analytically in Sec. 6.4, which we compare to the numerical results from Ch. 5 in Sec. 6.6 after numerically investigating the density fluctuation correlations $\langle\delta\rho(\boldsymbol{x}, t)\delta\rho(\boldsymbol{x}, t)\rangle$ and $\langle\delta\varepsilon(\boldsymbol{x}, t)\delta\varepsilon(\boldsymbol{x}, t)\rangle$ in Sec. 6.5. We find that, while the density fluctuation corrections cause a slight shift of the analytic values for the mass gap towards the numerical ones at high q, the effect is not significant.

6.1. A higher-order expansion in the density fluctuations

In order to obtain a low-energy effective field theory for φ_S including higher orders in the density fluctuations, we again perform the coordinate transformation and expansion as in Sec. 5.1 at first. However, instead of just expanding to the second order in the density fluctuations as in Eq. (5.7), we expand the Lagrangian to the fourth order

$$\mathcal{L} = \mathcal{L}^0 + \mathcal{L}^1 + \mathcal{L}^2 + \mathcal{L}^3 + \mathcal{L}^4 + \mathcal{O}(\delta\boldsymbol{\rho}^5) \tag{6.1}$$

with

$$\mathcal{L}^0 = -\frac{n}{4m}(\nabla\varphi_L)^2 - \frac{\tilde{\rho}-2n}{8m}(\nabla\varphi_S)^2 - 2c_1 n(\tilde{\rho}-2n)(1+\cos\varphi_S) \tag{6.2}$$

$$\mathcal{L}^1 = \begin{pmatrix} \dot{\varphi}_S - 2q - \frac{1}{4m}\left((\nabla\varphi_L)^2 - (\nabla\varphi_S)^2\right) - 2c_1(\tilde{\rho}-4n)(1+\cos\varphi_S) \\ -\dot{\varphi}_L \end{pmatrix} \begin{pmatrix} \delta\rho \\ \delta\varepsilon \end{pmatrix} \tag{6.3}$$

$$\mathcal{L}^2 = \begin{pmatrix} \delta\rho & \delta\varepsilon \end{pmatrix} \begin{pmatrix} \frac{\tilde{\rho}}{\tilde{\rho}-2n}\frac{\nabla^2}{4mn} + 4c_1(1+\cos\varphi_S) & 0 \\ 0 & \frac{\nabla^2}{4mn} - c_1\left(2 + \left(2-\frac{\tilde{\rho}}{n}\right)\cos\varphi_S\right) \end{pmatrix} \begin{pmatrix} \delta\rho \\ \delta\varepsilon \end{pmatrix} \tag{6.4}$$

$$\mathcal{L}^3 = -\frac{c_1\tilde{\rho}}{n^2}\delta\rho\delta\varepsilon^2\cos\varphi_S \tag{6.5}$$

$$\mathcal{L}^4 = \frac{c_1}{4}\frac{\tilde{\rho}-2n}{n^3}\delta\varepsilon^4\cos\varphi_S + \frac{c_1\tilde{\rho}}{n^3}\delta\rho^2\delta\varepsilon^2\cos\varphi_S, \tag{6.6}$$

where we have again neglected terms involving $\nabla\theta$ as well as all terms the order of $\nabla^2\delta^3$ and $\nabla^2\delta^4$ in $\mathcal{L}^3$ and $\mathcal{L}^4$, respectively, that appear when expanding the density derivative parts as shown in App B.2. The argument for the latter is again that the low momenta we consider make these terms irrelevant, as even the spin healing momentum only amounts to $k_{\xi_S} = 1/\xi_S = \sqrt{2m\tilde{\rho}|c_1|}$.

To still be able to perform a Gaussian integration and get rid of the functional dependence on $\delta\rho$ and $\delta\varepsilon$, we further expand the terms of third and fourth order in the fluctuations around the average density-density correlations

$$\delta\rho\delta\varepsilon^2 = \delta\rho\langle\delta\varepsilon\delta\varepsilon\rangle + 2\delta\varepsilon\langle\delta\rho\delta\varepsilon\rangle \tag{6.7}$$

$$\delta\varepsilon^4 = 6\langle\delta\varepsilon\delta\varepsilon\rangle\delta\varepsilon^2 \tag{6.8}$$

$$\delta\rho^2\delta\varepsilon^2 = \langle\delta\rho\delta\rho\rangle\delta\varepsilon^2 + \langle\delta\varepsilon\delta\varepsilon\rangle\delta\rho^2 + 4\langle\delta\rho\delta\varepsilon\rangle\delta\rho\delta\varepsilon. \tag{6.9}$$

For an interpretation of these correlators, let us remind ourselves that $\delta\varepsilon$ describes the difference between the densities of the $m_F = -1$ and $m_F = 1$ component while $\delta\rho$ corresponds to the fluctuation of the depletion of the $m_F = 0$ component around the mean-field value. Thus, the correlators that appear in the expansions Eq. (6.9) are the expectation values of products of these differences and depletions at some space-time point $(\boldsymbol{x}, t)$. This space-time dependence comes from the s-wave interactions being local in space and time.

Carrying out this expansion around the correlators, we again have a quadratic Lagrangian

$$\mathcal{L} = \mathcal{L}^0 + \mathcal{L}^1_{\text{fluc}} + \mathcal{L}^2_{\text{fluc}} + \mathcal{O}(\delta\rho^5) = \mathcal{L}^0 + \boldsymbol{\delta\rho}^T\boldsymbol{J}_{\mathbf{0}\text{fluc}} + \frac{1}{2}\boldsymbol{\delta\rho}^T\boldsymbol{G}^{-1}_{\mathbf{0}\text{fluc}}\cdot\boldsymbol{\delta\rho} \tag{6.10}$$

with

$$\boldsymbol{J}_{\mathbf{0}\text{fluc}} = \begin{pmatrix} \dot{\varphi}_S - 2q - \frac{1}{4m}\left((\nabla\varphi_L)^2 - (\nabla\varphi_S)^2\right) - 2c_1(\tilde{\rho} - 4n)(1+\cos\varphi_S) - \frac{c_1\tilde{\rho}}{n^2}\langle\delta\varepsilon\delta\varepsilon\rangle\cos\varphi_S \\ -\dot{\varphi}_L - \frac{2c_1\tilde{\rho}}{n^2}\langle\delta\rho\delta\varepsilon\rangle\cos\varphi_S \end{pmatrix} \tag{6.11}$$

and

$$\boldsymbol{G}_{\mathbf{0}\text{fluc}}^{-1} = \begin{pmatrix} G_{11} & G_{12} \\ G_{21} & G_{22} \end{pmatrix} \tag{6.12}$$

with

$$\begin{aligned} G_{11} &= \frac{\tilde{\rho}}{\tilde{\rho}-2n}\frac{\nabla^2}{2mn} + 8c_1(1+\cos\varphi_S) + \frac{2c_1\tilde{\rho}}{n^3}\langle\delta\varepsilon\delta\varepsilon\rangle\cos\varphi_S \\ G_{22} &= \frac{\nabla^2}{4mn} - 2c_1\left(2 + \left(2 - \frac{\tilde{\rho}}{n}\right)\cos\varphi_S\right) + \frac{2c_1\tilde{\rho}}{n^3}\langle\delta\rho\delta\rho\rangle\cos\varphi_S + 3c_1\frac{\tilde{\rho}-2n}{n^3}\langle\delta\varepsilon\delta\varepsilon\rangle\cos\varphi_S \\ G_{12} &= G_{21} = \frac{4c_1\tilde{\rho}}{n^3}\langle\delta\rho\delta\varepsilon\rangle\cos\varphi_S. \end{aligned} \tag{6.13}$$

Note that against our hopes, $\boldsymbol{G}_{\mathbf{0}\text{fluc}}$ is not regularized by $\langle\delta\varepsilon\delta\varepsilon\rangle$ and $\langle\delta\rho\delta\rho\rangle$ for $k = 0$. Instead, $\boldsymbol{G}_{\mathbf{0}\text{fluc}}$ now becomes singular at twice as many points places if $k = 0$, namely at

$$\varphi_S^{\text{divergence}} = \pm\arccos\left(-1 - \frac{\tilde{\rho}}{4n^3}\langle\delta\varepsilon\delta\varepsilon\rangle\right)^{-1} + 2\mathbb{Z}\pi. \tag{6.14}$$

Moreover, as all density fluctuation corrections entering the action like this will multiply $\cos\varphi_S$, no order of such corrections will stabilize the theory at the divergences.

6.1.1. A note on the divergences

To make sense of these divergences, let us look at mean-field dynamics on the spin-nematic sphere spanned by $\{F_x, Q_{yz}, Q_{z^2-y^2}\}$. Of course the mean-field dynamics on this sphere, for which we will assume $F_z = 0$ and $\varphi_L = 0$ for simplicity, cannot give us a full picture of what is happening. However, it can help us develop an intuition about why the divergences occur at $\varphi_S = (2\mathbb{Z}+1)\,\pi$ if we ignore the kinetic part of the inverse free propagator.

In Fig. 6.1, the mean-field dynamics on a sphere spanned by $\{F_x, Q_{yz}, Q_0\}$, where Q_0 only differs by a constant term from $Q_{z^2-y^2}$ in the mean-field approximation and for $\varphi_L = 0$[86][1]. We see in the right panel of Fig. 6.1 that the Hamiltonian generates dynamics of the mean field in which either the system stays in a self-trapping region (red), in which φ_S fluctuates around 0, or it has a wrap-around trajectory on which the spinor phase can change by 2π. Experimental

[1]Note that in the easy-plane phase, $\{F_x, Q_{yz}, Q_0\}$ also span a representation of $SU(2)$ as long as $\varphi_L = 0$ and the system is in the easy-plane phase.

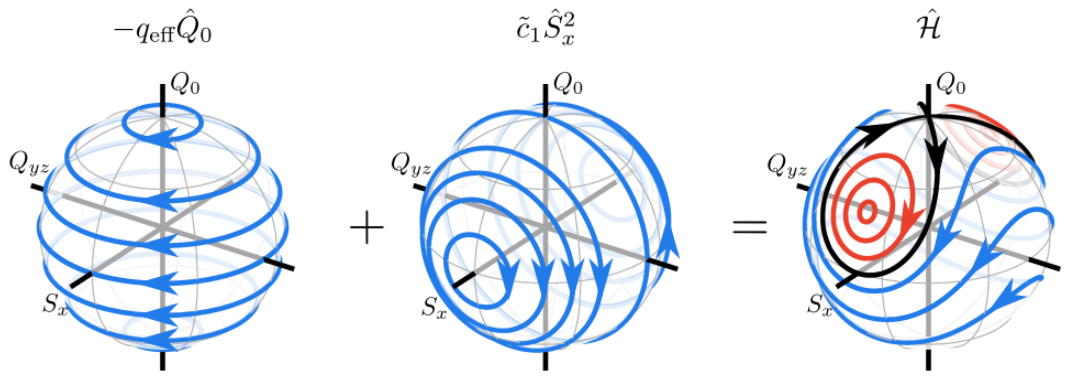

Figure 6.1.: Mean-field dynamics on the spin-nematic sphere, taken from [86]. Neglecting the kinetic terms in Eq. (2.5), we find that, up to irrelevant constants $\propto q\tilde{\rho}$ and $\propto c_0/2\tilde{\rho}^2$, the Hamiltonian is given by $\hat{H} = -q\hat{Q}_0 + c_1/2 : \left(\hat{F}_x^2 + \hat{F}_y^2 + \hat{F}_z^2\right) :$ where we have defined $\hat{Q}_0 = \hat{n}_0 - \hat{n}_1 - \hat{n}_{-1}$. If we are in the easy-plane phase such that $F_z = 0$ and assume zero Larmor phase, i.e. $F_y = 0$, we find that the mean-field dynamics can be illustrated on this spin-nematic sphere, with the quadratic Zeeman shift generating rotations around the Q_0-axis and the $c_1/2F_x^2$ term rotations around the F_x-axis. Thus, in total, the mean-field dynamics in the easy-plane phase can be illustrated as the trajectories on the right sphere, with some self-trapping regions (red) and wrap-around modes (blue) separated by a separatrix (black).

and numerical data showing us that the spinor phase φ_S is around multiples of 2π for most of the time corresponds to the system and, especially, the mean field being located in one of the self-trapping regions. We also note that in the mean-field approximation, $\langle\hat{Q}_0\rangle = \tilde{\rho} - 4n$. Given this information combined with the picture of the dynamics on the nematic sphere, it makes sense that fluctuation modes $\delta\rho(k)$ with $k \neq 0$ above the mean field are necessary to leave the self-trapping region and go into a wrap-around trajectory and, thus, enable φ_S to cross $(2\mathbb{Z}+1)\,\pi$ as such a fluctuation can lower Q_0.

Thus, the divergence of the theory simply tells us that we require non-zero momentum for the density fluctuation $\delta\rho$ to populate a wrap-around trajectory and "hop" from one potential minimum to the other.

6.2. Expansion around $\varphi_S = 2\pi\mathbb{Z}$

Let us still continue to investigate this improved theory around $\varphi_S = 2\pi\mathbb{Z}$ for the sake of including higher-order density fluctuation corrections in the coefficients of Eqs. (5.24) and (5.31), which could potentially diminish the differences between analytics and numerical simulations in Fig. 5.3b.

As we assume small φ_S around $\varphi_S = 2\pi\mathbb{Z}$, we can again neglect all terms $\mathcal{O}(k^2\delta^2)$ as we are far from the divergences, such that the ∇^2-terms in $\boldsymbol{G_0}^{-1}$ vanish. Moreover, because numerical simulations show that the cross-density correlator $\langle\delta\varepsilon\delta\rho\rangle$ is several orders of magnitude smaller than the already small $\langle\delta\varepsilon\delta\varepsilon\rangle$ and $\langle\delta\rho\delta\rho\rangle$, we will also neglect the off-diagonal parts of $\boldsymbol{G}_{\mathbf{0}\text{fluc}}^{-1}$ (note that approximation is very similar to the Hartree-Fock-Bogoliubov-Popov approximation in Sec. 4.3.1). With these approximations, we find

$$\begin{aligned}
&\frac{1}{2}\boldsymbol{J}_{\mathbf{0}\text{ fluc}}^{\boldsymbol{T}}\boldsymbol{G}_{\mathbf{0}\text{fluc}}\boldsymbol{J}_{\mathbf{0}\text{fluc}} \qquad (6.15)\\
=&\frac{1}{2}\left[\frac{n^3\left(\dot{\varphi}_L\right)^2}{-2n^2c_1(2n+(2n-\tilde{\rho})\cos\varphi_S)+3c_1(\tilde{\rho}-2n)\langle\delta\varepsilon\delta\varepsilon\rangle\cos\varphi_S+2c_1\tilde{\rho}\langle\delta\rho\delta\rho\rangle\cos\varphi_S}\right.\\
&\left.+\frac{\left(\dot{\varphi}_S-2q-\frac{(\nabla\varphi_L)^2-(\nabla\varphi_S)^2}{4m}-2c_1(\tilde{\rho}-4n)(1+\cos\varphi_S)-\frac{c_1\tilde{\rho}}{n^2}\langle\delta\varepsilon\delta\varepsilon\rangle\cos\varphi_S\right)^2}{8c_1(1+\cos\varphi_S)+\frac{2c_1\tilde{\rho}}{n^3}\langle\delta\varepsilon\delta\varepsilon\rangle\cos\varphi_S}\right],
\end{aligned}$$

and, thus,

$$\begin{aligned}
\Re\mathcal{L}^{\text{eff}} =& -\frac{n}{4m}\left(\nabla\varphi_L\right)^2-\left(\frac{\tilde{\rho}-2n}{8m}\right)\left(\nabla\varphi_S\right)^2-2c_1n(\tilde{\rho}-2n)\cos\varphi_S \qquad (6.16)\\
&-\frac{1}{2}\left[\frac{n^3\dot{\varphi}_L^2}{-2n^2c_1(2n+(2n-\tilde{\rho})\cos\varphi_S)+3c_1(\tilde{\rho}-2n)\langle\delta\varepsilon\delta\varepsilon\rangle\cos\varphi_S+2c_1\tilde{\rho}\langle\delta\rho\delta\rho\rangle\cos\varphi_S}\right.\\
&\left.+\frac{\left(\dot{\varphi}_S-2q-\frac{(\nabla\varphi_L)^2-(\nabla\varphi_S)^2}{4m}-2c_1(\tilde{\rho}-4n)(1+\cos\varphi_S)-\frac{c_1\tilde{\rho}}{n^2}\langle\delta\varepsilon\delta\varepsilon\rangle\cos\varphi_S\right)^2}{8c_1(1+\cos\varphi_S)+\frac{2c_1\tilde{\rho}}{n^3}\langle\delta\varepsilon\delta\varepsilon\rangle\cos\varphi_S}\right].
\end{aligned}$$

Here, we have omitted the imaginary part because, just like in the last chapter, we want to focus on the real part as the imaginary part only contributes to a damping of the partition function. A detailed discussion of the imaginary part can be found in App. C.1.

We will now expand around $\varphi_S \approx 2\pi\mathbb{Z}$ again up to order $\sin^4\frac{\varphi_S}{2}$ and neglect any terms of the order of $\dot{\varphi}_i\sin^2\frac{\varphi_S}{2}$ and $(\nabla\varphi_i)^2\sin^2\frac{\varphi_S}{2}$ as well as any terms involving three or more derivatives. Moreover, we will only include linear orders in the fluctuations. Performing this expansion, as well as using the relations Eqs. (5.28) and (5.29), we again find that the theories for φ_L and φ_S decouple. The effective Lagrangian for φ_L is obtained as

$$\begin{aligned}
\mathcal{L}_{\varphi_L}^{\text{eff}} =& -\frac{{\dot{\varphi_L}}^2}{-2\frac{q}{n}+6c_1\frac{\tilde{\rho}-2n}{n3}\langle\delta\varepsilon\delta\varepsilon\rangle+4c_1\frac{\tilde{\rho}}{n^3}\langle\delta\rho\delta\rho\rangle}-\left[\frac{n}{4m}+\frac{\tilde{\rho}}{64mn^2c_1}\langle\delta\varepsilon\delta\varepsilon\rangle\right]\left(\nabla\varphi_L\right)^2\\
&+\mathcal{O}(\langle\delta\delta\rangle^2,\dot{\varphi}\sin^2,\nabla\varphi\sin^2,\dot{\varphi}\nabla^2\varphi,\nabla^3\varphi). \qquad (6.17)
\end{aligned}$$

Meanwhile, the real part of the effective Lagrangian for φ_S is given by

$$\begin{aligned}\Re\mathcal{L}^{\text{eff}}_{\varphi_S} =& -\frac{\dot{\varphi}_S^2}{32c_1\left(1+\frac{\tilde{\rho}}{8n^3}\langle\delta\varepsilon\delta\varepsilon\rangle\right)}+\frac{\tilde{\rho}}{16n^2}\langle\delta\varepsilon\delta\varepsilon\rangle\dot{\varphi}_S \\ &-\left[\frac{\tilde{\rho}-2n}{8m}-\frac{\tilde{\rho}}{64mn^2}\langle\delta\varepsilon\delta\varepsilon\rangle\right](\nabla\varphi_S)^2 - A_R\cos\varphi_S + B_R\sin^2\varphi_S \\ &+\text{const.}+\mathcal{O}(\langle\delta\delta\rangle^2,\sin^6,\dot{\varphi}\sin^2,\nabla\varphi\sin^2,\dot{\varphi}\nabla^2\varphi,\nabla^3\varphi)\end{aligned} \tag{6.18}$$

where

$$A_R = 2c_1 n(\tilde{\rho}-2n)-\frac{q^2}{16c_1}-\frac{q^2\tilde{\rho}}{128c_1n^3}\langle\delta\varepsilon\delta\varepsilon\rangle \tag{6.19}$$

and

$$B_R = \frac{q^2}{32c_1}-\frac{q^2\tilde{\rho}}{128c_1n^3}\langle\delta\varepsilon\delta\varepsilon\rangle-\frac{q\tilde{\rho}}{32n^2}\langle\delta\varepsilon\delta\varepsilon\rangle \tag{6.20}$$

The details of this calculation can be found in App. B.3.

These Lagrangians of course reduce to Eqs. (5.24) and Eq. (5.31), respectively, when we set $\langle\delta\varepsilon\delta\varepsilon\rangle$ and $\langle\delta\rho\delta\rho\rangle$ to zero. Moreover, the type of Lagrangians has not changed, with $\mathcal{L}^{\text{eff}}_{\varphi_L}$ still describing a free theory and $\mathcal{L}^{\text{eff}}_{\varphi_S}$ a sine-squared-Gordon model. Nevertheless, if sufficiently large, the density fluctuation expectation values may significantly change the order of magnitude of the coefficients of the Lagrangian, and, therefore, also change the non-thermal RG flow of the theory.

6.3. Self-consistent equations for the density fluctuations

We note that for our expansion Eq. (6.9) and the effective theories Eq. (6.17) and (6.18) to be self-consistent, the correlation functions involving $\delta\rho$ and $\delta\varepsilon$ at equal space and time have to fulfill the equation

$$\langle\boldsymbol{\delta\rho}_i\boldsymbol{\delta\rho}_j\rangle = \frac{\delta^2}{i\delta\boldsymbol{J}_i i\delta\boldsymbol{J}_j}\frac{\tilde{Z}[\boldsymbol{J}]}{\tilde{Z}[0]}\bigg|_{\boldsymbol{J}=0} \tag{6.21}$$

with

$$\tilde{Z}[\boldsymbol{J}] = \int\mathcal{D}\delta\rho\mathcal{D}\delta\varepsilon\mathcal{D}\varphi_S\mathcal{D}\varphi_L e^{i\int_{t,x}\mathcal{L}^0_{\text{fluc}}+\boldsymbol{\delta\rho}^T\boldsymbol{J}_{\mathbf{0}\text{fluc}}+\frac{1}{2}\boldsymbol{\delta\rho}^T\boldsymbol{G}^{-1}_{\mathbf{0}\text{fluc}}\boldsymbol{\delta\rho}+\boldsymbol{J}^T\boldsymbol{\delta\rho}} \tag{6.22}$$

$$= C\int\mathcal{D}\varphi_S\mathcal{D}\varphi_L e^{i\int_{t,x}\left[\mathcal{L}-\frac{1}{2}(\boldsymbol{J}_{\mathbf{0}\text{fluc}}+\boldsymbol{J})^T\boldsymbol{G}_{\mathbf{0}\text{fluc}}(\boldsymbol{J}_{\mathbf{0}\text{fluc}}+\boldsymbol{J})\right]-\frac{1}{2}\log\det\boldsymbol{G}^{-1}_{\mathbf{0}\text{fluc}}}, \tag{6.23}$$

where we have again used the notation $\boldsymbol{\delta\rho} = (\delta\rho, \delta\varepsilon)^T$.

Applying the functional derivatives to this, we find for the self-consistent equations

$$\boldsymbol{G}_{\mathbf{0}\text{fluc},ij}(\langle\boldsymbol{\delta\rho}\boldsymbol{\delta\rho}\rangle) = \langle\boldsymbol{\delta\rho}_i\boldsymbol{\delta\rho}_j\rangle. \tag{6.24}$$

As $\boldsymbol{G}_{\mathbf{0}\text{fluc}}$ also includes $\langle\boldsymbol{\delta\rho}_i\boldsymbol{\delta\rho}_j\rangle$, Eq. (6.24) can only be solved perturbatively, and such a solution would exceed the scope of this work. Instead, we turn to numerical simulations to determine the numerical values for the full propagators $\langle\delta\rho\delta\rho\rangle$ and $\langle\delta\varepsilon\delta\varepsilon\rangle$ in Sec. 6.5.

6.4. Mass Gap of the Effective Theory

Like in Ch. 5, we again want to compare the mass gap of the effective theory for φ_S against numerical simulations. Including the $\langle\delta\varepsilon\delta\varepsilon\rangle$ corrections but still neglecting the imaginary parts, the equation of motion for φ_S with density fluctuation corrections becomes, neglecting the time dependence for $\langle\delta\varepsilon\delta\varepsilon\rangle$ as it is very slow (see Sec. 6.5),

$$\begin{aligned}
&-\frac{\ddot{\varphi}_S}{16c_1\left(1+\frac{\tilde{\rho}}{8n^3}\langle\delta\varepsilon\delta\varepsilon\rangle\right)} \\
&= \left(\frac{\tilde{\rho}-2n}{4m} - \frac{\tilde{\rho}}{32mn^2}\langle\delta\varepsilon\delta\varepsilon\rangle\right)\nabla^2\varphi_S + A_R\sin\varphi_S + 2B_R\sin\varphi_S\cos\varphi_S \\
&\approx \left(\frac{\tilde{\rho}-2n}{4m} - \frac{\tilde{\rho}}{32mn^2}\langle\delta\varepsilon\delta\varepsilon\rangle\right)\nabla^2\varphi_S + [A_R+2B_R]\varphi_S \\
&= \left(\frac{\tilde{\rho}-2n}{4m} - \frac{\tilde{\rho}}{32mn^2}\langle\delta\varepsilon\delta\varepsilon\rangle\right)\nabla^2\varphi_S + \left[2c_1n(\tilde{\rho}-2n) - \frac{3q^2\tilde{\rho}}{128c_1n^3}\langle\delta\varepsilon\delta\varepsilon\rangle - \frac{q\tilde{\rho}}{16n^2}\langle\delta\varepsilon\delta\varepsilon\rangle\right]\varphi_S,
\end{aligned} \tag{6.25}$$

where we have again linearized the equation of motion in the second step. Thus, the mass gap corrected by fluctuations to leading order in the latter is given by

$$m_{\text{GAP}} = \sqrt{32c_1^2n(\tilde{\rho}-2n) + 6\frac{\tilde{\rho}^2c_1^2}{n^2}\langle\delta\varepsilon\delta\varepsilon\rangle - 16\frac{\tilde{\rho}c_1^2}{n}\langle\delta\varepsilon\delta\varepsilon\rangle - \frac{3}{8}\frac{\tilde{\rho}q^2}{n^3}\langle\delta\varepsilon\delta\varepsilon\rangle}, \tag{6.26}$$

or, as a function of only q and $\langle\delta\varepsilon\delta\varepsilon\rangle$,

$$m_{\text{GAP}} = \sqrt{4\left(1-\frac{q^2}{(2\tilde{\rho}|c_1|)^2}\right) - \frac{64\langle\delta\varepsilon\delta\varepsilon\rangle}{\tilde{\rho}^2\left(1-\frac{q}{2\tilde{\rho}|c_1|}\right)} + \frac{96\langle\delta\varepsilon\delta\varepsilon\rangle}{\tilde{\rho}^2\left(1-\frac{q}{2\tilde{\rho}|c_1|}\right)^2} - \frac{24q^2\langle\delta\varepsilon\delta\varepsilon\rangle}{\tilde{\rho}^4c_1^2\left(1-\frac{q}{2\tilde{\rho}|c_1|}\right)^3}}\tilde{\rho}|c_1| \tag{6.27}$$

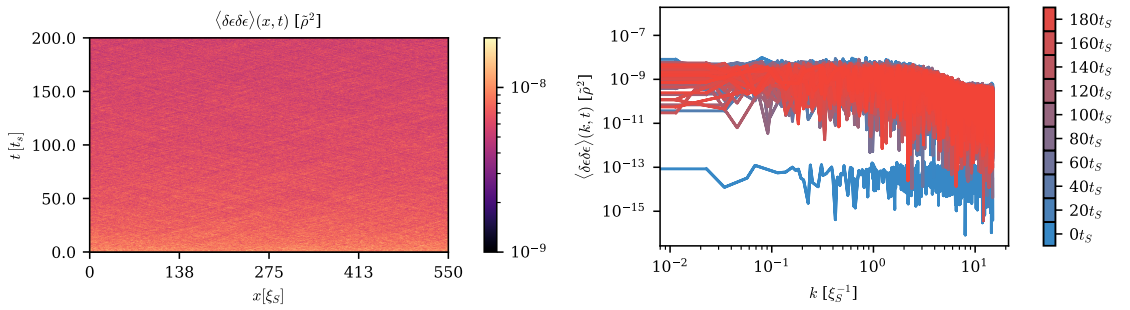

(a) (b)

Figure 6.2.: (a) Fluctuation correlation function $\langle\delta\varepsilon(\boldsymbol{x},t)\delta\varepsilon(\boldsymbol{x},t)\rangle$ in (1+1)d after a quench from the polar phase to the easy-plane phase with $q = -0.9\tilde{\rho}c_1$. The numerical data stems from 1000 independent truncated Wigner simulations of the full spin-1 Bose gas. (b) Numerical Fourier transform $\langle\delta\varepsilon\delta\varepsilon\rangle(k,t) = \int dx e^{ikx}\langle\delta\varepsilon(x,t)\delta\varepsilon(x,t)\rangle$ of the same fluctuation correlation function at different times.

6.5. Numerical results for the density fluctuation corrections

To determine how much the density fluctuation correlators $\langle\delta\varepsilon\delta\varepsilon\rangle$ and $\langle\delta\rho\delta\rho\rangle$ change the numerical value of the analytical mass gap Eq. (6.26) and the effective Lagrangians Eqs. (6.17) and (6.18), we must first know the order of magnitude of those fluctuations. As we do not solve the self-consistent equation in Sec. 6.3 in the current work, we study the density fluctuation correlators numerically. In this section, we will present the results for $\langle\delta\varepsilon\delta\varepsilon\rangle$ and $\langle\delta\rho\delta\rho\rangle$ from (1+1)d TWA simulations.

$\langle\delta\varepsilon(\boldsymbol{x},t)\delta\varepsilon(\boldsymbol{x},t)\rangle$ has the biggest influence on the effective actions for φ_S and φ_L, as this correlator renormalizes every part of the Lagrangians while $\langle\delta\rho(\boldsymbol{x},t)\delta\rho(\boldsymbol{x},t)\rangle$ only appears in the imaginary parts of the sine-squared-Gordon potential for φ_S (see App. C.1). Fig. 6.2 shows $\langle\delta\varepsilon(\boldsymbol{x},t)\delta\varepsilon(\boldsymbol{x},t)\rangle$ after a quench from the polar to the easy-plane phase with $q = -0.9\tilde{\rho}c_1$. The fluctuations are quite spatially homogeneous for each timeslice, while in the Fourier space, they plateau for $k_\Lambda \lesssim k \lesssim k_{\xi_S}$, with significantly lower values for even higher k. Moreover, it is apparent from this figure that the ε-fluctuation corrections are very small, with values no greater than $2 \times 10^{-8}\tilde{\rho}^2$. It can also be seen that the fluctuations increase in time at first, as they are several orders of magnitude smaller in the beginning, and then get slightly smaller over time. This is also illustrated well in Fig. 6.4a, where the spatial average of $\langle\delta\varepsilon(\boldsymbol{x},t)\delta\varepsilon(\boldsymbol{x},t)\rangle$ is plotted over time. There, we see that starting around $t = 2t_S$ and throughout the entire period in which the spin-1 Bose gas shows self-similar scaling [41], also the ε-fluctuation corrections decrease with a power law with scaling exponent $\sigma_\varepsilon = -0.12850(33)$.

The correlations $\langle\delta\rho(\boldsymbol{x},t)\delta\rho(\boldsymbol{x},t)\rangle$ behave similarly to $\langle\delta\varepsilon(\boldsymbol{x},t)\delta\varepsilon(\boldsymbol{x},t)\rangle$, as Fig. 6.3 shows. The

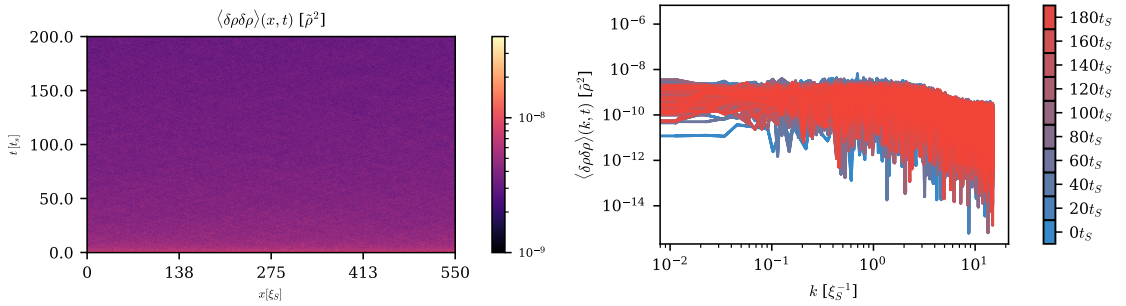

(a) (b)

Figure 6.3.: (a) Fluctuation correlation function $\langle\delta\rho(\boldsymbol{x},t)\delta\rho(\boldsymbol{x},t)\rangle$ in (1+1)d after a quench from the polar phase to the easy-plane phase with $q=-0.9\tilde{\rho}c_1$. The numerical data stems from 1000 independent truncated Wigner simulations of the full spin-1 Bose gas. (b) Numerical Fourier transform $\langle\delta\rho\delta\rho\rangle(k,t)=\int dx e^{ikx}\langle\delta\rho(x,t)\delta\rho(x,t)\rangle$ of the same fluctuation correlation function at different times.

main difference is that the fluctuation correlations of $\delta\rho$ are generally smaller than those for $\delta\varepsilon$, except at very early times where $|\delta\rho|$ is rather large due to our definition of $\delta\rho$ as the fluctuation around the easy-plane mean-field value n, which has not developed shortly after the quench. Moreover, $\langle\delta\rho(\boldsymbol{x},t)\delta\rho(\boldsymbol{x},t)\rangle$ already starts at quite high values, such that over time, $\langle\delta\rho(\boldsymbol{x},t)\delta\rho(\boldsymbol{x},t)\rangle$ only exhibits a decreasing trend, with a power law behavior after around $t=2t_S$ as Fig. 6.4b shows. The scaling exponent for this power law is slightly higher than for $\langle\delta\varepsilon(\boldsymbol{x},t)\delta\varepsilon(\boldsymbol{x},t)\rangle$ with $\sigma_\rho=-0.14538(31)$.

So far, we have looked at correlators at equal time and space, as they are what corrects our effective action. If we consider $\langle\delta\varepsilon(\boldsymbol{x},t)\delta\varepsilon(\boldsymbol{y},t)\rangle$ and $\langle\delta\rho(\boldsymbol{x},t)\delta\rho(\boldsymbol{y},t)\rangle$ as shown in Figs. 6.5a and 6.5b, we see no big difference in the spectra of the correlators at late times. However, at early times, the spectrum of the fluctuations $\langle\delta\varepsilon(\boldsymbol{x},t)\delta\varepsilon(\boldsymbol{y},t)\rangle$, $\langle|\delta\varepsilon(k,t)|^2\rangle$, has a clear peak at ξ_S, while $\langle|\delta\rho(k,t)|^2\rangle$ has a similar "plateau-spectrum" form at all times. The dominance of k_{ξ_S} for $\langle\delta\varepsilon(\boldsymbol{x},t)\delta\varepsilon(\boldsymbol{y},t)\rangle$ at early times could be related to the overpopulation of that mode in the initial spin density occupation $S(k,t)$.

6.6. Numerical results for the fluctuation-corrected mass gap

Now that we know how big the density fluctuation correlation functions are for the quench scenario of interest in the current work, we want to look at whether they have a big quantitative impact on the effective action parameters. For that, let us consider the mass gap of the theory, as analytically determined in Eq. (6.26). We have compared this analytical formula with the same numerical simulations as in Fig. 5.3b, now using the maximal value of $\langle\delta\varepsilon(\boldsymbol{x},t)\delta\varepsilon(\boldsymbol{x},t)\rangle\approx 2\times10^{-8}\tilde{\rho}^2$. If we do this, we see that for low values of q, there is no

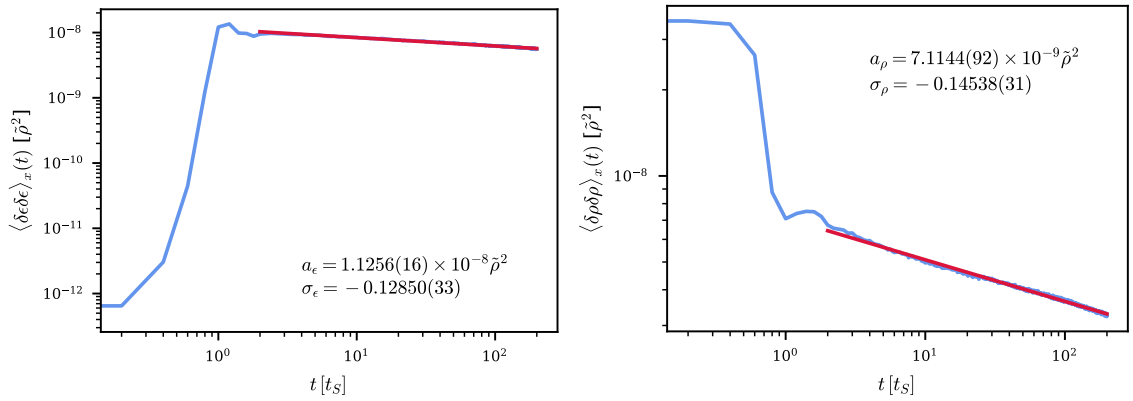

(a) (b)

Figure 6.4.: Time dependence of $\langle \delta\rho(\boldsymbol{x}, t)\delta\rho(\boldsymbol{x}, t)\rangle$ averaged over space in (1+1)d after a quench from the polar phase to the easy-plane phase with $q = -0.9\tilde{\rho}c_1$. The numerical data stems from 1000 independent truncated Wigner simulations of the full spin-1 Bose gas. For times greater than $2t_S$, the fluctuations decay following a power law according to $\langle \delta\varepsilon\delta\varepsilon\rangle = a_\varepsilon \times (t/t_S)^{\sigma_\varepsilon}$ and $\langle \delta\rho\delta\rho\rangle = a_\rho \times (t/t_S)^{\sigma_\rho}$.

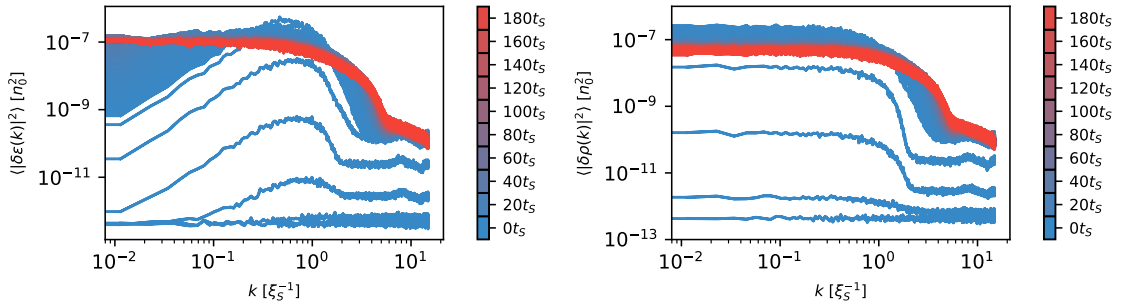

(a) (b)

Figure 6.5.: (a) Fluctuation correlation function $\langle |\delta\varepsilon(k, t)|^2\rangle$ and $\langle |\delta\rho(k, t)|^2\rangle$ in (1+1)d after a quench from the polar phase to the easy-plane phase with $q = -0.9\tilde{\rho}c_1$. Note that compared to Figs. 6.2b and 6.3b, these are the Fourier transforms of the full equal-time correlators $\langle \delta\varepsilon(\boldsymbol{x}, t)\delta\varepsilon(\boldsymbol{y}, t)\rangle$ and $\langle \delta\rho(\boldsymbol{x}, t)\delta\rho(\boldsymbol{y}, t)\rangle$. The numerical data stems from 1000 independent truncated Wigner simulations of the full spin-1 Bose gas. (b) Numerical Fourier transform of the same fluctuation correlation function at different times.

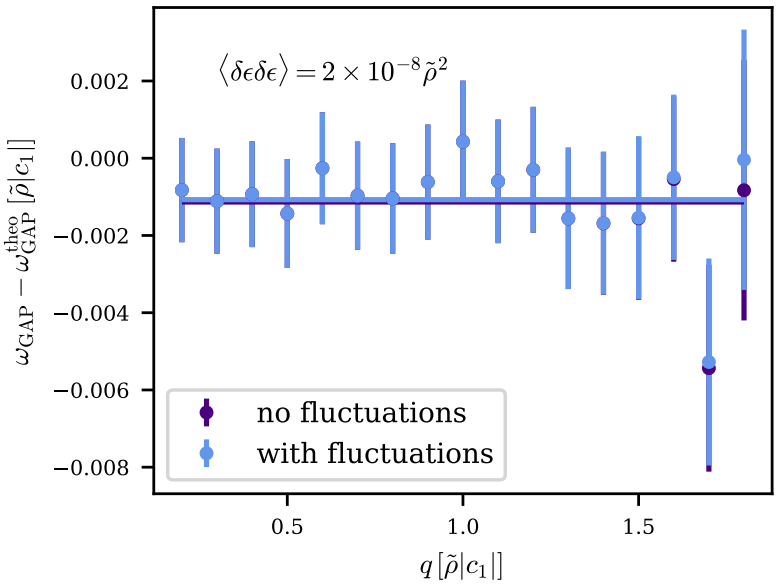

Figure 6.6.: Difference between the analytical results for the mass gap for φ_S according to Eqs. (5.37) and (6.26) and the numerical results detailed in Sec. 5.2. For the density fluctuation corrections $\langle \delta\varepsilon\delta\varepsilon \rangle$ in the analytical formula, we have used the maximal value encountered in Fig. 6.2. As can be seen, there is no big difference for low values of q, but the mass gap with fluctuations is slightly closer to what is observed in numerical simulations than if the additional density fluctuation corrections are not taken into account. The horizontal lines are given by the mean of the data points.

visible difference between the mass gap with and without including the density fluctuation corrections. However, for high values of q, it does make a small difference, and in fact it decreases the difference between numerics and analytics. Because this decrease is much smaller than the errors from determining the mass gap via fit, we cannot speak of a significant effect due to the low values of $\langle \delta\varepsilon(\boldsymbol{x}, t)\delta\varepsilon(\boldsymbol{x}, t) \rangle$, however.

We must note, though, that in the derivation of Eq. (6.26), we have neglected the time dependence of $\langle \delta\varepsilon(\boldsymbol{x}, t)\delta\varepsilon(\boldsymbol{x}, t) \rangle$, despite the fluctuation correlations varying in time. However, because the time evolution follows a scaling law with a very low exponent, not making this assumption would not make big quantitative differences in Fig. 6.6.

Even though the quantitative difference that the density fluctuation corrections make for the mass gap is not huge, the fact that the coupling constants of the sine-squared-Gordon model scale with time could make a qualitative difference influencing the scaling behavior observed of that theory. This will be further discussed in the conclusion.

7. A not-so-low-energy effective field theory

In the past two chapters, we have developed effective field theories for the phase degrees of freedom of the spin-1 Bose gas expanded around $\varphi_S = 2\pi\mathbb{Z}$ as numerical simulations and experiments show φ_S to be close to these values for most of the dynamics after a quench from the polar to the easy-plane phase. In doing so, we have seen that if we neglect the kinetic part in the inverse free propagator $\boldsymbol{G_0^{-1}}$, the effective theories diverge around $\varphi_S = (2\mathbb{Z}+1)\,\pi$ and no inclusion of density fluctuation corrections can fix this. This has led us to the conclusion that in order for φ_S to jump between the minima of the periodic potential, there needs to be non-zero momentum of the fluctuations $\delta\rho$.

As these jumps are seen in numerical simulations of a quench from the polar to the easy-plane phase in the form of real-time (anti)-instantons [41], we want to develop a theory that can describe what happens for the phases at these jumps in this chapter. We find that if we assume a characteristic momentum k_I for the density fluctuations, the effective field theory for φ_S and φ_L becomes regular around the $\varphi_S = (2\mathbb{Z}+1)\,\pi$. Moreover, if we expand this theory around $\varphi_S = (2\mathbb{Z}+1)\,\pi$ for a characteristic momentum $k_I = k_{\xi_S}$, the potential for φ_S shows shallow local minima on top of the global maxima. These qualitatively match numerical observations of φ_S at times of instanton occurrences.

7.1. A characteristic momentum

If we want to consider what happens around $\varphi_S = (2\mathbb{Z}+1)\,\pi$, we must not neglect the ∇^2-terms in $\boldsymbol{G_0^{-1}}$ (Eq. (6.12)). If we include these terms, however, we face another problem: Without the ∇^2-terms, $\boldsymbol{G_0^{-1}}$ is diagonal in position space, allowing us the analytical evaluation of $\frac{1}{2}\boldsymbol{J_0^T G_0 J_0}$ pointwise at each x and immensely simplifying the evaluation of the log det terms in the imaginary part of the effective action. Meanwhile, the ∇^2-terms are only diagonal in momentum space, where the x-dependent other parts of $\boldsymbol{G_0}$ are non-diagonal. To invert $\boldsymbol{G_0^{-1}}$, we would, therefore, have to find the general Green's function $\boldsymbol{G_0}$ such that

$$\int_z \boldsymbol{G_0^{-1}}(\boldsymbol{x}-\boldsymbol{z})\boldsymbol{G_0}(\boldsymbol{z}-\boldsymbol{y}) = \delta(\boldsymbol{x}-\boldsymbol{y}) \tag{7.1}$$

which involves solving differential equations like

$$\left[\frac{\tilde{\rho}}{\tilde{\rho}-2n}\frac{\nabla^2}{2mn}+8c_1(1+\cos\varphi_S(\boldsymbol{x}))+\frac{2c_1\tilde{\rho}}{n^3}\langle\delta\varepsilon(\boldsymbol{x})\delta\varepsilon(\boldsymbol{x})\rangle\cos\varphi_S(\boldsymbol{x})\right]G_{11}(\boldsymbol{x}-\boldsymbol{y})=\delta(\boldsymbol{x}-\boldsymbol{y}) \tag{7.2}$$

or, without the density fluctuation corrections,

$$\left[\frac{\tilde{\rho}}{\tilde{\rho}-2n}\frac{\nabla^2}{2mn}+8c_1(1+\cos\varphi_S(\boldsymbol{x}))\right]G_{11}(\boldsymbol{x}-\boldsymbol{y})=\delta(\boldsymbol{x}-\boldsymbol{y}), \tag{7.3}$$

which do not have solutions for a general function φ_S.

Thus, we cannot analytically include the full momentum-dependence of $\boldsymbol{G}_{\boldsymbol{0}}^{-1}$. However, if we assume that the fluctuations $\boldsymbol{\delta\rho}_i$ have support mainly in a narrow region of k centered around some characteristic tunneling momentum k_I, we can approximate

$$\begin{aligned}\int_x \boldsymbol{\delta\rho}_i(\boldsymbol{x})\nabla^2\boldsymbol{\delta\rho}_i(\boldsymbol{x}) &= -\int_k k^2\boldsymbol{\delta\rho}_i(\boldsymbol{k})\boldsymbol{\delta\rho}_i(-\boldsymbol{k})\\ &\approx -k_I^2\int_k \boldsymbol{\delta\rho}_i(\boldsymbol{k})\boldsymbol{\delta\rho}_i(-\boldsymbol{k})\\ &= -k_I^2\int_x \boldsymbol{\delta\rho}_i(\boldsymbol{x})^2,\end{aligned} \tag{7.4}$$

where we explicitly do not use the Einstein sum convention. Consequently, we obtain

$$\boldsymbol{G}_{\boldsymbol{0}_{\text{fluc}}}^{-1}=\begin{pmatrix}G_{11} & 0\\ 0 & G_{22}\end{pmatrix} \tag{7.5}$$

with

$$G_{11}=-\frac{k_I^2}{2mn}\frac{\tilde{\rho}}{(\tilde{\rho}-2n)}+8c_1(1+\cos\varphi_S)+\frac{2c_1\tilde{\rho}}{n^3}\langle\delta\varepsilon\delta\varepsilon\rangle\cos\varphi_S \tag{7.6}$$

$$G_{22}=-\frac{k_I^2}{2mn}-2c_1\left(2+\left(2-\frac{\tilde{\rho}}{n}\right)\cos\varphi_S\right)+\frac{2c_1\tilde{\rho}}{n^3}\langle\delta\rho\delta\rho\rangle\cos\varphi_S+3c_1\frac{\tilde{\rho}-2n}{n^3}\langle\delta\varepsilon\delta\varepsilon\rangle\cos\varphi_S \tag{7.7}$$

which now, again, is diagonal in position space for a constant k_I.

The k_I-terms then act as a regulator for the theory and the real part of the effective Lagrangian

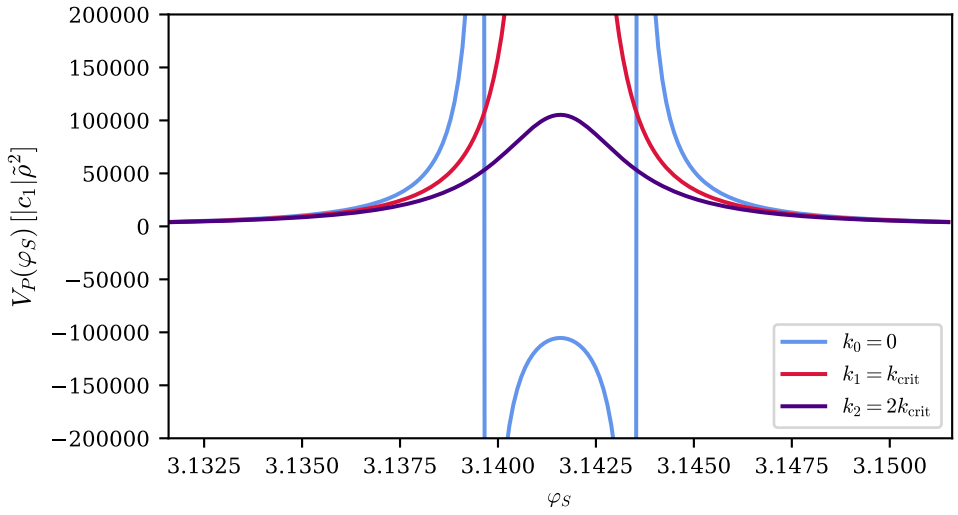

Figure 7.1.: Terms in $\Re\mathcal{L}^{\mathrm{eff}}$ (Eq. (7.9)) involving no derivatives for different values of the regularization momentum k_I in units of $\tilde{\rho}^2|c_1|$. For $k_I = 0$, this pseudopotential exhibits two divergences (blue curve). For $-\frac{k_I^2}{2mn}\frac{\tilde{\rho}}{(\tilde{\rho}-2n)} = -\frac{k_{\mathrm{crit}}^2}{2mn}\frac{\tilde{\rho}}{(\tilde{\rho}-2n)} = \frac{2c_1\tilde{\rho}}{n^3}\langle\delta\varepsilon\delta\varepsilon\rangle$, there is only one divergence left (red curve). If k_I is increased further, the divergences disappear completely (indigo curve). For this plot, we have assumed $q = -0.9\tilde{\rho}|c_1|$ and $\langle\delta\varepsilon\delta\varepsilon\rangle = 2\times10^{-8}$.

becomes

$$\Re\mathcal{L}^{\mathrm{eff}} = -\frac{n}{4m}(\nabla\varphi_L)^2 - \left(\frac{\tilde{\rho}-2n}{8m}\right)(\nabla\varphi_S)^2 - 2c_1 n(\tilde{\rho}-2n)\cos\varphi_S \tag{7.8}$$
$$-\frac{1}{2}\left[\frac{n^3\dot{\varphi}_L^2}{-\frac{k_I^2}{2mn} - 2n^2c_1(2n+(2n-\tilde{\rho})\cos\varphi_S) + 3c_1(\tilde{\rho}-2n)\langle\delta\varepsilon\delta\varepsilon\rangle\cos\varphi_S + 2c_1\tilde{\rho}\langle\delta\rho\delta\rho\rangle\cos\varphi_S}\right.$$
$$\left.+\frac{\left(\dot{\varphi}_S - 2q - \frac{(\nabla\varphi_L)^2-(\nabla\varphi_S)^2}{4m} - 2c_1(\tilde{\rho}-4n)(1+\cos\varphi_S) - \frac{c_1\tilde{\rho}}{n^2}\langle\delta\varepsilon\delta\varepsilon\rangle\cos\varphi_S\right)^2}{-\frac{k_I^2}{2mn}\frac{\tilde{\rho}}{(\tilde{\rho}-2n)} + 8c_1(1+\cos\varphi_S) + \frac{2c_1\tilde{\rho}}{n^3}\langle\delta\varepsilon\delta\varepsilon\rangle\cos\varphi_S}\right].$$

Fig. 7.1 shows that as we increase k_I, the two divergences that occur in the effective Lagrangian around π first become one and then disappear completely.

After the theory is regularized, the density fluctuation corrections play no crucial role anymore as they are numerically small, so that in the following, we will work with the theory without

those corrections, leaving us with

$$\begin{aligned}\Re\mathcal{L}^{\text{eff}} = &-\frac{n}{4m}\left(\nabla\varphi_L\right)^2 - \left(\frac{\tilde{\rho}-2n}{8m}\right)\left(\nabla\varphi_S\right)^2 - 2c_1 n(\tilde{\rho}-2n)\cos\varphi_S \\ &-\frac{1}{2}\left[\frac{n^3\left(\dot{\varphi}_L\right)^2}{-\frac{k_I^2 n^2}{2m} - 2n^2 c_1(2n+(2n-\tilde{\rho})\cos\varphi_S)}\right. \\ &\left.+\frac{\left(\dot{\varphi}_S - 2q - \frac{(\nabla\varphi_L)^2-(\nabla\varphi_S)^2}{4m} - 2c_1(\tilde{\rho}-4n)(1+\cos\varphi_S)\right)^2}{-\frac{k_I^2}{2mn}\frac{\tilde{\rho}}{(\tilde{\rho}-2n)} + 8c_1(1+\cos\varphi_S)}\right].\end{aligned} \tag{7.9}$$

Note that we have again omitted the imaginary part of the effective action, as our analysis in this work concentrates on the real part. Discussion of the imaginary part can be found in App. C.2.

7.2. Expansion around $\varphi_S = \pi$

As the assumption of a characteristic momentum for $\delta\rho$ is only really valid for instantons and, thus, around $\varphi_S = (2\mathbb{Z}+1)\pi$, we can now proceed similarly to before and perform an expansion of $\mathcal{L}^{\text{eff}}$ around small absolute values of $1+\cos\varphi_s$ up to $\mathcal{O}(1+\cos\varphi_s)^2$. If we also again neglect any terms of the order $\dot{\varphi}_i(1+\cos\varphi_s)$ and $(\nabla\varphi_i)^2(1+\cos\varphi_s)$ as well as higher than quadratic terms in the derivatives, the theories for φ_S and φ_L decouple again and we get (see details in App. B.4)

$$\mathcal{L}^{\text{eff}}_{\varphi_L} = -\frac{\dot{\varphi}_L^2}{\frac{4c_1\tilde{\rho}}{n} + \frac{k_I^2}{mn}} - \left[\frac{n}{4m} + \frac{q}{\frac{k_I^2}{2mn}\frac{\tilde{\rho}}{\tilde{\rho}-2n}}\frac{1}{2m}\right]\left(\nabla\varphi_L\right)^2 + \mathcal{O}\left(\dot{\varphi}(1+\cos), \nabla\varphi(1+\cos)\right) \tag{7.10}$$

for the Lagrangian for φ_L and

$$\begin{aligned}\Re\mathcal{L}^{\text{eff}}_{\varphi_S} = &-\frac{\dot{\varphi}_S^2}{\frac{k_I^2}{mn}\frac{\tilde{\rho}}{\tilde{\rho}-2n}} - \left[\frac{\tilde{\rho}-2n}{8m} - \frac{q}{\frac{k_I^2}{2mn}\frac{\tilde{\rho}}{\tilde{\rho}-2n}}\frac{1}{2m}\right]\left(\nabla\varphi_S\right)^2 \\ &- A_R\cos\varphi_S - B_R\sin^2\varphi_S + \text{const.} + \mathcal{O}\left((1+\cos)^3, \dot{\varphi}(1+\cos), \nabla\varphi(1+\cos)\right)\end{aligned} \tag{7.11}$$

for the real part of the Lagrangian for φ_S with

$$A = 2c_1 n(\tilde{\rho} - 2n) + \frac{4q^2}{\frac{k_I^2}{mn}\frac{\tilde{\rho}}{\tilde{\rho}-2n}} \left[\frac{1}{2} + \frac{8c_1}{\frac{k_I^2}{2mn}\frac{\tilde{\rho}}{\tilde{\rho}-2n}} - 2\left(\frac{8c_1}{\frac{k_I^2}{2mn}\frac{\tilde{\rho}}{\tilde{\rho}-2n}} \right)^2 \right] \tag{7.12}$$

$$B = \frac{4q^2}{\frac{k_I^2}{mn}\frac{\tilde{\rho}}{\tilde{\rho}-2n}} \left[\frac{1}{4} - \frac{8c_1}{\frac{k_I^2}{2mn}\frac{\tilde{\rho}}{\tilde{\rho}-2n}} + \left(\frac{8c_1}{\frac{k_I^2}{2mn}\frac{\tilde{\rho}}{\tilde{\rho}-2n}} \right)^2 \right]. \tag{7.13}$$

In this calculation, we have used $(1+\cos\varphi_S)^2 = 2 + 2\cos\varphi_S - \sin^2\varphi_S$ as well as the Taylor expansion $\frac{1}{1+x} = 1 - x + x^2 + \mathcal{O}(x^3)$ and neglected any constant terms. The imaginary part can be found in App. C.2.

Note that the prefactor of the time derivative for the Larmor phase in Eq. (7.10) diverges for twice the spin healing momentum $k_I = 2k_{\xi_S}$, such that the Larmor phase becomes static. Because at $\varphi_S = (2\mathbb{Z}+1)\pi$, which we assume approximately in this expansion, the Larmor phase is not well-defined anymore as there is no elongation of $F_\perp$ in the spin sphere (see Fig. 2.4), this is not a problem, however.

In the following, we will now use the spin healing momentum $k_I = k_{\xi_S} = \sqrt{-2c_1\tilde{\rho}m} = \sqrt{2|c_1|\tilde{\rho}m}$ as the characteristic momentum for two reasons. Firstly, ξ_S is generally the characteristic lengthscale for defects in the system to occur. Secondly, it was found in [38] that the healing momentum is overpopulated, especially shortly after the quench. Thus, the (anti)-instantons at momentum k_{ξ_S} could be associated with the cascades driving the scaling observed in [38, 41]. If we insert k_ξ into Eqs. (7.10) and (7.12), we find

$$\mathcal{L}^{\text{eff}}_{\varphi_L} = \frac{n\dot{\varphi}_L^2}{2c_1\tilde{\rho}} - \left[\frac{n}{4m} - \frac{qn(\tilde{\rho}-2n)}{c_1\tilde{\rho}^2}\frac{1}{2m} \right] (\nabla\varphi_L)^2 + \mathcal{O}\left(\dot{\varphi}(1+\cos), \nabla\varphi(1+\cos)\right) \tag{7.14}$$

and

$$\begin{aligned} \Re\mathcal{L}^{\text{eff}}_{\varphi_S} = &- \frac{\dot{\varphi}_L^2 n(\tilde{\rho}-2n)}{2c_1\tilde{\rho}^2} - \left[\frac{\tilde{\rho}-2n}{8m} + \frac{qn(\tilde{\rho}-2n)}{c_1\tilde{\rho}^2}\frac{1}{2m} \right] (\nabla\varphi_S)^2 \\ &- A_R\cos\varphi_S + B_R\sin^2\varphi_S + \text{const.} + \mathcal{O}\left(\langle\delta\delta\rangle^2, (1+\cos)^3, \dot{\varphi}(1+\cos), \nabla\varphi(1+\cos)\right) \end{aligned} \tag{7.15}$$

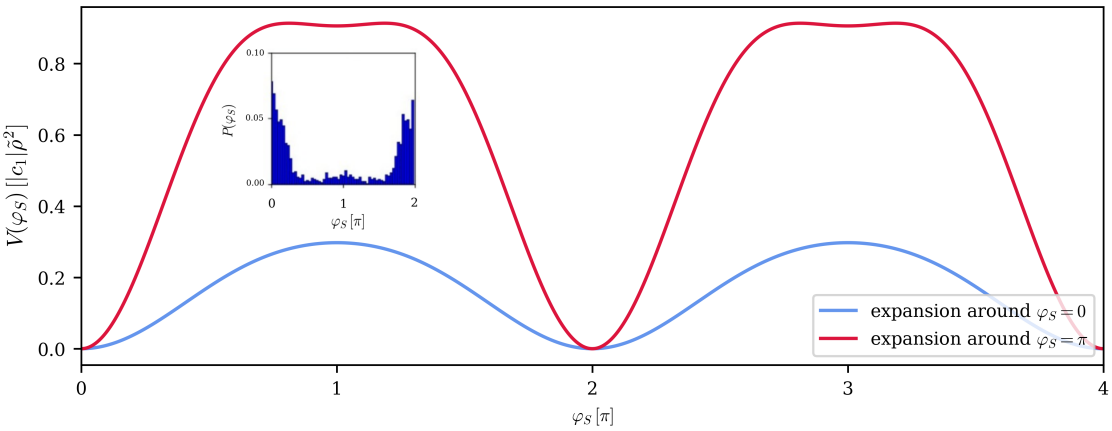

Figure 7.2.: Sine-squared-Gordon potentials for φ_S after expansion of the effective action around $\varphi_S = 2\pi\mathbb{Z}$ assuming $\nabla^2 = 0$ and $\varphi_S = (2\mathbb{Z}+1)\pi$ assuming regulator momentum k_{ξ_S}. For both, we have once again used $q = -0.9\tilde{\rho}c_1$ and shown the potentials in units of $\tilde{\rho}^2|c_1|$. The inset shows a histogram of the spinor phase φ_S at the occurrence of an instanton. The data for this comes from [41] It can be clearly seen that at the time of the instanton, there is a non-zero population at $\varphi_S = (2\mathbb{Z}+1)\pi$, with the structure of the histogram corresponding to the potential stemming from the expansion around $\varphi_S = \pi$.

where

$$A_R = 2c_1 n(\tilde{\rho} - 2n) - \frac{2q^2 n(\tilde{\rho} - 2n)}{c_1\tilde{\rho}^2}\left[\frac{1}{2} - \frac{8(\tilde{\rho} - 2n)n}{\tilde{\rho}^2} - \frac{128(\tilde{\rho} - 2n)^2 n^2}{\tilde{\rho}^4}\right] \tag{7.16}$$

$$B_R = \frac{2q^2 n(\tilde{\rho} - 2n)}{c_1\tilde{\rho}^2}\left[\frac{1}{4} + \frac{8(\tilde{\rho} - 2n)n}{\tilde{\rho}^2} + \frac{64(\tilde{\rho} - 2n)^2 n^2}{\tilde{\rho}^4}\right] \tag{7.17}$$

$$\tag{7.18}$$

In Fig. 7.2, this sine-squared-Gordon potential is compared to the one obtained from the expansion around $\varphi_S = 2\pi\mathbb{Z}$ in Sec. 5.1.3. Of course, this figure again has to be taken with a grain of salt as the two expansions are only valid around $\varphi_S = (2\mathbb{Z}+1)\,\pi$ and $\varphi_S = 2\pi\mathbb{Z}$, respectively.

The main takeaway of this figure is, of course, that there is no divergence around $\varphi_S = (2\mathbb{Z}+1)\,\pi$ anymore if we include a cutoff momentum. Moreover, it is worth noting that the expansion around $\varphi_S = (2\mathbb{Z}+1)\,\pi$ leads to broader maxima and narrower minima as well as higher potential barriers compared to the expansion around $2\pi\mathbb{Z}$, which may further explain why numerical simulations show φ_S to be so centered around $\varphi_S = 2\pi\mathbb{Z}$ (see Fig. 5.2b). In addition, the potential for this expansion shows small dips in the global potential maxima at $\varphi_S = (2\mathbb{Z}+1)\,\pi$. These perfectly coincide with the histograms of φ_S around an instanton seen in numerical simulations [84] in the inlay in Fig. 7.2.

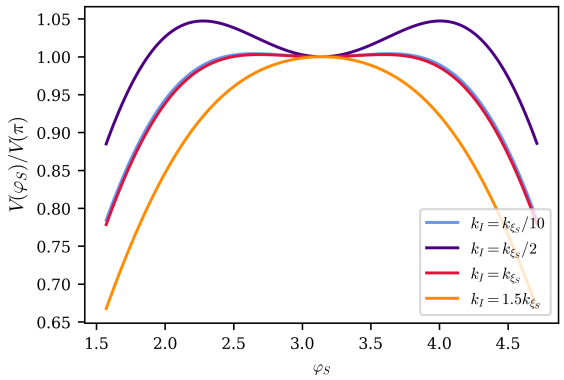

Figure 7.3.: Global maxima for the spinor phase potential expanded around π assuming different characteristic momenta k_I. The potential is normalized by its value at π and we have used $q = -0.9\tilde{\rho}c_1$ for plotting.

The fact that the expansion around $(2\mathbb{Z}+1)\,\pi$ is regular at all manifests our discussion from Sec. 6.1.1 that we need non-zero momenta for the fluctuations $\delta\rho$ to be able to see any hopping between the periodic potential minima. Moreover, this form of the potential including flat dips on top of the potential peaks implies that it should be possible for the spinor phase to stay in the local minimum at $(2\mathbb{Z}+1)\,\pi$ for a while, leading to an elongated dip in $F_\perp$ before jumping to the next global minimum, causing a phase jump in the Larmor phase Eq. (2.38), r jumping back into the original minimum. However, this is of course limited by the shallowness of the minimum at $(2\mathbb{Z}+1)\,\pi$, with the (anti)-instantons being subject to false vacuum decay as detailed in [51].

It is interesting to consider what happens if, against our original assumptions, the characteristic momentum is not in the realm of k_{ξ_S}. If we look at the potentials for different characteristic momenta as plotted in Fig. 7.3, we see that for low values of k_I, there also only is a shallow minimum on top of the global maxima as if the characteristic momentum for $\delta\rho$ was that low, there would not be many tunneling occurrences, thus not many quasiparticles even seeing the maximum. The local minimum at $(2\mathbb{Z}+1)\,\pi$ then first grows deeper with higher characteristic momentum, as more and more occurrences of quasiparticles hopping the maximum would be possible with increasing k_I but they would get stuck at the top, not being able to escape anymore. Then, for $k_I = k_\xi$ the momentum of $\delta\rho$ is high enough that most quasiparticles tunnel directly without getting stuck on top, again leading to a shallow minimum. Lastly, if the characteristic momentum for $\delta\rho$ was even higher, the minimum on top of the global maxima would vanish as no quasiparticles would get stuck on top of the maximum anymore.

Fig. 7.2 captures the essence of this work: We now have two theories describing the phase degrees of freedom of the spin-1 Bose gas near the easy-plane phase - one valid for small

angles and small momenta, and one that is valid around the maxima of the potential where we have assumed the hopping between the potential wells to take place with the spin healing momentum $k_I = k_{\xi_S}$. In future works, one could interpolate between these potentials in order to perform numerical simulations of the dynamics of φ_S in a potential that is as realistic as possible.

8. Conclusion

In this work, we have developed different effective field theories for the spin-1 Bose gas far from equilibrium after a quench from the polar to the easy-plane phase. At first, we have used the 2PI effective action formalism to derive an effective action, as well as a closed set of evolution equations for both the field expectation value and the full propagator to leading order. While this formalism is useful for including far from equilibrium initial conditions, it does not allow us to reduce the degrees of freedom of the theory. Moreover, as we have seen the importance of the gapped spinor phase in the effective theories developed in Ch. 5-7, we could question whether the large N expansion, which we have argued to be applicable also in the spin-1 Bose gas for describing mostly the Goldstone modes, should be used in the way done in Ch. 4. Further analytical investigation of this formalism is subject to future work.

For the remainder of the thesis, we have used a different approach, integrating out the density fluctuations around the mean-field values of the easy-plane phase, leaving us with a theory only for the phase degrees of freedom in the easy-plane phase: the spinor phase φ_S and the Larmor phase φ_L. We have found that if we neglect the kinetic part of the density fluctuations, our effective theory diverges periodically at φ_S around $(2\mathbb{Z}+1)\,\pi$. We could explain this fact by considering the mean-field trajectories of the spin-1 Bose gas on the spin-nematic sphere, which illustrate that density fluctuations at non-zero momentum are necessary for the system to leave closed, self-trapping trajectories around $\varphi_S = 2\pi\mathbb{Z}$.

For φ_S around these values, we have been able to expand this divergent effective theory into a regular one, finding that under some reasonable approximations, φ_L and φ_S decouple, yielding a free theory for φ_L and a sine-Gordon theory with additional $\sin^2\varphi$-term for φ_S. This sine-squared-Gordon theory qualitatively agrees with the form of the periodic potential for φ_S observed in numerical simulations as well as the experiment. Moreover, the mass gap for this effective theory for φ_S agrees with the Bogoliubov prediction.

Using this method, we have also included higher orders in the density fluctuation by expanding the Lagrangian up to fourth order in the density fluctuations and then expanding higher than quadratic terms in $\delta\rho$ and $\delta\varepsilon$ around correlations like $\langle\delta\rho\delta\rho\rangle$ and $\langle\delta\varepsilon\delta\varepsilon\rangle$ at equal space and time. We have found that such terms do not regularize the effective theory at $k = 0$ and due

to small numerical values of the correlators after a quench far from equilibrium, they do not have a large qualitative impact on the parameters of the effective theory if we expand around $\varphi_S = 2\pi\mathbb{Z}$. However, for high q, they seem to move the analytical mass gap slightly closer to the numerics compared to the Bogoliubov result.

In the last chapter, we have been able to regularize the effective theory around $\varphi_S = (2\mathbb{Z}+1)\pi$ by introducing a characteristic momentum for the fluctuations $\delta\rho$. Expanding around the maxima of the periodic potential for φ_S at $\varphi_S = (2\mathbb{Z}+1)\pi$, we have once more found that the theories for φ_L and φ_S decouple, yielding again a free theory for φ_S and a sine-squared-Gordon theory for φ_S. Compared to the theories found before by expanding around $\varphi_S = 2\mathbb{Z}\pi$ and not including the kinetic terms for the density fluctuations, the potential for φ_S in this theory has narrower minima as well as broader and higher global potential maxima that include a shallow local minimum at $\varphi_S = (2\mathbb{Z}+1)\,\pi$ if we assume the characteristic momentum to be the spin healing momentum $k_I = k_{\xi_S}$.

With this theory, we could explain the instantons observed in [84] despite the initial effective theories seeming not to allow for these defects. The form of the potential for φ_S around the maxima has even been found to qualitatively correspond to the numerical spinor phase histogram around the time that an instanton occurs. Moreover, due to the shallow minimum at the top of the global maxima, we could connect the instantons to false vacuum decay.

In this work, we have mostly focussed our discussion on the real part of the effective field theories. The imaginary parts are considered in the Appendix. We have found for the theories expanded around $\varphi_S = 2\mathbb{Z}\pi$ that the imaginary part of the effective action simply leads to a damping of the partition function in the relevant region of φ_S. For the theory expanded around $\varphi_S = (2\mathbb{Z}+1)\pi$, this is also the case except when the system gets very near to the quantum phase transition. In this case, we hypothesize that defects such as instantons can lead to exponentially growing modes during the small time that they spend around the potential maxima of φ_S. A thorough investigation of the imaginary parts is subject to future works.

Of course, the theories developed in this work have their limitations. In general, we have neglected any terms that could lead to potentials dependent on the derivatives of the Larmor and the spinor phase, which is only valid for low momenta and energies. Moreover, because we cannot include the full momentum dependence of the density fluctuations in our effective theory, we had to make approximations, neglecting the kinetic part for these fluctuations when we expanded around $\varphi_S = 2\mathbb{Z}\pi$ and assuming a characteristic momentum corresponding to the spin healing momentum when we expanded around the potential maxima at $\varphi_S = (2\mathbb{Z}+1)\pi$. While these approximations are inspired by numerical observations and the typically low momenta

present in ultra-cold Bose gases, they still limit the applicability of the theories. It would be interesting to combine the theories expanded around $\varphi_S = 2\mathbb{Z}\pi$ and around $\varphi_S = (2\mathbb{Z}+1)\pi$, for example through interpolation between the two, to obtain a theory that is approximately valid for all values of φ_S.

In future works, it would also be highly interesting to use the effective theories developed in this thesis in numerical investigations of their respective scaling behavior. First numerical simulations of the effective theory for φ_S in Ch. 5 have already been carried out [84]. Assuming far-from-equilibrium initial conditions, it has been observed that the phase correlator $\langle|\varphi_S(k)|^2\rangle$ in (1+1)d can exhibit spatio-temporal self-similar scaling with the same scaling exponent $\alpha \approx 1/4 \approx \beta$ as numerically observed for $S(k,t)$ in the full (1+1)d spin-1 Bose gas [38]. Moreover, for the (2+1)d effective theory, the results of [9] for the (2+1)d spin-1 Bose gas with $\beta \approx 1/2$ and $\alpha \approx 1$ could be reproduced [84]. Furthermore, scaling in the (1+1)d sine-squared Gordon model with $\alpha \approx 1/3 \approx \beta$ could be observed as well, as it has been analytically predicted for the sine-Gordon model using the 2PI action formalism [87].

We could now investigate how the theories developed in this work would influence these numerical results. It would, for example, be interesting to numerically study how including the scaling density fluctuation corrections affects the scaling behavior observed in the sine-squared Gordon model. Moreover, one could interpolate between the potential expanded around $\varphi_S = 2\mathbb{Z}\pi$ and that expanded around $\varphi_S = (2\mathbb{Z}+1)\pi$, including the small dips at the global maxima to obtain a more realistic effective theory for φ_S and to probe this theory numerically. Using this interpolated theory for a scaling analysis, we could possibly make some conclusions about the instantons' effect on the scaling of the theory, as only they "see" the global potential maxima.

It is well-known that the pure sine-Gordon model effectively describes or can be mapped to a plethora of different condensed matter systems, from two coupled condensates [88] to the BKT transition in superfluids and superconductors [89, 90]. Thus, we hope that, similarly, the considerations of the sine-squared Gordon model in the current work may help develop effective theories for systems beyond those considered in the present work and in [51], either as improved effective theories for systems approximately described by the sine-Gordon model or as effective theories for systems with more complex interactions.

One such example has been seen in [51], where they have found that a 2-component BEC can also be described via a sine-squared-Gordon theory, allowing for quantum simulation of false vacuum decay with such a system. According to our results showing periodic false vacuums for φ_S in Ch. 7 for appropriate momenta of the fluctuations $\delta\rho$, such a study of false vacuum decay

could also be a possibility in the 3-component BEC. However, due to the approximations made in our theory and the fact that the false vacuum of the potential seems to depend on the momentum of the density fluctuations, it is not clear whether an experimental realization would be feasible. Regardless, it would be interesting to investigate in the future whether higher-spin BECs can also be described by a sine-squared Gordon theory under certain conditions, potentially also allowing for quantum simulations of false vacuum decay.

A. Numerical parameters

For the numerical simulations in the present work, we have used the following parameters unless otherwise stated:

Quantity	Numerical value	Physical value
Particle number	3×10^6	3×10^6
Lattice spacing Δx	1.00	$5.371 \times 10^{-8}\,\mu\mathrm{m}$
c_0	1.233×10^{-3}	$1.768 \times 10^{-39}\,\mathrm{J\,m}$
c_1	-5.702×10^{-6}	$-8.181 \times 10^{-42}\,\mathrm{J\,m}$
Healing length ξ	0.7442	$3.997 \times 10^{-8}\,\mu\mathrm{m}$
Spin healing length ξ_S	10.94	$5.87 \times 10^{-7}\,\mu\mathrm{m}$
System length L	4096	$374.4\,\xi_S$
Total density $\tilde{\rho}$	732.4	$8014\,\xi_S^{-1}$
Spin healing time t_S	1504	$5.939 \times 10^{-3}\,\mathrm{s}$

Table A.1.: Values used in the numerical simulations of the (1+1)d spin-1 Bose gas, given to four significant digits. Numerical values in dimensionless units as defined in Sec. 3.1

For c_0 and c_1 specifically, these are the values for ^{87}Rb adjusted to quasi-1d as in Eq. (2.71)

B. Derivations and Expansions

In the following, we provide some more derivations and the details of some tedious calculations that have been omitted in the main text for brevity.

B.1. The 1PI effective action

In this section, we will demonstrate the derivation of the 1PI effective action to 1-loop order, explaining the result Eq. (4.35). We will follow [91] for this and set $R = 0$ in this section.

As explained in Sec. 4.1.5, we find the quantum equations of motion Eqs. (4.34a) and (4.34b) for the effective action $\Gamma^{R=0}$. Using the definition Eq.(4.33), we can write

$$e^{i\Gamma^{R=0}[\Phi]} = e^{i(W[J]-J^\dagger\cdot\Phi)} = \int \mathcal{D}\phi e^{i\left(S[\phi]+J^\dagger\cdot(\phi-\Phi)\right)} \tag{B.1}$$

$$= \int \mathcal{D}f e^{i\left(S[\Phi+f]+J^\dagger\cdot f\right)} \tag{B.2}$$

where we have defined $f = \phi - \Phi$. To get $\Gamma^{R=0}$ to 1-loop order, we can now expand

$$S[\Phi + f] = S[\Phi] + \frac{\delta S}{\delta\Phi}\cdot f + \frac{1}{2} f\cdot\frac{\delta^2 S}{\delta\Phi\delta\Phi}\cdot f + \mathcal{O}(f^3) \tag{B.3}$$

and use Eq. (4.34a) to obtain

$$e^{i\Gamma^{R=0}[\Phi]} = \int \mathcal{D}f e^{i\left(S[\Phi]+\left(\frac{\delta S}{\delta\Phi}-\frac{\delta\Gamma^{R=0}}{\delta\Phi}\right)\cdot f+\frac{1}{2}f\cdot\frac{\delta^2 S}{\delta\Phi\delta\Phi}\cdot f+\mathcal{O}(f^3)\right)} \tag{B.4}$$

Using now that

$$\Gamma^{R=0} = S + 1 - \text{loop}, \tag{B.5}$$

we find that to 1-loop order

$$\frac{\delta\Gamma^{R=0}}{\delta\Phi} = \frac{\delta S}{\delta\Phi} + 1 - \text{loop} \tag{B.6}$$

such that to this order, the linear term in Eq. (B.4) cancels and we are left with

$$e^{i\Gamma^{R=0,1-\text{loop}}[\Phi]} = \int \mathcal{D}f e^{i\left(S[\Phi]+\frac{1}{2}f\cdot\frac{\delta^2 S}{\delta\Phi\delta\Phi}\cdot f+\mathcal{O}(f^3)\right)} \tag{B.7}$$

$$\propto \det\left(G_0^{-1}\right)^{-1/2} e^{iS[\Phi]} \tag{B.8}$$

where we have used Eq. (4.36) and, thus,

$$\Gamma^{R=0,1-\text{loop}} = S[\Phi] + \frac{i}{2}\log\det\left[G_0^{-1}\right] \tag{B.9}$$

$$= S[\Phi] + \frac{i}{2}\text{Tr}\log\left[G_0^{-1}\right] \tag{B.10}$$

up to irrelevant constants.

B.2. Expansion in the density fluctuations

Here, we carry out the expansion of Lagrangian Eq. (??) up to the fourth order in the density fluctuations. This Lagrangian has two terms where the $\delta\rho$ and $\delta\varepsilon$ appear non-linearly: For once, they are found in the potential in the prefactor of the cosine term, which involves

$$\sqrt{n^2+\delta\rho^2+2n\delta\rho-\delta\varepsilon^2} \tag{B.11}$$

$$= n\left(1+\frac{\delta\rho}{n}-\frac{\delta\varepsilon^2}{2n^2}+\frac{\delta\rho\delta\varepsilon^2}{2n^3}-\frac{\delta\rho^2\delta\varepsilon^2}{2n^4}-\frac{\delta\varepsilon^4}{8n^4}\right)+\mathcal{O}(\delta^5). \tag{B.12}$$

Moreover, the spatial derivative terms of the densities can be expanded as

$$(n+\delta\rho-\delta\varepsilon)(\nabla\log(n+\delta\rho-\delta\varepsilon))^2+(n+\delta\rho+\delta\varepsilon)(\nabla\log(\rho+\varepsilon))^2 \tag{B.13}$$

$$+(\tilde{\rho}-2n-2\delta\rho)(\nabla\log(\tilde{\rho}-2n-2\delta\rho))^2$$

$$=2\left(\frac{1}{n}-\frac{\delta\rho}{n^2}+\frac{\delta\rho^2+\delta\varepsilon^2}{n^3}\right)\left((\nabla\delta\rho)^2+(\nabla\delta\varepsilon)^2\right)+4\left(-\frac{\delta\varepsilon}{n}+\frac{2\delta\varepsilon\delta\rho}{n^2}\right)\nabla\delta\varepsilon\nabla\delta\rho$$

$$+\frac{4}{\tilde{\rho}-2n}\left(1+\frac{2\delta\rho}{\tilde{\rho}-2n}+\frac{4\delta\rho^2}{(\tilde{\rho}-2n)^2}\right)(\nabla\delta\rho)^2+\mathcal{O}(\delta^5) \tag{B.14}$$

if we use that n and $\tilde{\rho}$ are approximately constant.

B.3. Expanding the real part of the effective Lagrangian for small φ_S including density fluctuation corrections

In this section, we want to detail the expansion of the effective Lagrangian in Sec. 6.1 for small angles to obtain the effective theory in Sec. 6.2. For that, we first consider its real part involving

the $\frac{1}{2}\boldsymbol{J}^T\boldsymbol{G}\boldsymbol{J}$ term Eq. (6.16)

$$\begin{aligned}&\frac{1}{2}\boldsymbol{J^T G J} \\ =&\frac{1}{2}\left[\frac{n^3\dot{\varphi}_L^2}{-2n^2c_1(2n+(2n-\tilde{\rho})\cos\varphi_S)+3c_1(\tilde{\rho}-2n)\langle\delta\varepsilon\delta\varepsilon\rangle\cos\varphi_S+2c_1\tilde{\rho}\langle\delta\rho\delta\rho\rangle\cos\varphi_S}\right. \\ &\left.+\frac{\left(\dot{\varphi}_S-2q-\frac{(\nabla\varphi_L)^2-(\nabla\varphi_S)^2}{4m}-2c_1(\tilde{\rho}-4n)(1+\cos\varphi_S)-\frac{c_1\tilde{\rho}}{n^2}\langle\delta\varepsilon\delta\varepsilon\rangle\cos\varphi_S\right)^2}{8c_1(1+\cos\varphi_S)+\frac{2c_1\tilde{\rho}}{n^3}\langle\delta\varepsilon\delta\varepsilon\rangle\cos\varphi_S}\right],\end{aligned} \tag{B.15}$$

Neglecting the terms $\mathcal{O}(\dot{\varphi}\sin^2, \nabla^2\sin^2, \nabla^3, \dot{\varphi}\nabla^2)$ and higher, we have

$$\begin{aligned}&\frac{n^3\dot{\varphi}_L^2}{-2n^2c_1(2n+(2n-\tilde{\rho})\cos\varphi_S)+3c_1(\tilde{\rho}-2n)\langle\delta\varepsilon\delta\varepsilon\rangle\cos\varphi_S+2c_1\tilde{\rho}\langle\delta\rho\delta\rho\rangle\cos\varphi_S} \\ =&\frac{{\dot{\varphi_L}}^2}{-\frac{q}{n}+3c_1\frac{\tilde{\rho}-2n}{n3}\langle\delta\varepsilon\delta\varepsilon\rangle+2c_1\frac{\tilde{\rho}}{n^3}\langle\delta\rho\delta\rho\rangle}+\mathcal{O}(\dot{\varphi}\sin^2,\nabla^3,\dot{\varphi}\nabla^2))\end{aligned} \tag{B.16}$$

and

$$\begin{aligned}&\frac{\left(\dot{\varphi}_S-2q-\frac{(\nabla\varphi_L)^2-(\nabla\varphi_S)^2}{4m}-2c_1(\tilde{\rho}-4n)(1+\cos\varphi_S)-\frac{c_1\tilde{\rho}}{n^2}\langle\delta\varepsilon\delta\varepsilon\rangle\right)^2\cos\varphi_S}{8c_1(1+\cos\varphi_S)+\frac{2c_1\tilde{\rho}}{n^3}\langle\delta\varepsilon\delta\varepsilon\rangle\cos\varphi_S} \\ =&\frac{\dot{\varphi}_S^2}{8c_1(1+\cos\varphi_S)+\frac{2c_1\tilde{\rho}}{n^3}\langle\delta\varepsilon\delta\varepsilon\rangle\cos\varphi_S}+\frac{2\dot{\varphi}_S\left(-2q-2c_1(\tilde{\rho}-4n)(1+\cos\varphi_S)-\frac{c_1\tilde{\rho}}{n^2}\langle\delta\varepsilon\delta\varepsilon\rangle\cos\varphi_S\right)}{8c_1(1+\cos\varphi_S)+\frac{2c_1\tilde{\rho}}{n^3}\langle\delta\varepsilon\delta\varepsilon\rangle\cos\varphi_S} \\ &+\frac{\frac{(\nabla\varphi_L)^2-(\nabla\varphi_S)^2}{2m}\left(2q+2c_1(\tilde{\rho}-4n)(1+\cos\varphi_S)+\frac{c_1\tilde{\rho}}{n^2}\langle\delta\varepsilon\delta\varepsilon\rangle\cos\varphi_S\right)}{8c_1(1+\cos\varphi_S)+\frac{2c_1\tilde{\rho}}{n^3}\langle\delta\varepsilon\delta\varepsilon\rangle\cos\varphi_S} \\ &+\frac{\left(2q+\frac{c_1\tilde{\rho}}{n^2}\langle\delta\varepsilon\delta\varepsilon\rangle\cos\varphi_S\right)^2}{8c_1(1+\cos\varphi_S)+\frac{2c_1\tilde{\rho}}{n^3}\langle\delta\varepsilon\delta\varepsilon\rangle\cos\varphi_S}+\frac{4c_1^2(\tilde{\rho}-4n)^2(1+\cos\varphi_S)^2}{8c_1(1+\cos\varphi_S)+\frac{2c_1\tilde{\rho}}{n^3}\langle\delta\varepsilon\delta\varepsilon\rangle\cos\varphi_S} \\ &+\frac{4c_1(\tilde{\rho}-4n)(1+\cos\varphi_S)\left(2q+\frac{c_1\tilde{\rho}}{n^2}\langle\delta\varepsilon\delta\varepsilon\rangle\cos\varphi_S\right)}{8c_1(1+\cos\varphi_S)+\frac{2c_1\tilde{\rho}}{n^3}\langle\delta\varepsilon\delta\varepsilon\rangle\cos\varphi_S}+\mathcal{O}(\nabla^3,\dot{\varphi}\nabla^2)\end{aligned} \tag{B.17}$$

We now want to expand terms now for small φ_S up to to order $\sin^4\frac{\varphi_S}{2}$. Moreover, assuming that $\sin^2\frac{\varphi_S}{2}$ is small, we also neglect any terms of the order of $\dot{\varphi}_i\sin^2\frac{\varphi_S}{2}$ and $(\nabla\varphi_i)^2\sin^2\frac{\varphi_S}{2}$ and only include linear orders in the fluctuations.

To carry out this expansion, the following reoccurring approximations are helpful, in which

we have included $\langle\delta\varepsilon\delta\varepsilon\rangle$ up to linear order:

$$\begin{aligned}
&\frac{1}{8c_1(1+\cos\varphi_S)+\frac{2c_1\tilde{\rho}}{n^3}\langle\delta\varepsilon\delta\varepsilon\rangle\cos\varphi_S} \\
&= \frac{1}{16c_1\left(1+\frac{\tilde{\rho}}{8n^3}\langle\delta\varepsilon\delta\varepsilon\rangle\right)\left(1-\frac{1+\frac{\tilde{\rho}}{4n^3}\langle\delta\varepsilon\delta\varepsilon\rangle}{1+\frac{\tilde{\rho}}{8n^3}\langle\delta\varepsilon\delta\varepsilon\rangle}\sin^2\frac{\varphi_S}{2}\right)} \\
&\approx \frac{1}{16c_1\left(1+\frac{\tilde{\rho}}{8n^3}\langle\delta\varepsilon\delta\varepsilon\rangle\right)}\sum_{k=0}^{\infty}\sin^{2k}(\frac{\varphi_S}{2})\left(1+\frac{k\tilde{\rho}}{8n^3}\langle\delta\varepsilon\delta\varepsilon\rangle\right) \\
&= \frac{1}{16c_1}\sum_{k=0}^{\infty}\sin^{2k}(\frac{\varphi_S}{2})\left(1+\frac{(k-1)\tilde{\rho}}{8n^3}\langle\delta\varepsilon\delta\varepsilon\rangle\right)
\end{aligned} \tag{B.18}$$

$$\begin{aligned}
&\frac{1+\cos\varphi_S}{8c_1(1+\cos\varphi_S)+\frac{2c_1\tilde{\rho}}{n^3}\langle\delta\varepsilon\delta\varepsilon\rangle\cos\varphi_S} \\
&\approx \frac{2(1-\sin^2\frac{\varphi_S}{2})}{16c_1}\sum_{k=0}^{\infty}\sin^{2k}(\frac{\varphi_S}{2})\left(1+\frac{(k-1)\tilde{\rho}}{8n^3}\langle\delta\varepsilon\delta\varepsilon\rangle\right) \\
&= \frac{1}{8c_1}\left(1-\frac{\tilde{\rho}}{8n^3}\langle\delta\varepsilon\delta\varepsilon\rangle+\sum_{k=1}^{\infty}\left[1+\frac{(k-1)\tilde{\rho}}{8n^3}\langle\delta\varepsilon\delta\varepsilon\rangle-1-\frac{(k-2)\tilde{\rho}}{8n^3}\langle\delta\varepsilon\delta\varepsilon\rangle\right]\sin^{2k}(\frac{\varphi_S}{2})\right) \\
&\approx \frac{1}{8c_1\left(1+\frac{\tilde{\rho}}{8n^3}\langle\delta\varepsilon\delta\varepsilon\rangle\right)}+\sum_{k=1}^{\infty}\frac{\sin^{2k}(\frac{\varphi_S}{2})}{8c_1}\frac{\tilde{\rho}}{8n^3}\langle\delta\varepsilon\delta\varepsilon\rangle
\end{aligned} \tag{B.19}$$

$$\begin{aligned}
&\frac{(1+\cos\varphi_S)^2}{8c_1(1+\cos\varphi_S)+\frac{2c_1\tilde{\rho}}{n^3}\langle\delta\varepsilon\delta\varepsilon\rangle\cos\varphi_S} \\
&\approx 2(1-\sin^2\frac{\varphi_S}{2})\left[\frac{1}{8c_1\left(1+\frac{\tilde{\rho}}{8n^3}\langle\delta\varepsilon\delta\varepsilon\rangle\right)}+\sum_{k=1}^{\infty}\frac{\sin^{2k}(\frac{\varphi_S}{2})}{8c_1}\frac{\tilde{\rho}}{8n^3}\langle\delta\varepsilon\delta\varepsilon\rangle\right] \\
&= \frac{1}{4c_1\left(1+\frac{\tilde{\rho}}{8n^3}\langle\delta\varepsilon\delta\varepsilon\rangle\right)}-\frac{\sin^2(\frac{\varphi_S}{2})}{4c_1}+\frac{\sin^2(\frac{\varphi_S}{2})}{16c_1}\frac{\tilde{\rho}}{n^3}\langle\delta\varepsilon\delta\varepsilon\rangle
\end{aligned} \tag{B.20}$$

$$\begin{aligned}
&\frac{(1+\cos\varphi_S)\cos\varphi_S}{8c_1(1+\cos\varphi_S)+\frac{2c_1\tilde{\rho}}{n^3}\langle\delta\varepsilon\delta\varepsilon\rangle\cos\varphi_S} \\
&\approx (1-2\sin^2\frac{\varphi_S}{2})\left[\frac{1}{8c_1\left(1+\frac{\tilde{\rho}}{8n^3}\langle\delta\varepsilon\delta\varepsilon\rangle\right)}+\sum_{k=1}^{\infty}\frac{\sin^{2k}(\frac{\varphi_S}{2})}{8c_1}\frac{\tilde{\rho}}{8n^3}\langle\delta\varepsilon\delta\varepsilon\rangle\right]
\end{aligned} \tag{B.21}$$

$$\begin{aligned}
&= \frac{1}{8c_1\left(1+\frac{\tilde{\rho}}{8n^3}\langle\delta\varepsilon\delta\varepsilon\rangle\right)}-\frac{\sin^2\frac{\varphi_S}{2}}{8c_1\left(1+\frac{3\tilde{\rho}}{16n^3}\langle\delta\varepsilon\delta\varepsilon\rangle\right)}-\sum_{k=2}^{\infty}\frac{\sin^{2k}(\frac{\varphi_S}{2})}{8c_1}\frac{\tilde{\rho}}{8n^3}\langle\delta\varepsilon\delta\varepsilon\rangle
\end{aligned} \tag{B.22}$$

Moreover, through linear combinations of these we find

$$\frac{\cos\varphi_S}{8c_1(1+\cos\varphi_S)+\frac{2c_1\tilde{\rho}}{n^3}\langle\delta\varepsilon\delta\varepsilon\rangle\cos\varphi_S} \tag{B.23}$$

$$\begin{aligned}
&\approx \frac{1}{8c_1\left(1+\frac{\tilde{\rho}}{8n^3}\langle\delta\varepsilon\delta\varepsilon\rangle\right)}+\sum_{k=1}^{\infty}\frac{\sin^{2k}(\frac{\varphi_S}{2})}{8c_1}\frac{\tilde{\rho}}{8n^3}\langle\delta\varepsilon\delta\varepsilon\rangle \\
&-\frac{1}{16c_1}\sum_{k=0}^{\infty}\sin^{2k}(\frac{\varphi_S}{2})\left(1+\frac{(k-1)\tilde{\rho}}{8n^3}\langle\delta\varepsilon\delta\varepsilon\rangle\right) \\
&=\frac{1}{16c_1\left(1+\frac{\tilde{\rho}}{8n^3}\langle\delta\varepsilon\delta\varepsilon\rangle\right)}-\frac{1}{16c_1}\sum_{k=1}^{\infty}\sin^{2k}(\frac{\varphi_S}{2})\left(1-\frac{(k+1)\tilde{\rho}}{8n^3}\langle\delta\varepsilon\delta\varepsilon\rangle\right).
\end{aligned} \tag{B.24}$$

With these approximations, we can then expand the different terms in Eq. (6.16) up to order

$\sin^4 \varphi/2$, yielding

$$\begin{aligned}
&\frac{\dot{\varphi}_S^2}{8c_1(1+\cos\varphi_S) + \frac{2c_1\tilde{\rho}}{n^3}\langle\delta\varepsilon\delta\varepsilon\rangle\cos\varphi_S} \\
&= \frac{\dot{\varphi}_S^2}{16c_1\left(1+\frac{\tilde{\rho}}{8n^3}\langle\delta\varepsilon\delta\varepsilon\rangle\right)} + \mathcal{O}(\dot{\varphi}_S\sin^2)
\end{aligned} \tag{B.25}$$

$$\begin{aligned}
&\frac{2\dot{\varphi}_S\left(-2q - 2c_1(\tilde{\rho}-4n)(1+\cos\varphi_S) - \frac{c_1\tilde{\rho}}{n^2}\langle\delta\varepsilon\delta\varepsilon\rangle\cos\varphi_S\right)}{8c_1(1+\cos\varphi_S) + \frac{2c_1\tilde{\rho}}{n^3}\langle\delta\varepsilon\delta\varepsilon\rangle\cos\varphi_S} \\
&= -\frac{2\dot{\varphi}_S\frac{c_1\tilde{\rho}}{n^2}\langle\delta\varepsilon\delta\varepsilon\rangle}{16c_1\left(1+\frac{\tilde{\rho}}{8n^3}\langle\delta\varepsilon\delta\varepsilon\rangle\right)} + \mathcal{O}(\dot{\varphi}_S\sin^2) \\
&= -\frac{\tilde{\rho}}{8n^2}\langle\delta\varepsilon\delta\varepsilon\rangle\dot{\varphi}_S + \mathcal{O}(\dot{\varphi}_S\sin^2, \langle\delta\delta\rangle^2)
\end{aligned} \tag{B.26}$$

$$\begin{aligned}
&\frac{\frac{(\nabla\varphi_L)^2-(\nabla\varphi_S)^2}{2m}\left(2q + 2c_1(\tilde{\rho}-4n)(1+\cos\varphi_S) + \frac{c_1\tilde{\rho}}{n^2}\langle\delta\varepsilon\delta\varepsilon\rangle\cos\varphi_S\right)}{8c_1(1+\cos\varphi_S) + \frac{2c_1\tilde{\rho}}{n^3}\langle\delta\varepsilon\delta\varepsilon\rangle\cos\varphi_S} \\
&= \frac{\frac{(\nabla\varphi_L)^2-(\nabla\varphi_S)^2}{2m}\frac{c_1\tilde{\rho}}{n^2}\langle\delta\varepsilon\delta\varepsilon\rangle}{16c_1\left(1+\frac{\tilde{\rho}}{8n^3}\langle\delta\varepsilon\delta\varepsilon\rangle\right)} + \mathcal{O}(\nabla\varphi_S\sin^2) \\
&= \frac{\tilde{\rho}}{32mn^2}\langle\delta\varepsilon\delta\varepsilon\rangle\left[(\nabla\varphi_L)^2 - (\nabla\varphi_S)^2\right] + \mathcal{O}(\nabla\varphi_S\sin^2, \langle\delta\delta\rangle^2)
\end{aligned} \tag{B.27}$$

$$\begin{aligned}
&\frac{\left(2q + \frac{c_1\tilde{\rho}}{n^2}\langle\delta\varepsilon\delta\varepsilon\rangle\cos\varphi_S\right)^2}{8c_1(1+\cos\varphi_S) + \frac{2c_1\tilde{\rho}}{n^3}\langle\delta\varepsilon\delta\varepsilon\rangle\cos\varphi_S} \\
&= 4q^2\left(\frac{\sin^2(\frac{\varphi_S}{2})}{16c_1} + \frac{\sin^4(\frac{\varphi_S}{2})}{16c_1}\left(1+\frac{\tilde{\rho}}{8n^3}\langle\delta\varepsilon\delta\varepsilon\rangle\right)\right) \\
&+ \frac{4qc_1\tilde{\rho}}{n^2}\langle\delta\varepsilon\delta\varepsilon\rangle\left(-\frac{\sin^2(\frac{\varphi_S}{2})}{16c_1} - \frac{\sin^4(\frac{\varphi_S}{2})}{16c_1}\right) + \text{const.} + \mathcal{O}(\sin^6, \langle\delta\delta\rangle^2)
\end{aligned} \tag{B.28}$$

$$\begin{aligned}
&\frac{4c_1^2(\tilde{\rho}-4n)^2(1+\cos\varphi_S)^2}{8c_1(1+\cos\varphi_S) + \frac{2c_1\tilde{\rho}}{n^3}\langle\delta\varepsilon\delta\varepsilon\rangle\cos\varphi_S} \\
&= q^2\frac{\sin^2(\frac{\varphi_S}{2})}{16c_1}\frac{\tilde{\rho}}{n^3}\langle\delta\varepsilon\delta\varepsilon\rangle + \text{const.} + \mathcal{O}(\langle\delta\delta\rangle^2)
\end{aligned} \tag{B.29}$$

$$\begin{aligned}
&\frac{4c_1(\tilde{\rho}-4n)(1+\cos\varphi_S)\left(2q + \frac{c_1\tilde{\rho}}{n^2}\langle\delta\varepsilon\delta\varepsilon\rangle\cos\varphi_S\right)}{8c_1(1+\cos\varphi_S) + \frac{2c_1\tilde{\rho}}{n^3}\langle\delta\varepsilon\delta\varepsilon\rangle\cos\varphi_S} \\
&= \frac{-4q^2(1+\cos\varphi_S) - 2\frac{qc_1\tilde{\rho}}{n^2}\langle\delta\varepsilon\delta\varepsilon\rangle\cos\varphi_S(1+\cos\varphi_S)}{8c_1(1+\cos\varphi_S) + \frac{2c_1\tilde{\rho}}{n^3}\langle\delta\varepsilon\delta\varepsilon\rangle\cos\varphi_S} \\
&= -\frac{q^2}{16c_1}\frac{\tilde{\rho}}{n^3}\langle\delta\varepsilon\delta\varepsilon\rangle\left(\sin^2\frac{\varphi_S}{2} + \sin^4\frac{\varphi_S}{2}\right) + \frac{q\tilde{\rho}}{2n^2}\langle\delta\varepsilon\delta\varepsilon\rangle\sin^2(\frac{\varphi_S}{2}) + \text{const.} + \mathcal{O}(\langle\delta\delta\rangle^2)
\end{aligned} \tag{B.30}$$

where we have always used the mean-field relation $q = -2c_1(\tilde{\rho} - 4n)$. Thus, we get

$$\begin{aligned}\frac{1}{2}\boldsymbol{J}_{\text{fluc}}^{\boldsymbol{T}}\boldsymbol{G}_{\text{fluc}}\boldsymbol{J}_{\text{fluc}} =& \frac{\dot{\varphi}_S^2}{32c_1\left(1+\frac{\tilde{\rho}}{8n^3}\langle\delta\varepsilon\delta\varepsilon\rangle\right)} - \frac{\tilde{\rho}}{16n^2}\langle\delta\varepsilon\delta\varepsilon\rangle\dot{\varphi}_S \qquad \text{(B.31)}\\ &+ \frac{\tilde{\rho}}{64mn^2}\langle\delta\varepsilon\delta\varepsilon\rangle\left[(\nabla\varphi_L)^2 - (\nabla\varphi_S)^2\right]\\ &+ \sin^2(\frac{\varphi_S}{2})\left[\frac{q\tilde{\rho}}{8n^2}\langle\delta\varepsilon\delta\varepsilon\rangle + \frac{q^2\tilde{\rho}}{64n^3c_1}\langle\delta\varepsilon\delta\varepsilon\rangle\right]\\ &+ \sin^4(\frac{\varphi_S}{2})\left[\frac{q^2}{8c_1} - \frac{q\tilde{\rho}}{8n^2}\langle\delta\varepsilon\delta\varepsilon\rangle - \frac{q^2\tilde{\rho}}{32n^3c_1}\langle\delta\varepsilon\delta\varepsilon\rangle\right] \qquad \text{(B.32)}\\ &+ \frac{{\dot{\varphi_L}}^2}{-4\frac{q}{n} + 6c_1\frac{\tilde{\rho}-2n}{n^3}\langle\delta\varepsilon\delta\varepsilon\rangle + 4c_1\frac{\tilde{\rho}}{n^3}\langle\delta\rho\delta\rho\rangle}\\ &+ \text{const.} + \mathcal{O}\left(\langle\delta\delta\rangle^2, \sin^6, \dot{\varphi}\sin^2, \nabla\varphi\sin^2, \dot{\varphi}\nabla^2\varphi, \nabla^3\varphi\right)\end{aligned}$$

We can now use the trigonometric identities

$$\sin^2(\varphi/2) = -\frac{1}{2}\cos(\varphi) + \text{const.} \qquad \text{(B.33)}$$

and

$$\sin^4(\varphi/2) = -\frac{1}{2}\cos(\varphi) - \frac{1}{4}\sin^2(\varphi) + \text{const.}, \qquad \text{(B.34)}$$

finding

$$\begin{aligned}\frac{1}{2}\boldsymbol{J}_{\boldsymbol{0}\,\text{fluc}}^{\boldsymbol{T}}\boldsymbol{G}_{\boldsymbol{0}\text{fluc}}\boldsymbol{J}_{\boldsymbol{0}\text{fluc}} =& \frac{\dot{\varphi}_S^2}{32c_1\left(1+\frac{\tilde{\rho}}{8n^3}\langle\delta\varepsilon\delta\varepsilon\rangle\right)} - \frac{\tilde{\rho}}{16n^2}\langle\delta\varepsilon\delta\varepsilon\rangle\dot{\varphi}_S \qquad \text{(B.35)}\\ &+ \frac{\tilde{\rho}}{64mn^2}\langle\delta\varepsilon\delta\varepsilon\rangle\left[(\nabla\varphi_L)^2 - (\nabla\varphi_S)^2\right]\\ &+ \sin^2\frac{\varphi_S}{2}\left[\frac{q\tilde{\rho}}{8n^2}\langle\delta\varepsilon\delta\varepsilon\rangle + \frac{q^2\tilde{\rho}}{64n^3c_1}\langle\delta\varepsilon\delta\varepsilon\rangle\right]\\ &+ \sin^4\frac{\varphi_S}{2}\left[\frac{q^2}{8c_1} - \frac{q\tilde{\rho}}{8n^2}\langle\delta\varepsilon\delta\varepsilon\rangle - \frac{q^2\tilde{\rho}}{32n^3c_1}\langle\delta\varepsilon\delta\varepsilon\rangle\right] \qquad \text{(B.36)}\\ &+ \frac{{\dot{\varphi_L}}^2}{-2\frac{q}{n} + 6c_1\frac{\tilde{\rho}-2n}{n^3}\langle\delta\varepsilon\delta\varepsilon\rangle + 4c_1\frac{\tilde{\rho}}{n^3}\langle\delta\rho\delta\rho\rangle}\\ &+ \text{const.} + \mathcal{O}\left(\langle\delta\delta\rangle^2, \sin^6, \dot{\varphi}\sin^2, \nabla\varphi\sin^2, \dot{\varphi}\nabla^2\varphi, \nabla^3\varphi\right).\end{aligned}$$

This then just has to be inserted in Eq. (5.13) in order to obtain the real part of the effective actions for φ_S and φ_L.

B.4. Expanding the real part of the effective Lagrangian around $\varphi_S = \pi$ including a momentum cutoff

In this section, we want to detail the expansion of the effective Lagrangian in Ch. 7 for φ_S around $(2\mathbb{Z}+1)\pi$ to obtain the effective theory in Sec. 7.2. Around $\varphi_S = (2\mathbb{Z}+1)\pi$, we can expand

$$\begin{aligned}\frac{1}{2}\boldsymbol{J}^{\boldsymbol{T}}\boldsymbol{G}_{\boldsymbol{0}}^{-1}\boldsymbol{J} = \frac{1}{2}\Bigg[&\frac{n^3\left(\dot{\varphi}_L\right)^2}{-\frac{k_I^2}{2mn} - 2n^2c_1(2n+(2n-\tilde{\rho})\cos\varphi_S)} \\ &+\frac{\left(\dot{\varphi}_S - 2q - \frac{(\nabla\varphi_L)^2-(\nabla\varphi_S)^2}{4m} - 2c_1(\tilde{\rho}-4n)(1+\cos\varphi_S)\right)^2}{-\frac{k_I^2}{2mn}\frac{\tilde{\rho}}{(\tilde{\rho}-2n)} + 8c_1(1+\cos\varphi_S)}\Bigg]\end{aligned} \tag{B.37}$$

to second order in $1+\cos\varphi_S$. We find, neglecting terms of the order $\dot{\varphi}(1+\cos)$, $\nabla\varphi(1+\cos)$, as well as any terms involving more than 2 derivatives

$$\begin{aligned}\frac{1}{2}\boldsymbol{J}^{\boldsymbol{T}}\boldsymbol{G}_{\boldsymbol{0}}^{-1}\boldsymbol{J} =& -\frac{\dot{\varphi}_S^2}{\frac{k_I^2}{mn}+\frac{4c_1\tilde{\rho}}{n}} - \frac{\dot{\varphi}_L^2}{\frac{k_I^2}{mn}\frac{\tilde{\rho}}{\rho-2n}} - \frac{(\nabla\varphi_L)^2-(\nabla\varphi_S)^2}{4m}\frac{1}{\frac{k_I^2}{mn}\frac{\tilde{\rho}}{\rho-2n}} \\ &+\frac{1}{2}\frac{(2q-q(1+\cos\varphi_S))}{-\frac{k_I^2}{2mn}\frac{\tilde{\rho}}{(\tilde{\rho}-2n)}+8c_1(1+\cos\varphi_S)} \\ &+\mathcal{O}(\dot{\varphi}(1+\cos),\nabla^2\varphi(1+\cos),\dot{\varphi}\nabla^2\varphi+\nabla^3\varphi).\end{aligned} \tag{B.38}$$

Expanding the second line, we find

$$\frac{1}{2}\frac{(2q-q(1+\cos\varphi_S))}{-\frac{k_I^2}{2mn}\frac{\tilde{\rho}}{(\tilde{\rho}-2n)}+8c_1(1+\cos\varphi_S)} \tag{B.39}$$

$$= -\frac{4q^2}{\frac{k_I^2}{2mn}\frac{\tilde{\rho}}{(\tilde{\rho}-2n)}}\left(1-(1+\cos\varphi_S)+\frac{1}{4}(1+\cos\varphi_S)^2\right) \tag{B.40}$$

$$\times\left(1+\frac{8c_1}{\frac{k_I^2}{2mn}\frac{\tilde{\rho}}{(\tilde{\rho}-2n)}}(1+\cos\varphi_S)+\left(\frac{8c_1}{\frac{k_I^2}{2mn}\frac{\tilde{\rho}}{(\tilde{\rho}-2n)}}\right)^2(1+\cos\varphi_S)^2\right) \tag{B.41}$$

$$=\frac{4q^2}{\frac{k_I^2}{2mn}\frac{\tilde{\rho}}{(\tilde{\rho}-2n)}}\left(\frac{1}{2}+\frac{8c_1}{\frac{k_I^2}{2mn}\frac{\tilde{\rho}}{(\tilde{\rho}-2n)}}-2\left(\frac{8c_1}{\frac{k_I^2}{2mn}\frac{\tilde{\rho}}{(\tilde{\rho}-2n)}}\right)^2\right)\cos\varphi_S \tag{B.42}$$

$$-\frac{4q^2}{\frac{k_I^2}{2mn}}\left(\frac{1}{4}-\frac{8c_1}{\frac{k_I^2}{2mn}\frac{\tilde{\rho}}{(\tilde{\rho}-2n)}}+\left(\frac{8c_1}{\frac{k_I^2}{2mn}\frac{\tilde{\rho}}{(\tilde{\rho}-2n)}}\right)^2\right)\cos^2\varphi_S + \text{const.} + \mathcal{O}((1+\cos\varphi_S)^3) \tag{B.43}$$

Using $\cos^2 = -\sin^2 + \text{const.}$, we find the Lagrangians Eq. (7.10) and (7.12).

C. Imaginary parts

In the main text, we have mainly focussed on the real parts of the effective Lagrangians. Here, we will go into some more detail on the imaginary parts of the theories developed in Ch. 6 and Ch. 7.

C.1. Imaginary part of the effective Lagrangian for small φ_S including density fluctuation corrections

After having derived the real part of the effective Lagrangian for φ_S shown in Sec. 5.1.3 in App. B.3, we now want to show the expansion of the imaginary part, which is given by

$$\begin{aligned}
&\Im S^{\text{eff}} = \frac{1}{2}\log\det \boldsymbol{G}_{\mathbf{0}_{\text{fluc}}}^{-1} = \frac{1}{2}\text{tr}\log \boldsymbol{G}_{\mathbf{0}_{\text{fluc}}}^{-1} \\
=&\frac{1}{2\Delta t(\Delta x)^d}\int_{t,x}\left[\log\left(\frac{8c_1(1+\cos\varphi_S)+\frac{2c_1\tilde{\rho}}{n^3}\langle\delta\varepsilon\delta\varepsilon\rangle\cos\varphi_S}{16c_1+\frac{2c_1\tilde{\rho}}{n^3}\langle\delta\varepsilon\delta\varepsilon\rangle}\right)\right. \\
&\left.+\log\left(\frac{-2c_1\left(2+\left(2-\frac{\tilde{\rho}}{n}\right)\cos\varphi_S\right)+\frac{2c_1\tilde{\rho}}{n^3}\langle\delta\rho\delta\rho\rangle\cos\varphi_S+3c_1\frac{\tilde{\rho}-2n}{n^3}\langle\delta\varepsilon\delta\varepsilon\rangle\cos\varphi_S}{2c_1\left(\frac{\tilde{\rho}}{n}-4\right)+\frac{2c_1\tilde{\rho}}{n^3}\langle\delta\rho\delta\rho\rangle+3c_1\frac{\tilde{\rho}-2n}{n^3}\langle\delta\varepsilon\delta\varepsilon\rangle}\right)\right],
\end{aligned}$$

where again Δt and Δx are the time- and lengthscales relevant for regularization, defined by $\sum_{t,x} = \frac{1}{\Delta t(\Delta x)^d}\int_{t,x}$ and we have normalized the term to vanish for $\varphi_S = 0$.

Using that $\log(1+x) = x - \frac{x^2}{2} + \mathcal{O}(x^3)$, we can expand the first of these terms as

$$\begin{aligned}
&\log\left(\frac{8c_1(1+\cos\varphi_S)+\frac{2c_1\tilde{\rho}}{n^3}\langle\delta\varepsilon\delta\varepsilon\rangle\cos\varphi_S}{16c_1+\frac{2c_1\tilde{\rho}}{n^3}\langle\delta\varepsilon\delta\varepsilon\rangle}\right) \qquad \text{(C.1)}\\
&= \log\left(1-2\sin^2\frac{\varphi_S}{2}\frac{8c_1+\frac{2c_1}{n^2}\langle\delta\varepsilon\delta\varepsilon\rangle}{16c_1+\frac{2c_1\tilde{\rho}}{n^3}\langle\delta\varepsilon\delta\varepsilon\rangle}\right) \\
&= \log\left(1-\sin^2\frac{\varphi_S}{2}\left(1+\frac{\tilde{\rho}}{8n^3}\langle\delta\varepsilon\delta\varepsilon\rangle\right)\right)+\mathcal{O}\left(\langle\delta\delta\rangle^2\right) \\
&= -\sin^2\frac{\varphi_S}{2}\left(1+\frac{\tilde{\rho}}{8n^3}\langle\delta\varepsilon\delta\varepsilon\rangle\right)-\sin^4\frac{\varphi_S}{2}\left(\frac{1}{2}+\frac{\tilde{\rho}}{8n^3}\langle\delta\varepsilon\delta\varepsilon\rangle\right)+\text{const.}+\mathcal{O}\left(\langle\delta\delta\rangle^2,\sin^6\right)
\end{aligned}$$

where in the last step we have only included fluctuations $\langle\delta\varepsilon\delta\varepsilon\rangle$ to linear order, just like for

the real part. Moreover,

$$\log\left(\frac{-2c_1\left(2+\left(2-\frac{\tilde{\rho}}{n}\right)\cos\varphi_S\right)+\frac{2c_1\tilde{\rho}}{n^3}\langle\delta\rho\delta\rho\rangle\cos\varphi_S+3c_1\frac{\tilde{\rho}-2n}{n^3}\langle\delta\varepsilon\delta\varepsilon\rangle\cos\varphi_S}{2c_1\left(\frac{\tilde{\rho}}{n}-4\right)+\frac{2c_1\tilde{\rho}}{n^3}\langle\delta\rho\delta\rho\rangle+3c_1\frac{\tilde{\rho}-2n}{n^3}\langle\delta\varepsilon\delta\varepsilon\rangle}\right) \tag{C.2}$$
$$\begin{aligned}
&= \log\left(1-\sin^2\frac{\varphi_S}{2}\frac{4(\tilde{\rho}-2n)+\frac{4\tilde{\rho}}{n^2}\langle\delta\rho\delta\rho\rangle+6\frac{\tilde{\rho}-2n}{n^2}\langle\delta\varepsilon\delta\varepsilon\rangle}{2(\tilde{\rho}-4n)+\frac{2\tilde{\rho}}{n^2}\langle\delta\rho\delta\rho\rangle+3\frac{\tilde{\rho}-2n}{n^2}\langle\delta\varepsilon\delta\varepsilon\rangle}\right)\\
&= -\sin^2\frac{\varphi_S}{2}\left[2\frac{\tilde{\rho}-2n}{\tilde{\rho}-4n}+\left(2\frac{\tilde{\rho}}{\tilde{\rho}-4n}-\frac{1}{2}\frac{\tilde{\rho}}{\tilde{\rho}-2n}\right)\frac{\langle\delta\rho\delta\rho\rangle}{n^2}+\left(3\frac{\tilde{\rho}-2n}{\tilde{\rho}-4n}-\frac{3}{4}\right)\frac{\langle\delta\varepsilon\delta\varepsilon\rangle}{n^2}\right]\\
&\quad-\sin^4\frac{\varphi_S}{2}\left[2\left(\frac{\tilde{\rho}-2n}{\tilde{\rho}-4n}\right)^2+\left(2\frac{\tilde{\rho}}{\tilde{\rho}-4n}-\frac{1}{2}\frac{\tilde{\rho}}{\tilde{\rho}-2n}\right)\frac{\tilde{\rho}-2n}{\tilde{\rho}-4n}\frac{\langle\delta\rho\delta\rho\rangle}{n^2}\right.\\
&\quad\left.+\left(3\frac{\tilde{\rho}-2n}{\tilde{\rho}-4n}-\frac{3}{4}\right)\frac{\tilde{\rho}-2n}{\tilde{\rho}-4n}\frac{\langle\delta\varepsilon\delta\varepsilon\rangle}{n^2}\right]+\mathcal{O}\left(\langle\delta\delta\rangle^2,\sin^6\right).
\end{aligned}$$

We can now use

$$\sin^2(\varphi/2) = -\frac{1}{2}\cos(\varphi)+\text{const.} \tag{C.3}$$

and

$$\sin^4(\varphi/2) = -\frac{1}{2}\cos(\varphi)-\frac{1}{4}\sin^2(\varphi)+\text{const.} \tag{C.4}$$

to find for the imaginary part of the effective Lagrangian for φ_S

$$\Im\mathcal{L}^{\text{eff}} = \frac{1}{4\Delta t(\Delta x)^d}\left[A_I\cos\varphi_S+B_I\sin^2\varphi_S\right]+\text{const.}+\mathcal{O}(\langle\delta\delta\rangle^2,\sin^6) \tag{C.5}$$

where

$$\begin{aligned}
A_I = \Bigg[&\frac{3}{2}+2\frac{\tilde{\rho}-2n}{\tilde{\rho}-4n}+2\left(\frac{\tilde{\rho}-2n}{\tilde{\rho}-4n}\right)^2\\
&+\left(\frac{\tilde{\rho}}{4n}+\frac{9}{4}\frac{\tilde{\rho}-2n}{\tilde{\rho}-4n}+3\left(\frac{\tilde{\rho}-2n}{\tilde{\rho}-4n}\right)^2-\frac{3}{4}\right)\frac{\langle\delta\varepsilon\delta\varepsilon\rangle}{n^2}\\
&+\left(\frac{3}{2}\frac{\tilde{\rho}}{\tilde{\rho}-4n}-\frac{1}{2}\frac{\tilde{\rho}}{\tilde{\rho}-2n}+\frac{2\tilde{\rho}(\tilde{\rho}-2n)}{(\tilde{\rho}-4n)^2}\right)\frac{\langle\delta\rho\delta\rho\rangle}{n^2}\Bigg]
\end{aligned}$$

and

$$\begin{aligned}
B_I = \Bigg[&\frac{1}{4}+\left(\frac{\tilde{\rho}-2n}{\tilde{\rho}-4n}\right)^2+\frac{1}{2}\left(\frac{\tilde{\rho}}{8n}-\frac{3}{4}\frac{\tilde{\rho}-2n}{\tilde{\rho}-4n}+3\left(\frac{\tilde{\rho}-2n}{\tilde{\rho}-4n}\right)^2\right)\frac{\langle\delta\varepsilon\delta\varepsilon\rangle}{n^2}\\
&+\left(\frac{\tilde{\rho}(\tilde{\rho}-2n)}{(\tilde{\rho}-4n)^2}-\frac{1}{4}\frac{\tilde{\rho}}{\tilde{\rho}-4n}\right)\frac{\langle\delta\rho\delta\rho\rangle}{n^2}\Bigg].
\end{aligned}$$

For the small fluctuations shown in Sec. 6.5, the positivity of the imaginary part in the theory without fluctuations discussed in Sec. 5.1.3 translates to the case with fluctuations, such that

also here, the imaginary part only accounts for a damping of the partition function.

C.2. Imaginary part of the effective Lagrangian around $\varphi_S = \pi$ including a momentum cutoff

The imaginary part of the effective Lagrangian in Sec. 7.1 is given by

$$\Im\mathcal{L}^{\text{eff}} = \frac{1}{2\Delta t(\Delta x)^d} \log\left(\frac{-\frac{k_I^2}{2mn}\frac{\tilde{\rho}}{(\tilde{\rho}-2n)} + 8c_1(1+\cos\varphi_S)}{-\frac{k_I^2}{2mn}\frac{\tilde{\rho}}{(\tilde{\rho}-2n)}} \cdot \frac{-\frac{k_I^2}{2mn} - 2c_1\left(2+\left(2-\frac{\tilde{\rho}}{n}\right)\cos\varphi_S\right)}{-\frac{k_I^2}{2mn} - 2c_1\frac{\tilde{\rho}}{n}} \right), \tag{C.6}$$

where again Δt and Δx are the time- and lengthscales relevant for regularization, defined by $\sum_{t,x} = \frac{1}{\Delta t(\Delta x)^d}\int_{t,x}$ and we have now normalized the term to vanish for $\varphi_S = \pi$. Expanding these logarithms for small $(1+\cos\varphi_S)$ using $\log(1+x) = x - \frac{x^2}{2} + \mathcal{O}(x^3)$, we get

$$\log\left(\frac{-\frac{k_I^2}{2mn}\frac{\tilde{\rho}}{(\tilde{\rho}-2n)} + 8c_1(1+\cos\varphi_S)}{-\frac{k_I^2}{2mn}\frac{\tilde{\rho}}{(\tilde{\rho}-2n)}} \right) \tag{C.7}$$

$$= -\frac{8c_1}{\frac{k_I^2}{2mn}\frac{\tilde{\rho}}{(\tilde{\rho}-2n)}}(1+\cos\varphi_S) - \frac{1}{2}\left(\frac{8c_1}{\frac{k_I^2}{2mn}\frac{\tilde{\rho}}{(\tilde{\rho}-2n)}}\right)^2 (1+\cos\varphi_S)^2 + \mathcal{O}((1+\cos\varphi_S)^3) \tag{C.8}$$

and

$$\log\left(\frac{-\frac{k_I^2}{2mn} - 2c_1\left(2+\left(2-\frac{\tilde{\rho}}{n}\right)\cos\varphi_S\right)}{-\frac{k_I^2}{2mn} - 2c_1\frac{\tilde{\rho}}{n}} \right) \tag{C.9}$$

$$= -\frac{2c_1\left(\frac{\tilde{\rho}}{n}-2\right)}{\frac{k_I^2}{2mn} + 2c_1\frac{\tilde{\rho}}{n}}(1+\cos\varphi_S) - \frac{1}{2}\left(\frac{2c_1\left(\frac{\tilde{\rho}}{n}-2\right)}{\frac{k_I^2}{2mn} + 2c_1\frac{\tilde{\rho}}{n}}\right)^2 (1+\cos\varphi_S)^2 + \mathcal{O}((1+\cos\varphi_S)^3) \tag{C.10}$$

Using $\sin^2\varphi + \cos^2\varphi = 1$ and ignoring any constants, we then find

$$\Im\mathcal{L}^{\text{eff}}_{\varphi_S} = \frac{1}{2\Delta t(\Delta x)^d}\left[-A_I\cos\varphi_S + B_I\sin^2\varphi_S\right] + \text{const.} + \mathcal{O}\left((1+\cos)^3\right)$$

with

$$A_I = \frac{8c_1}{\frac{k_I^2}{2mn}\frac{\tilde{\rho}}{\tilde{\rho}-2n}} + \left(\frac{8c_1}{\frac{k_I^2}{2mn}\frac{\tilde{\rho}}{\tilde{\rho}-2n}}\right)^2 + \frac{2c_1\left(\frac{\tilde{\rho}}{n}-2\right)}{\frac{k_I^2}{2mn}+2c_1\frac{\tilde{\rho}}{n}} + \left(\frac{2c_1\left(\frac{\tilde{\rho}}{n}-2\right)}{\frac{k_I^2}{2mn}+2c_1\frac{\tilde{\rho}}{n}}\right)^2 \tag{C.11}$$
$$B_I = \left[\frac{1}{2}\left(\frac{8c_1}{\frac{k_I^2}{2mn}\frac{\tilde{\rho}}{\tilde{\rho}-2n}}\right)^2 + \frac{1}{2}\left(\frac{2c_1\left(\frac{\tilde{\rho}}{n}-2\right)}{\frac{k_I^2}{2mn}+2c_1\frac{\tilde{\rho}}{n}}\right)^2\right]$$

Inserting $k_I = k_{\xi_S}$, the coefficients become

$$A_I = -\frac{8(\tilde{\rho}-2n)n}{\tilde{\rho}^2} + \frac{64(\tilde{\rho}-2n)^2n^2}{\tilde{\rho}^4} + \frac{2\left(\tilde{\rho}-2n\right)}{\tilde{\rho}} + \left(\frac{2\left(\tilde{\rho}-2n\right)}{\tilde{\rho}}\right)^2 \tag{C.12}$$
$$B_I = \left[\frac{32(\tilde{\rho}-2n)^2n^2}{\tilde{\rho}^4} + \frac{2\left(\tilde{\rho}-2n\right)^2}{\tilde{\rho}^2}\right].$$

Note that this leads to a positive imaginary part for $|\varphi_S - \pi| \mod 2\pi < \pi/2$ and $q > 0.188\tilde{\rho}|c_1|$, such that if we are far enough away from the quantum phase transition at $q = 0$ and in the range in which our approximation is valid, the imaginary part is again only a damping of the partition function. If q gets smaller than that, the imaginary part becomes negative, first only at $\varphi_S = (2\mathbb{Z}+1)\pi$ and then also in an increasingly bigger area around the maxima.

Thus, for small q, the partition function growing exponentially is possible whenever φ_S is around $\varphi_S = (2\mathbb{Z}+1)\pi$. This could be interpreted as the instantons leading to exponentially growing modes in the vicinity of the phase transition where the description with φ_S and φ_L breaks down.

Acknowledgements

Als erstes möchte ich mich ganz herzlich bei Prof. Dr. Thomas Gasenzer für die Betreuung meiner Masterarbeit bedanken - für die neuen Impulse für meine Forschung, die sich aus jedem Treffen mit dir ergaben, deine Wissbegier nach physikalischen Interpretationen und Erklärungen, die geholfen hat, die endlosen Formeln, die ich hergeleitet habe, mit "Physik" zu füllen, und deine Gabe, meine Resultate oft in den Kontext mit anderen physikalischen Phänomenen zu setzen. Außerdem möchte ich Ihnen, Prof. Dr. Jan Pawlowski, dafür danken, dass Sie sich bereit erklärt haben, der Zweitkorrektor für meine Arbeit zu sein.

Mein großer Dank gilt auch Ido Siovitz, der als Doktorand mein unmittelbarer Betreuer war und dessen Arbeit die Inspiration und Grundlage für dieses Projekt war. Als Numerik-Gott hast du immer gewusst, wie man meine Analytik durch numerische Simulationen unterstützen und überprüfen kann, und du hast mir bei meinen Simulationen durch deine Expertise tagelanges Stack-Exchange-Durchpflügen erspart. Außerdem konnte ich mich mit jeder noch so dummen Frage über das Spin-1 Bose Gas an dich wenden. Abgesehen davon möchte ich dir für deine emotionale Unterstützung in den Situationen danken, in denen ich dachte, nicht gut genug für die Wissenschaft zu sein.

Weiterhin möchte ich Dr. Philipp Heinen dafür danken, dass du mir durch deine große Erfahrung und Expertise im Feld der ultrakalten Atome und den damit assoziierten Methoden mehr als einmal weitergeholfen hast. Auch Hannes Köper möchte ich dafür danken, dass du dein großes Wissen über Analytik mit mir geteilt hast. Außerdem danke ich Niklas Rasch dafür, dass du mich immer wieder auf die richtigen Paper verwiesen hast.

Außerdem möchte ich mich bei Prof. Dr. Markus Oberthaler und der BEC-Gruppe bestehend aus Dr. Helmut Strobel, Yannick Deller, Alexander Schmutz und Felix Klein bedanken. Ohne die Kollaboration mit euch und die Motivation aus euren experimentellen Ergebnissen wäre meine Masterarbeit nicht möglich gewesen.

Ich möchte mich auch bei Andreea Oros bedanken, dafür, dass du die beste Bürokollegin warst, und mich nicht nur mit den richtigen Plotting- oder Clusterkommandos sondern auch immer mit aufmunternden Worten, Umarmungen, Stricktips, Memes, und Kinderriegeln unterstützt

hast.

Allgemein möchte ich mich bei allen Matterwavern aus der SynQS-Gruppe bedanken - explizit erwähnen möchte ich hier zusätzlich zu den schon genannten vor allem Mai Anh, Yvette Werner, Toni Eberhardt, Alexandra Beikert und Magdalena Winkelvoss. Die Zeit in der Gruppe war für mich eine sehr lehrreiche Erfahrung dank dem Retreat in Italien, der DPG Tagung, den regelmäßigen Chatterwaves, Laborführungen, und allgemein dem Dialog mit vielen Menschen, die sich experimentell oder theoretisch mit Quantendynamik beschäftigen. Über das fachliche hinaus werde ich auch die gemeinsamen Aktivitäten wie die (Pool)parties auf dem Retreat, das gemeinsame Frühstück jeden Freitag, und die monatlichen Kranzmittwoche in guter Erinnerung behalten.

Außerdem möchte ich mich bei Christiane Jäger und Petra Hübler bedanken. Ohne eure organisatorische Hilfe wäre meine Teilnahme an der Konferenz und dem Retreat nie so reibungslos möglich gewesen, und ich habe mich immer gefreut, euch auf dem Flur zu sehen.

Schließlich möchte ich mich bei meinen Eltern bedanken. Nur durch eure unendliche Unterstützung habe ich das gesamte Studium und die Masterarbeit geschafft. Ihr wart immer bei mir - ob physisch oder am Telefon - und habt mich aufgeheitert und motiviert, wenn ich dachte, etwas nicht mehr zu schaffen. Ich habe euch sehr lieb! Emotional unterstützt haben mich im letzten Jahr auch meine Freund:innen, allen voran Flora Vollmer, Annika Oligschläger, Emilia Schaaf und Leon Patzig, sowie meine WG mit Isabel Schwenk, Jakob Burgi, Fabian Schulte und Julia Raffetseder. Ich werde euch und die schönen und lustigen Stunden, die wir zusammen verbracht haben, sehr vermissen, wenn ich für die Promotion in die USA gehe.

Für die finanzielle Unterstützung während dieser Masterarbeit und des Großteils meines Studiums möchte ich mich außerdem bei der Bischöflichen Studienförderung Cusanuswerk bedanken.

The numerical simulations in this work have been carried out on the GPU computing cluster of the European Institute for Neuromorphic Computing (EINC) in Heidelberg as well as the bwForCluster Helix. For the latter, I acknowledge support by the state of Baden-Württemberg through bwHPC and the German Research Foundation (DFG) through grant INST 35/1597-1 FUGG.

Bibliography

[1] Pasquale Di Bari. *Cosmology and the early universe*. CRC Press, 2018.

[2] Rudolf Baier et al. ""Bottom-up" thermalization in heavy ion collisions." In: *Physics Letters B* 502.1–4 (Mar. 2001), pp. 51–58. ISSN: 0370-2693. DOI: 10.1016/s0370-2693(01)00191-5. URL: http://dx.doi.org/10.1016/S0370-2693(01)00191-5.

[3] Jürgen Berges et al. "Turbulent thermalization process in heavy-ion collisions at ultrarelativistic energies." In: *Physical Review D* 89.7 (Apr. 2014). ISSN: 1550-2368. DOI: 10.1103/physrevd.89.074011. URL: http://dx.doi.org/10.1103/PhysRevD.89.074011.

[4] Lev Kofman, Andrei Linde, and Alexei A. Starobinsky. "Reheating after Inflation." In: *Physical Review Letters* 73.24 (Dec. 1994), pp. 3195–3198. ISSN: 0031-9007. DOI: 10.1103/physrevlett.73.3195. URL: http://dx.doi.org/10.1103/PhysRevLett.73.3195.

[5] Raphael Micha and Igor I. Tkachev. "Relativistic Turbulence: A Long Way from Preheating to Equilibrium." In: *Physical Review Letters* 90.12 (Mar. 2003). ISSN: 1079-7114. DOI: 10.1103/physrevlett.90.121301. URL: http://dx.doi.org/10.1103/PhysRevLett.90.121301.

[6] Jürgen Berges. *Nonequilibrium Quantum Fields: From Cold Atoms to Cosmology*. 2015. arXiv: 1503.02907 [hep-ph].

[7] Jürgen Berges. "What ultracold atoms tell us about the real-time dynamics of QCD in extreme conditions." In: *EPJ Web Conf.* 296 (2024), p. 01021. DOI: 10.1051/epjconf/202429601021. arXiv: 2312.10673 [hep-ph].

[8] Immanuel Bloch, Jean Dalibard, and Wilhelm Zwerger. "Many-body physics with ultracold gases." In: *Rev. Mod. Phys.* 80 (3 July 2008), pp. 885–964. DOI: 10.1103/RevModPhys.80.885. URL: https://link.aps.org/doi/10.1103/RevModPhys.80.885.

[9] Christian-Marcel Schmied, Aleksandr N. Mikheev, and Thomas Gasenzer. "Non-thermal fixed points: Universal dynamics far from equilibrium." In: *International Journal of Modern Physics A* 34.29 (Oct. 2019), p. 1941006. ISSN: 1793-656X. DOI: 10.1142/s0217751x19410069. URL: http://dx.doi.org/10.1142/S0217751X19410069.

[10] T. Kinoshita, T. Wenger, and D. Weiss. "A quantum Newton's cradle." In: *Nature* 440 (2006), pp. 900–903. DOI: 10.1038/nature04693.

[11] S. Hofferberth et al. "Non-equilibrium coherence dynamics in one-dimensional Bose gases." In: *Nature* 449.7160 (Sept. 2007), pp. 324–327. ISSN: 1476-4687. DOI: 10.1038/nature06149. URL: http://dx.doi.org/10.1038/nature06149.

[12] Stefan Trotzky et al. "Probing the relaxation towards equilibrium in an isolated strongly correlated one-dimensional Bose gas." In: *Nature Physics* 8.4 (Feb. 2012), pp. 325–330. ISSN: 1745-2481. DOI: 10.1038/nphys2232. URL: http://dx.doi.org/10.1038/nphys2232.

[13] Luís M.A. Bettencourt and Christof Wetterich. "Time evolution of correlation functions in non-equilibrium field theories." In: *Physics Letters B* 430.1–2 (June 1998), pp. 140–150. ISSN: 0370-2693. DOI: 10.1016/s0370-2693(98)00509-7. URL: http://dx.doi.org/10.1016/S0370-2693(98)00509-7.

[14] Gert Aarts, Gian Franco Bonini, and Christof Wetterich. "Exact and truncated dynamics in nonequilibrium field theory." In: *Phys. Rev. D* 63 (2 Dec. 2000), p. 025012. DOI: 10.1103/PhysRevD.63.025012. URL: https://link.aps.org/doi/10.1103/PhysRevD.63.025012.

[15] Jürgen Berges. "Introduction to Nonequilibrium Quantum Field Theory." In: *AIP Conference Proceedings*. AIP, 2004. DOI: 10.1063/1.1843591. URL: https://doi.org/10.1063%2F1.1843591.

[16] Michael Gring et al. "Relaxation and Prethermalization in an Isolated Quantum System." In: *Science* 337.6100 (2012), pp. 1318–1322. DOI: 10.1126/science.1224953. eprint: https://www.science.org/doi/pdf/10.1126/science.1224953. URL: https://www.science.org/doi/abs/10.1126/science.1224953.

[17] Tim Langen, Thomas Gasenzer, and Jörg Schmiedmayer. "Prethermalization and universal dynamics in near-integrable quantum systems." In: *Journal of Statistical Mechanics: Theory and Experiment* 2016.6 (June 2016), p. 064009. ISSN: 1742-5468. DOI: 10.1088/1742-5468/2016/06/064009. URL: http://dx.doi.org/10.1088/1742-5468/2016/06/064009.

[18] Edwin T. Jaynes. "Information Theory and Statistical Mechanics." In: *Phys. Rev.* 106 (4 May 1957), pp. 620–630. DOI: 10.1103/PhysRev.106.620. URL: https://link.aps.org/doi/10.1103/PhysRev.106.620.

[19] Edwin T. Jaynes. "Information Theory and Statistical Mechanics. II." In: *Phys. Rev.* 108 (2 Oct. 1957), pp. 171–190. DOI: 10.1103/PhysRev.108.171. URL: https://link.aps.org/doi/10.1103/PhysRev.108.171.

[20] Marcos Rigol et al. "Relaxation in a Completely Integrable Many-Body Quantum System: An Ab Initio Study of the Dynamics of the Highly Excited States of 1D Lattice Hard-Core Bosons." In: *Phys. Rev. Lett.* 98 (5 Feb. 2007), p. 050405. DOI: 10.1103/PhysRevLett.98.050405. URL: https://link.aps.org/doi/10.1103/PhysRevLett.98.050405.

[21] Tim Langen et al. "Experimental observation of a generalized Gibbs ensemble." In: *Science* 348.6231 (2015), pp. 207–211. DOI: 10.1126/science.1257026. eprint: https://www.science.org/doi/pdf/10.1126/science.1257026. URL: https://www.science.org/doi/abs/10.1126/science.1257026.

[22] Lev Vidmar and Marcos Rigol. "Generalized Gibbs ensemble in integrable lattice models." In: *Journal of Statistical Mechanics: Theory and Experiment* 2016.6 (June 2016), p. 064007. ISSN: 1742-5468. DOI: 10.1088/1742-5468/2016/06/064007. URL: http://dx.doi.org/10.1088/1742-5468/2016/06/064007.

[23] Rahul Nandkishore and David A Huse. "Many-body localization and thermalization in quantum statistical mechanics." In: *Annu. Rev. Condens. Matter Phys.* 6.1 (2015), pp. 15–38.

[24] Michael Schreiber et al. "Observation of many-body localization of interacting fermions in a quasirandom optical lattice." In: *Science* 349.6250 (2015), pp. 842–845. DOI: 10.1126/science.aaa7432. eprint: https://www.science.org/doi/pdf/10.1126/science.aaa7432. URL: https://www.science.org/doi/abs/10.1126/science.aaa7432.

[25] Romain Vasseur and Joel E Moore. "Nonequilibrium quantum dynamics and transport: from integrability to many-body localization." In: *Journal of Statistical Mechanics: Theory and Experiment* 2016.6 (June 2016), p. 064010. ISSN: 1742-5468. DOI: 10.1088/1742-5468/2016/06/064010. URL: http://dx.doi.org/10.1088/1742-5468/2016/06/064010.

[26] Dmitry A. Abanin et al. "Colloquium : Many-body localization, thermalization, and entanglement." In: *Reviews of Modern Physics* 91.2 (May 2019). ISSN: 1539-0756. DOI: 10.1103/revmodphys.91.021001. URL: http://dx.doi.org/10.1103/RevModPhys.91.021001.

[27] Simon Braun et al. "Emergence of coherence and the dynamics of quantum phase transitions." In: *Proceedings of the National Academy of Sciences* 112.12 (2015), pp. 3641–3646. DOI: 10.1073/pnas.1408861112. eprint: https://www.pnas.org/doi/pdf/10.1073/pnas.1408861112. URL: https://www.pnas.org/doi/abs/10.1073/pnas.1408861112.

[28] Eike Nicklas et al. "Observation of Scaling in the Dynamics of a Strongly Quenched Quantum Gas." In: *Physical Review Letters* 115.24 (Dec. 2015). ISSN: 1079-7114. DOI: 10.1103/physrevlett.115.245301. URL: http://dx.doi.org/10.1103/PhysRevLett.115.245301.

[29] Nir Navon et al. "Critical dynamics of spontaneous symmetry breaking in a homogeneous Bose gas." In: *Science* 347.6218 (Jan. 2015), pp. 167–170. ISSN: 1095-9203. DOI: 10.1126/science.1258676. URL: http://dx.doi.org/10.1126/science.1258676.

[30] Christoph Eigen et al. "Universal prethermal dynamics of Bose gases quenched to unitarity." In: *Nature* 563.7730 (Nov. 2018), pp. 221–224. ISSN: 1476-4687. DOI: 10.1038/s41586-018-0674-1. URL: http://dx.doi.org/10.1038/s41586-018-0674-1.

[31] Vladimir E Zakharov, Victor S L'vov, and Gregory Falkovich. *Kolmogorov spectra of turbulence I: Wave turbulence*. Springer Science & Business Media, 2012.

[32] Nir Navon et al. "Emergence of a turbulent cascade in a quantum gas." In: *Nature* 539.7627 (Nov. 2016), pp. 72–75. ISSN: 1476-4687. DOI: 10.1038/nature20114. URL: http://dx.doi.org/10.1038/nature20114.

[33] Bernhard Rauer et al. "Recurrences in an isolated quantum many-body system." In: *Science* 360.6386 (2018), pp. 307–310. DOI: 10.1126/science.aan7938. eprint: https://www.science.org/doi/pdf/10.1126/science.aan7938. URL: https://www.science.org/doi/abs/10.1126/science.aan7938.

[34] Jürgen Berges, Alexander Rothkopf, and Jonas Schmidt. "Nonthermal Fixed Points: Effective Weak Coupling for Strongly Correlated Systems Far from Equilibrium." In: *Phys. Rev. Lett.* 101 (4 July 2008), p. 041603. DOI: 10.1103/PhysRevLett.101.041603. URL: https://link.aps.org/doi/10.1103/PhysRevLett.101.041603.

[35] Asier Piñeiro Orioli, Kirill Boguslavski, and Jürgen Berges. "Universal self-similar dynamics of relativistic and nonrelativistic field theories near nonthermal fixed points." In: *Physical Review D* 92.2 (July 2015). ISSN: 1550-2368. DOI: 10.1103/physrevd.92.025041. URL: http://dx.doi.org/10.1103/PhysRevD.92.025041.

[36] Sebastian Erne et al. "Universal dynamics in an isolated one-dimensional Bose gas far from equilibrium." In: *Nature* 563.7730 (Nov. 2018), pp. 225–229. ISSN: 1476-4687. DOI: 10.1038/s41586-018-0667-0. URL: http://dx.doi.org/10.1038/s41586-018-0667-0.

[37] Maximilian Prüfer et al. "Observation of universal dynamics in a spinor Bose gas far from equilibrium." In: *Nature* 563.7730 (Nov. 2018), pp. 217–220. ISSN: 1476-4687. DOI: 10.1038/s41586-018-0659-0. URL: http://dx.doi.org/10.1038/s41586-018-0659-0.

[38] Christian-Marcel Schmied et al. "Bidirectional universal dynamics in a spinor Bose gas close to a nonthermal fixed point." In: *Physical Review A* 99.3 (Mar. 2019). ISSN: 2469-9934. DOI: 10.1103/physreva.99.033611. URL: http://dx.doi.org/10.1103/PhysRevA.99.033611.

[39] Christian-Marcel Schmied, Thomas Gasenzer, and P. Blaire Blakie. "Violation of single-length scaling dynamics via spin vortices in an isolated spin-1 Bose gas." In: *Phys. Rev. A* 100.3 (2019), p. 033603. DOI: 10.1103/PhysRevA.100.033603. arXiv: 1904.13222 [cond-mat.quant-gas].

[40] Aleksandr N. Mikheev, Ido Siovitz, and Thomas Gasenzer. *Universal dynamics and non-thermal fixed points in quantum fluids far from equilibrium*. 2023. arXiv: 2304.12464 [cond-mat.quant-gas]. URL: https://arxiv.org/abs/2304.12464.

[41] Ido Siovitz et al. "Universal Dynamics of Rogue Waves in a Quenched Spinor Bose Condensate." In: *Physical Review Letters* 131.18 (Nov. 2023). ISSN: 1079-7114. DOI: 10.1103/physrevlett.131.183402. URL: http://dx.doi.org/10.1103/PhysRevLett.131.183402.

[42] Christian-Marcel Schmied, Aleksandr N. Mikheev, and Thomas Gasenzer. "Prescaling in a far-from-equilibrium Bose gas." In: *Phys. Rev. Lett.* 122.17 (2019), p. 170404. DOI: 10.1103/PhysRevLett.122.170404. arXiv: 1807.07514 [cond-mat.quant-gas].

[43] Benjamin Widom. "Equation of state in the neighborhood of the critical point." In: *The Journal of Chemical Physics* 43.11 (1965), pp. 3898–3905.

[44] Leo P. Kadanoff. "Scaling laws for ising models near T_c." In: *Physics Physique Fizika* 2 (6 June 1966), pp. 263–272. DOI: 10.1103/PhysicsPhysiqueFizika.2.263. URL: https://link.aps.org/doi/10.1103/PhysicsPhysiqueFizika.2.263.

[45] Kenneth G. Wilson. "Renormalization Group and Critical Phenomena. I. Renormalization Group and the Kadanoff Scaling Picture." In: *Phys. Rev. B* 4 (9 Nov. 1971), pp. 3174–3183. DOI: 10.1103/PhysRevB.4.3174. URL: https://link.aps.org/doi/10.1103/PhysRevB.4.3174.

[46] Kenneth G. Wilson. "Renormalization Group and Critical Phenomena. II. Phase-Space Cell Analysis of Critical Behavior." In: *Phys. Rev. B* 4 (9 Nov. 1971), pp. 3184–3205. DOI: 10.1103/PhysRevB.4.3184. URL: https://link.aps.org/doi/10.1103/PhysRevB.4.3184.

[47] Kenneth G. Wilson and Michael E. Fisher. "Critical Exponents in 3.99 Dimensions." In: *Phys. Rev. Lett.* 28 (4 Jan. 1972), pp. 240–243. DOI: 10.1103/PhysRevLett.28.240. URL: https://link.aps.org/doi/10.1103/PhysRevLett.28.240.

[48] Michael E. Fisher. "The renormalization group in the theory of critical behavior." In: *Rev. Mod. Phys.* 46 (4 Oct. 1974), pp. 597–616. DOI: 10.1103/RevModPhys.46.597. URL: https://link.aps.org/doi/10.1103/RevModPhys.46.597.

[49] Jürgen Berges and David Mesterházy. "Introduction to the nonequilibrium functional renormalization group." In: *Nuclear Physics B - Proceedings Supplements* 228 (2012). "Physics at all scales: The Renormalization Group" Proceedings of the 49th Internationale Universitätswochen für Theoretische Physik, pp. 37–60. ISSN: 0920-5632. DOI: https://doi.org/10.1016/j.nuclphysbps.2012.06.003. URL: https://www.sciencedirect.com/science/article/pii/S0920563212001600.

[50] J. Stenger et al. "Spin domains in ground-state Bose–Einstein condensates." In: *Nature* 396.6709 (Nov. 1998), pp. 345–348. ISSN: 1476-4687. DOI: 10.1038/24567. URL: http://dx.doi.org/10.1038/24567.

[51] Jonathan Braden et al. "Towards the cold atom analog false vacuum." In: *Journal of High Energy Physics* 2018.7 (July 2018). ISSN: 1029-8479. DOI: 10.1007/jhep07(2018)014. URL: http://dx.doi.org/10.1007/JHEP07(2018)014.

[52] Philipp Kunkel et al. "Simultaneous Readout of Noncommuting Collective Spin Observables beyond the Standard Quantum Limit." In: *Phys. Rev. Lett.* 123 (6 Aug. 2019), p. 063603. DOI: 10.1103/PhysRevLett.123.063603. URL: https://link.aps.org/doi/10.1103/PhysRevLett.123.063603.

[53] Stefan Lannig et al. "Collisions of Three-Component Vector Solitons in Bose-Einstein Condensates." In: *Phys. Rev. Lett.* 125 (17 Oct. 2020), p. 170401. DOI: 10.1103/PhysRevLett.125.170401. URL: https://link.aps.org/doi/10.1103/PhysRevLett.125.170401.

[54] Maximilian Prüfer et al. "Experimental extraction of the quantum effective action for a non-equilibrium many-body system." In: *Nature Physics* 16.10 (June 2020), pp. 1012–1016. ISSN: 1745-2481. DOI: 10.1038/s41567-020-0933-6. URL: http://dx.doi.org/10.1038/s41567-020-0933-6.

[55] Philipp Kunkel et al. "Detecting Entanglement Structure in Continuous Many-Body Quantum Systems." In: *Phys. Rev. Lett.* 128 (2 Jan. 2022), p. 020402. DOI: 10.1103/PhysRevLett.128.020402. URL: https://link.aps.org/doi/10.1103/PhysRevLett.128.020402.

[56] Maximilian Prüfer et al. "Condensation and thermalization of an easy-plane ferromagnet in a spinor Bose gas." In: *Nature Physics* 18.12 (Oct. 2022), pp. 1459–1463. ISSN: 1745-2481. DOI: 10.1038/s41567-022-01779-6. URL: http://dx.doi.org/10.1038/s41567-022-01779-6.

[57] Yannick Deller et al. *Area laws and thermalization from classical entropies in a Bose-Einstein condensate*. 2024. arXiv: 2404.12321.

[58] Yuki Kawaguchi and Masahito Ueda. "Spinor Bose–Einstein condensates." In: *Physics Reports* 520.5 (2012). Spinor Bose–Einstein condensates, pp. 253–381. ISSN: 0370-1573. DOI: https://doi.org/10.1016/j.physrep.2012.07.005. URL: https://www.sciencedirect.com/science/article/pii/S0370157312002098.

[59] Tetsuo Ohmi and Kazushige Machida. "Bose-Einstein Condensation with Internal Degrees of Freedom in Alkali Atom Gases." In: *Journal of the Physical Society of Japan* 67.6 (June 1998), pp. 1822–1825. ISSN: 1347-4073. DOI: 10.1143/jpsj.67.1822. URL: http://dx.doi.org/10.1143/JPSJ.67.1822.

[60] Tin-Lun Ho. "Spinor Bose Condensates in Optical Traps." In: *Physical Review Letters* 81.4 (July 1998), pp. 742–745. ISSN: 1079-7114. DOI: 10.1103/physrevlett.81.742. URL: http://dx.doi.org/10.1103/PhysRevLett.81.742.

[61] Stefan Lannig. "Experimental Control of a Spin-1 Bose-Einstein Condensate." MA thesis. Heidelberg University, 2018.

[62] Christopher David Hamley. "Spin-Nematic Squeezing in a Spin-1 Bose-Einstein Condensate." PhD thesis. Georgia Institute of Technology, 2018.

[63] Jürgen Berges and Thomas Gasenzer. "Quantum versus classical statistical dynamics of an ultracold Bose gas." In: *Phys. Rev. A* 76 (3 Sept. 2007), p. 033604. DOI: 10.1103/PhysRevA.76.033604. URL: https://link.aps.org/doi/10.1103/PhysRevA.76.033604.

[64] Michael E. Peskin and Daniel V. Schroeder. *An Introduction to quantum field theory*. Reading, USA: Addison-Wesley, 1995. DOI: 10.1201/9780429503559.

[65] Christian-Marcel Schmied. "Universal Scaling Dynamics at Non-thermal Fixed Points in Multi-Component Bose Gases Far from Eqilibrium." PhD thesis. Heidelberg University, 2020.

[66] Shun Uchino, Michikazu Kobayashi, and Masahito Ueda. "Bogoliubov theory and Lee-Huang-Yang corrections in spin-1 and spin-2 Bose-Einstein condensates in the presence of the quadratic Zeeman effect." In: *Phys. Rev. A* 81 (6 June 2010), p. 063632. DOI: 10.1103/PhysRevA.81.063632. URL: https://link.aps.org/doi/10.1103/PhysRevA.81.063632.

[67] Ido Siovitz. "Topological Excitations and Universal Scaling of the One-Dimensional Spin-1 Bose-Einstein Condensate Far from Equilibrium." MA thesis. Heidelberg University, 2022.

[68] Shun Uchino. "Spinor Bose gas in an elongated trap." In: *Phys. Rev. A* 91 (3 Mar. 2015), p. 033605. DOI: 10.1103/PhysRevA.91.033605. URL: https://link.aps.org/doi/10.1103/PhysRevA.91.033605.

[69] Weizhu Bao, Dieter Jaksch, and Peter A. Markowich. "Numerical solution of the Gross–Pitaevskii equation for Bose–Einstein condensation." In: *Journal of Computational Physics* 187.1 (May 2003), pp. 318–342. ISSN: 0021-9991. DOI: 10.1016/s0021-9991(03)00102-5. URL: http://dx.doi.org/10.1016/S0021-9991(03)00102-5.

[70] Markus Karl, Boris Nowak, and Thomas Gasenzer. "Universal scaling at nonthermal fixed points of a two-component Bose gas." In: *Phys. Rev. A* 88 (6 Dec. 2013), p. 063615. DOI: 10.1103/PhysRevA.88.063615. URL: https://link.aps.org/doi/10.1103/PhysRevA.88.063615.

[71] Thomas Gasenzer et al. "Gauge turbulence, topological defect dynamics, and condensation in Higgs models." In: *Nuclear Physics A* 930 (2014), pp. 163–186. ISSN: 0375-9474. DOI: https://doi.org/10.1016/j.nuclphysa.2014.07.030. URL: https://www.sciencedirect.com/science/article/pii/S0375947414002310.

[72] Markus Karl and Thomas Gasenzer. "Strongly anomalous non-thermal fixed point in a quenched two-dimensional Bose gas." In: *New Journal of Physics* 19.9 (Sept. 2017), p. 093014. ISSN: 1367-2630. DOI: 10.1088/1367-2630/aa7eeb. URL: http://dx.doi.org/10.1088/1367-2630/aa7eeb.

[73] JAC Weideman and Ben M Herbst. "Split-step methods for the solution of the nonlinear Schrödinger equation." In: *SIAM Journal on Numerical Analysis* 23.3 (1986), pp. 485–507.

[74] P.Blaire Blakie et al. "Dynamics and statistical mechanics of ultra-cold Bose gases using c-field techniques." In: *Advances in Physics* 57.5 (2008), pp. 363–455. DOI: 10.1080/00018730802564254. eprint: https://doi.org/10.1080/00018730802564254. URL: https://doi.org/10.1080/00018730802564254.

[75] Alex Kamenev. *Field Theory of Non-Equilibrium Systems*. Cambridge University Press, 2011. DOI: 10.1017/CBO9781139003667.

[76] Martin Rabel. "Dynamics of a One-Dimensional Two-Component Bose Gas Quenched to Criticality." MA thesis. Heidelberg University, 2018.

[77] Leonid V. Keldysh. "Diagram technique for nonequilibrium processes." In: *Soviet Physics JETP* 20 (4 1965).

[78] Philipp Heinen et al. *Non-thermal fixed points of universal sine-Gordon coarsening dynamics*. 2022. arXiv: 2212.01162 [cond-mat.quant-gas]. URL: https://arxiv.org/abs/2212.01162.

[79] Jürgen Berges and Jürgen Cox. "Thermalization of quantum fields from time-reversal invariant evolution equations." In: *Physics Letters B* 517.3–4 (Oct. 2001), pp. 369–374. ISSN: 0370-2693. DOI: 10.1016/s0370-2693(01)01004-8. URL: http://dx.doi.org/10.1016/S0370-2693(01)01004-8.

[80] Gert Aarts et al. "Far-from-equilibrium dynamics with broken symmetries from the 1/N expansion of the 2PI effective action." In: *Physical Review D* 66.4 (Aug. 2002). ISSN: 1089-4918. DOI: 10.1103/physrevd.66.045008. URL: http://dx.doi.org/10.1103/PhysRevD.66.045008.

[81] Mark Alford, Jürgen Berges, and Jack M. Cheyne. "Critical phenomena from the two-particle irreducible 1/N expansion." In: *Physical Review D* 70.12 (Dec. 2004). ISSN: 1550-2368. DOI: 10.1103/physrevd.70.125002. URL: http://dx.doi.org/10.1103/PhysRevD.70.125002.

[82] Aleksandr N. Mikheev, Christian-Marcel Schmied, and Thomas Gasenzer. "Low-energy effective theory of nonthermal fixed points in a multicomponent Bose gas." In: *Physical Review A* 99.6 (June 2019). ISSN: 2469-9934. DOI: 10.1103/physreva.99.063622. URL: http://dx.doi.org/10.1103/PhysRevA.99.063622.

[83] S. Sobkowiak et al. "Interacting multicomponent exciton gases in a potential trap: Phase separation and Bose-Einstein condensation." In: *Physical Review B* 82.6 (Aug. 2010). DOI: 10.1103/physrevb.82.064505. URL: https://doi.org/10.1103%2Fphysrevb.82.064505.

[84] Ido Siovitz et al. "Double sine-Gordon as effective theory of a spin-1 Bose gas." In: *in preparation* (2024).

[85] Christof Wetterich. *Field transformations in functional integral, effective action and functional flow equations*. 2024. arXiv: 2402.04679 [hep-th].

[86] Philipp Kunkel. "Splitting a Bose-Einstein condensate enables EPR steering and simultaneous readout of noncommuting observables." PhD thesis. Heidelberg University, 2019.

[87] Philipp Heinen, Aleksandr N. Mikheev, and Thomas Gasenzer. "Anomalous scaling at nonthermal fixed points of the sine-Gordon model." In: *Physical Review A* 107.4 (Apr. 2023). ISSN: 2469-9934. DOI: 10.1103/physreva.107.043303. URL: http://dx.doi.org/10.1103/PhysRevA.107.043303.

[88] Vladimir Gritsev, Anatoli Polkovnikov, and Eugene Demler. "Linear response theory for a pair of coupled one-dimensional condensates of interacting atoms." In: *Phys. Rev. B* 75 (17 May 2007), p. 174511. DOI: 10.1103/PhysRevB.75.174511. URL: https://link.aps.org/doi/10.1103/PhysRevB.75.174511.

[89] Jorge V. José et al. "Renormalization, vortices, and symmetry-breaking perturbations in the two-dimensional planar model." In: *Phys. Rev. B* 16 (3 Aug. 1977), pp. 1217–1241. DOI: 10.1103/PhysRevB.16.1217. URL: https://link.aps.org/doi/10.1103/PhysRevB.16.1217.

[90] Matthew P. A. Fisher and G. Grinstein. "Quantum Critical Phenomena in Charged Superconductors." In: *Phys. Rev. Lett.* 60 (3 Jan. 1988), pp. 208–211. DOI: 10.1103/PhysRevLett.60.208. URL: https://link.aps.org/doi/10.1103/PhysRevLett.60.208.

[91] Timo Weigand. *Lecture notes on "Quantum Field Theory I + II"*.

Selbstständigkeitserklärung

Ich versichere, dass ich diese Arbeit selbstständig verfasst und keine anderen als die angegebenen Quellen und Hilfsmittel benutzt habe.

Heidelberg, 02.08.2024